

# **Experimental Methods for the Assessment of Single Living**

**Cells:**

## **Dielectrophoresis for Cell Electro-Deformations**

Shahrzad Nouri

A thesis

in the Department

of

Mechanical and Industrial Engineering

Presented in Partial Fulfillment of the Requirements for the Degree of  
Master of Applied Science (Mechanical Engineering) at

Concordia University

Montreal, Quebec, Canada

October 2013

© Shahrzad Nouri, 2013

**CONCORDIA UNIVERSITY**  
**SCHOOL OF GRADUATE STUDIES**

This is to certify that the Thesis prepared,

By: **Shahrzad Nouri**

Entitled: **“Experimental Methods for the Assessment of Single Living Cells:  
Dielectrophoresis for Cell Electro-Deformations”**

and submitted in partial fulfillment of the requirements for the Degree of

**Master of Applied Science (Mechanical Engineering)**

complies with the regulations of this University and meets the accepted standards with respect to originality and quality.

Signed by the Final Examining Committee:

_____	Chair
Dr. K. Demirli	
_____	Examiner
Dr. R. Wuthrich	
_____	Examiner
Dr. S. Williamson	External
Electrical and Computer Engineering	
_____	Supervisor
Dr. I. Stiharu	
_____	Supervisor
Dr. R. Sedaghati	

Approved by:

\_\_\_\_\_  
Dr. S. Narayanswamy, MASc Program Director  
Department of Mechanical and Industrial Engineering

\_\_\_\_\_  
Dr. C.W. Trueman, Interim Dean  
Faculty of Engineering & Computer Science

Date: \_\_\_\_\_

## *Abstract*

### Experimental methods for the assessment of single living cells: Dielectrophoresis for cell electro-deformations

Shahrzad Nouri

Many diseases such as cancer are initiated in single cells which modify their functions and amplify certain biological activities of the normal cells. These changes affect and permanently change the mechanical properties of normal cells. The significant difference between mechanical properties of different malignant cell lines could be used as a label free biomarker to distinguish between invasive and non-invasive carcinoma cells whose shapes and sizes are roughly the same. Among recent experimental methods for single cell assessments, dielectrophoresis (DEP) based devices have been introduced as novel techniques to direct deformation measurement of the living cell. In this work the application of microdevices for trapping and stretching of two human breast carcinoma cell lines based on dielectrophoresis phenomena, is presented.

The results of electro-deformation process of two malignant cell lines, MDA-MB-231 (highly metastatic human breast carcinoma cell line) and MCF-7 (weakly metastatic human breast carcinoma cell line) using a positive DEP micro-device is presented in this work. The elastic constants of cells are measured by comparing the results of finite element simulation using COMSOL multiphysics with those of experimental studies. Concurring with the previous works, the results of this study show that highly metastatic breast cancer cells (MDA-MB-231) are much softer than weakly metastatic breast cancer

cells (MCF-7), such that they could squeeze easier and migrate into human tissue through capillary blood vessels.

An improved design to trap the suspended living cells in the middle of electrodes is presented and experimentally tested in the thesis. Inducing symmetric elongation on cells could improve the accuracy of calculated elastic constant of cells. Also, as the cells are positioning between electrodes (in the transparent zone) the visibility of captured images and accuracy of calibrated images could be improved.

## *ACKNOWLEDGMENTS*

First and foremost I would like to provide my heartfelt gratitude to my supervisors Dr. Ion Stiharu and Dr. Ramin Sedaghati whose comments and genuine suggestions were invaluable to the progress of this thesis. Without their guidance and support this work would have not been successful.

During my research and work, I have had the pleasure to benefit from expertise of Dr. Ala-Eddin Al Moustafa, Dr. Vahé Nerguizian and Dr. Dacian Roman. I would like to take the opportunity to thank them all for their convivial company and cordial conversation. I would also like to express my gratitude to Dr. Anas Alazzam for his helpful suggestions.

My dearest thanks are warmly extended to my husband, who has been a constant source of motivation and comfort, for his encouragement and care throughout my efforts in this work. I also extend my deep thanks to my parents and siblings for their unconditional love and support.

Finally, I would like to present my cordial thanks to those who helped me to become this thesis a successful one.

*To my beloved husband Amirhossein and my lovely kids Kian and Ariyan*

## Contents

List of Figures .....	xi
List of Tables .....	xv
List of Acronyms .....	xvi
List of Symbols .....	xviii
Chapter 1: INTRODUCTION.....	1
Motivation, rationale and objectives .....	1
1.1 Achieving single cell assessment .....	5
1.2 Mechanical and structural properties of living cells .....	5
1.3 Literature review .....	8
1.4.1 Atomic force microscopy (AFM) .....	9
1.4.2 Microneedle .....	16
1.4.3 Oscillatory cantilevers .....	18
1.4.4 Magnetic twisting cytometry (MTC) .....	19
1.4.5 Laser/optical tweezers.....	21
1.4.6 Microplates .....	23
1.4.8 Micropipette aspiration .....	25
1.5 Dielectrophoresis (DEP ) micro-devices.....	27
1.6 Mechanical models for single cell assessment.....	29
1.7 Thesis organizations.....	34
Concluding remarks on the experimental methods .....	36
Chapter 2: ELECTRO-DEFORMATION OF LIVING CELLS IN A NON-UNIFORM ELECTRIC FIELD .....	38

2.1	Introduction .....	38
2.1.1	Electromechanical model of a living cell.....	39
2.1.2	Governing equations .....	39
2.2	Dielectrophoresis phenomena .....	40
2.3	Maxwell stress tensor (MST) approach .....	41
2.4	DEP force calculation on the living cell membrane using MST approach .....	42
2.5	Electro-deformation of living cells in a non-uniform DC electric field.....	43
2.5.1	Problem description .....	43
2.6	Living cells in a uniform DC electric field .....	49
2.7	Effective dipole moment approximation.....	52
2.8	Finite Element simulation of the cell deformation using COMSOL .....	54
2.8.1	Theoretical background .....	55
2.8.2	Problem formulation .....	56
2.9	Summary .....	61
Chapter 3: PARAMETRIC STUDY AND OPTIMIZATION OF THE ELECTRO- DEFORMATION MEMS DEVICE TO INCREASE DEP FORCES ON BIOLOGICAL CELLS .....		62
3.1	Introduction .....	62
3.2	Parametric study.....	62
3.2.1	Influence of distance between electrodes on cell elongation.....	64
3.2.2	Influence of tip angle of electrodes on cell elongation .....	66
3.2.3	Influence of relative permittivity of the medium on cell elongation .....	68
3.2.4	Influence of length of electrodes on cell elongation .....	68
3.3	Optimization study .....	69



3.3.1	General formulation of the optimization problem .....	70
3.3.2	Optimization algorithm .....	71
3.3.3	General concepts of the genetic algorithm optimization method .....	72
3.3.4	Terminology of the genetic algorithm [96] .....	73
3.3.5	Optimization procedure .....	74
3.3.6	Optimum design of the problem .....	74
3.3.7	Results .....	78
3.3.8	Validation of the genetic algorithm based optimization results .....	79
3.3.9	Best Design .....	83
3.4	Conclusion .....	84
Chapter 4: EXPERIMENTAL ANALYSIS OF ELECTRO-DEFORMATIONS OF SINGLE LIVING CELLS AND VALIDATION OF THE MODEL .....		86
4.1	Introduction .....	86
4.2	Cell preparation protocol .....	86
4.3	Suspension medium .....	87
4.4	Specimen preparation .....	87
4.5	Experimental setup .....	89
4.6	Microdevice design and fabrication (P-DEP device) .....	90
4.7	Experimental analysis of cancer living cell lines .....	91
4.7.1	Electro-deformation of MDA-MB-231 and MCF-7 cell lines .....	91
4.7.2	Estimation of Young's modulus for the two cell lines .....	95
4.8	An improved design to trap the cells in the middle of electrodes .....	99
4.9	Comparison of the obtained results with the results presented in the literature .....	102
4.10	Conclusion .....	104

Chapter 5: SUMMARY AND FUTURE WORK.....	106
5.1 Summary of the research study .....	106
5.2 Areas of further study.....	108
References .....	110
Appendix.....	117
A.1: <i>model.m</i> , MATLAB function for transferring the result and modified parameters to COMSOL Desktop.....	117
A.2: Trapping-stretching procedure of MDA-MB-231 cells .....	124
A.3: Elastic parameters of MCF10A and MDA-MB-231 cells in different growth media [105].....	125

## List of Figures

Figure 1.1: Schematic of AFM for living cell probing [29].	9
Figure 1.2: A) Single force spectroscopy, B) Force-versus-distance curves [37]	15
Figure 1.3: Schematic of experiments done by Ahmad et al. [21]	17
Figure 1.4: a) Experimental setup for pulling cytometry of a BCE cell [51], b) SEM image of beads embedded in the cell surface [49].	20
Figure 1.5: Stretching a single human red blood cell using the optical tweezers method [53].	22
Figure 1.6: Stretching a single fibroblast cell using microplates technique [24].	23
Figure 1.7: The aspirated neutrophil and chondrocyte cells into glass pipettes [25].	26
Figure 1.8: Schematic drawing of DEP phenomena	28
Figure 2.1: Lipid bilayer forming a microsphere	38
Figure 2.2: Schematic drawing of DEP phenomena	41
Figure 2.3: Schematic drawing of a spherical cell in a non-uniform electric field	44
Figure 2.4: Electromechanical model of a living cell	45
Figure 2.5: A two-dimensional shell with finite thickness	48
Figure 2.6: Schematic drawing of a spherical cell in a uniform electric field	49
Figure 2.7: Contour plot of the electric field intensity around the cell	51
Figure 2.8: Outward Maxwell stress tensor over the boundary of the cell	52
Figure 2.9: Schematic drawing of a cell as a dipole particle in a non-uniform electric field	53
Figure 2.10: Schematic drawing of a linear elastic material (Material 1) placed in a medium (Material 2)	55

Figure 2.11: 3D representation of a single shelled spherical cell surrounded in a non-uniform DC electric field .....	57
Figure 2.12: Contour plot of electric field (a) when the cell is present, (b) no cell is present .....	58
Figure 2.13: 3D finite element model of the problem .....	59
Figure 2.14: Electric tractions inside (a) and outside (b) the cell .....	60
Figure 2.15: Electro deformation of the cell in a non-uniform electric field.....	60
Figure 3.1: Schematic drawing of a spherical cell in a non-uniform electric field and the input parameters of the model.....	63
Figure 3.2: Deformation of the cell versus distance between electrodes for different size of the cell.....	65
Figure 3.3: Deformation ratio ( $\Delta r/r$ ) of the cells versus size ratio ( $D/r$ ).....	65
Figure 3.4: Comparing the $X$ component of dielectrophoretic force on cell surfaces .....	66
Figure 3.5: Comparing the $X$ component of dielectrophoretic force on cell surfaces .....	67
Figure 3.6: Comparing the electric tractions on the cell surfaces regarding the tip angle of electrodes. (a) A cell placed between sharp electrodes. (b) A cell placed between flat electrodes. Arrows indicate the electric tractions on the cell membrane.....	67
Figure 3.7: Maximum deformation of the cell versus the medium permittivity.....	68
Figure 3.8: Maximum deformation of the cell versus the length of electrodes .....	69
Figure 3.9: Flow chart of optimization process [93].....	72
Figure 3.10: Result of the optimization algorithm for Crossover fraction of 0.9 .....	78
Figure 3.11: Maximum deformation of the cell membrane versus parameter $X_1$ .....	80
Figure 3.12: Maximum deformation of the cell membrane versus parameter $X_2$ .....	81

Figure 3.13: Maximum deformation of the cell membrane versus parameter $X_3$ .....	81
Figure 3.14: Maximum deformation of the cell membrane versus parameter $X_4$ .....	82
Figure 3.15: Comparing the maximum deformation of the cell in the initial design (a) and the best design (b) .....	83
Figure 4.1: (a) The P-DEP microdevice for trapping and stretching the living cells, (b) Electrode lines and electrical connections .....	89
Figure 4.2: Experimental setup for trapping and stretching the living cells .....	90
Figure 4.3: (a) MCF-7 cells are attached to the tips of electrodes, (b) Finite element simulation of electric field between the electrodes using COMSOL. The arrows indicate the direction of the dielectrophoretic force. The background contours indicate the electric field strength .....	91
Figure 4.4: MDA-MB-231 trapping- stretching-procedure (a) Trapping the cells upon applying 2 Volts(b) Stretching the cells after 10 minutes of exposure of 20 Volts.....	92
Figure 4.5: (a) & (c) Captured images of trapping - stretching of breast cancer cell lines	94
Figure 4.6: Deformation of the cell near one electrode is in equilibrium position .....	96
Figure 4.7: Histogram of calculated Young's modulus of MDA-MB-231(a), and MCF7 (b).....	97
Figure 4.8: Mean control chart of Young's modulus of MDA-MB-231 (a), and MCF-7 (b).....	98
Figure 4.9: Symmetric deformation of a cell positioned at the center line between electrodes .....	99
Figure 4.10: Configuration of two electrode circuits to apply symmetric deformations on cells .....	100

Figure 4.11: Trapping and stretching a MDA-MB-231 cell in the middle of thick electrodes ..... 101

Figure 4.12: Finite element simulation of electric field. The arrows indicate the direction of the dielectrophoretic force. The background contours indicate the electric field strength ..... 101

## List of Tables

Table 1.1: Young's modulus of two different cancerous cell lines [6].....	3
Table 1.2: Experimental methods for single cell assessment .....	8
Table 1.3: Linear elastic solid model used for single cell level.....	31
Table 2.1: Comparing the maximum and minimum tractions over the cell boundary based on FEM analysis (COMSOL) and theoretical analysis (Eq.22). .....	52
Table 2.2: Input parameters of the 3D electrostatic-mechanical analysis .....	57
Table 3.1: Input parameters of the parametric study .....	64
Table 3.2: Input parameters for 3D optimization analysis.....	75
Table 3.3: Comparing different optimum points found by optimization algorithms associated with the different crossover fractions .....	79
Table 4.1: Statistical results of the experimental electro-deformations of MDA-MB-231 and MCF-7 cells.....	93
Table 4.2: Input parameters of the electro-deformation model of cells.....	95
Table 4.3: Calculated values of Young's modulus of MDA-MB-231 and MCF-7 cells..	97

## **List of Acronyms**

AC	Altering Current
AFM	Atomic force microscopy
BCE	Bovine Capillary Endothelial cells
COMSOL	Finite Element Analysis Solver and Simulation Software
DC	Direct Current
DEP	Dielectrophoresis or Dielectrophoretic
ECM	Extracellular Matrixes of living cells
EDTA	EthyleneDiamineTetraacetic acid
ESEM	Environmental Scanning Electron Microscope
FBS	Fetal Bovine Serum
$F_{DEP}$	Dielectrophoretic Force
FEM	Finite Element Method
GA	Genetic Algorithm
HASM	Human Airway Smooth Muscle cells
HeLa	Immortal cervical cancer cell line
HUVE	Human Umbilical Vein Endothelial cells
kHz	Kilo Hertz, $10^3$ Hertz
LDV	Laser Doppler Vibrometer
MATLAB	MATrix LABoratory
MCF-10A	Non-cancerous human breast cell
MCF-7	weakly metastatic human breast carcinoma cell line
MDA-MB-231	highly metastatic human breast carcinoma cell line



MEMS	Micro-Electro-Mechanical System
MHz	Mega Hertz, $10^6$ Hertz
MN	Microneedle
MPa	Mega Pascal, $10^6$ Pascal
MST	Maxwell stress tensor approach
MTC	Magnetic Twisting Cytometry
n-DEP	Negative Dielectrophoresis
nm	Nano-Meter, $10^{-9}$ Meter
OT	Laser/optical tweezers
PBS	Phosphate Buffered Saline
P-DEP	Positive Dielectrophoresis
pN	Pico Newton, $10^{-12}$ Newton
Poly-L-lysine	Solution for use in adhering tissue sections to glass slides
RPMI	Roswell Park Memorial Institute Medium
$\mu\text{m}$	Micro-Meter, $10^{-6}$ Meter
2D	Two Dimensional
3D	Three Dimensional

## List of Symbols

$A$	Surface enclosing the particle
$\text{\AA}$	Angstrom
$G^*$	Frequency dependent shear modulus
$F^*$	Complex loading force
$L_p$	Length of the aspirated tongue of the cell
$R_p$	Radius of the micropipette
$\dot{L}_p$	Rate of change of the aspirated tongue length
$\Delta P$	Total suction pressure
$P_{cr}$	Critical pressure
$(\nabla)^n E$	Symmetric tensor of rank n
$\langle \bar{F}_{DEF} \rangle^n$	Overall time-average DEP force based on multipole assumption
$\langle \vec{f}_{DEF} \rangle$	Time-averaged net DEP force
$\vec{f}_{DEF}^s$	DEP force per unit area
$\vec{f}_{mem}^s$	Membrane mechanical force strength
$\vec{\vec{T}}_{in}$ or $T_{down}$	Downward Maxwell stress tensor
$\vec{\vec{T}}_{out}$ or $T_{up}$	Upward Maxwell stress tensor
$\vec{\vec{T}}_1$	Time-average stress tensor
$\vec{\vec{T}}_2$	Instantaneous term of stress tensor
$\vec{E}^*(r, t)$	Conjugate complex of electric field
$\vec{f}^s$	Total force strength acting on the cell membrane

$\vec{\hat{I}}$	Unit tensor
$\vec{\hat{T}}$	Time-average Maxwell stress tensor
$T^T_1$	Total stress tensor in the elastic material
$T^T_2$	Total stress tensor in the medium
$[\cdot]^n$	Dot product operations,
$\nabla^2$	Laplace Operator
$E_0$	Uniform electric field
$E_B$	Bending stiffness
$E_{in}$	Electric field inside the cell
$E_{out}$	Electric field outside the cell
$E_{rms}$	Root-mean-square of the applied electrical field
$E_s$	Shear modulus
$K(\omega)_n$	General multipole form of Clausius-Mossotti function
$\vec{n}$	Outward unit vector normal to the cell surface
$\vec{t}$	Unit tangent vector
$T^T$	Total stress tensor
$\epsilon^*$	Complex permittivity
$\epsilon_0$	Vacuum permittivity
$\epsilon_c$	Cytoplasm permittivity
$\epsilon_m$	Medium permittivity
$\epsilon_p$	Permittivity of the particle
$\epsilon_r$	Relative permittivity

$\sigma^*$	Complex conductivity
$\sigma_M$	Mechanical stress
$\sigma_p$	Conductivity of the particle
$\Phi_0$	Applied electric potential
$\Phi_{in}$	Electric potential inside the cell
$\Phi_{out}$	Electric potential outside the cell
$\bar{\mathbf{E}}$	Real part of the harmonic electric field
$\nabla$	Gradient vector
$\mu$	Shear viscosity
$D$	Electric field flux density
$d$	Distance between electrodes
$D/r$	Size ratio
$E$	electric filed
$f(\vec{X})$	Displacement of a specific point on the cell membrane
$f_{ext}$	External volume force
$H$	Magnetic field
$J$	Current density
$J(t)$	Creep function
$k$	Constant (stands for inside or outside the particle)
$k$	Resting curvature of the membrane
$K(\omega)$	Complex Clausius-Mossotti function
$lb$	Lower bound of the design variables
$n$	Number of observation per sample

$R_c$ or $r_c$	Radius of the cell
P	Pressure due to medium
s	Arc length along the cell membrane
S	Solution space
$T_0$	Constant tension
U	Applied electric potential
ub	Upper bound of the design variables
$\mathbf{X}^*$	Optimum points
X1 or D	Distance between electrodes
X2	Length of electrodes
X3	Angle of electrodes
X4	Relative permittivity of the medium
Z	Standard normal variable
$\Gamma$	Cell membrane
$\Delta r/r$	Deformation ratio
$\epsilon$	Tensile strain
$\sigma$	Electrical conductivity
$\Phi$	Electric potential
$\omega$	Angular frequency

## **Chapter 1: INTRODUCTION**

### **1.1 Motivation, rationale and objectives**

In the previous decade, the trend toward in depth assessment of living cells, as the fundamental entities of the human body, has led to the emergence of new experimental techniques and several thousands of research papers have been published. The living cells (typical cell diameter is around 10  $\mu\text{m}$  and a typical cell mass is around 1 nanogram) are the complex bio-dynamic systems which exhibit behaviors dependent on their type, size, shape, environment, local state (adhered or suspended), and other several known and unknown factors. Manipulation and assessment of such small particles creates more difficulties. Recent, extensive studies are trying to overcome these difficulties.

During life, living bodies are exposed to various kinds of stresses, including external (e.g. bio-chemicals) and internal (e.g. ageing). Although human body is prepared for these stresses by the natural immune system [1], millions of deaths per year indicate that our bodies' immune system is not always able to effectively act in the presence of cancers or heart attacks, which are two leading causes of death in the twentieth century [2] and current century [3], respectively.

Besides the immune system of the human body, diagnosis and treatment, or medical care, are also the two keys to health. Life is strongly dependent on the physical condition of the living units of the human body, from organisms to single cells. Regarding this fact, the investigation of the physical condition of the living units of

human body helps scientists and researchers find the most effective, and most cost effective, treatments for cancers.

It should be noted that the diagnosis of a disease or choice of the best medical treatment cannot be achieved without an in-depth understanding of the physiology of living cells. Assessing the properties of living cells, investigating the responses of living cells upon applying a stimulus, and observing and investigating how living cells carry out changes to their environment, are among the studies which lead to a better understanding of the physiology of these small, essential parts of human bodies.

There are certainly needs, gaps, and also difficulties in this regard, which scientists and researchers are trying to overcome based on their interests. For bio-engineers, the field of interest lies in the separation of living cells, cell-cell interaction, moving the single cells in mediums, cell adhesion to the substrate and the mechanical properties of the living cells. The above mentioned properties are seen as key factors in understanding the mechanism of cancer genesis and progression.

Measuring and investigating the local and global mechanical properties of living cells, especially when they are in their physiological environment is of great interest to research as these properties may reveal important information about the state of the cells. Mechanical properties of the living cells may alter when the condition of their environment changes or an external condition induces a permanent change into the cell structures. Mechanical properties of single cells are not only different from one cell line to another, but they also vary in different states of cell life, such as division, migration, fixing and ageing [4]. Regarding this fact, researchers are interested in measuring the

mechanical properties of the living cells. They believe this is an inverse method to recognize and evaluate the unknown cells, in order to choose the best treatment.

Here, it will be useful to mention some research works, which have shown the significant changes in living cell properties during different life conditions. The first example is related to the results of a research work published by M. Lekka and his colleagues in 1999 [5]. They demonstrated that the significant difference exists between the values of Young's modulus of cancerous cells and normal cells. They measured a value of  $0.99 \pm 0.47$  kPa for Young's modulus of a T24 cell (cancerous human epithelial cell line) and  $12.88 \pm 4.83$  kPa for Hu609 (normal human epithelial cell line). Thus, one can recognize cancer cells by evaluating the mechanical properties of the individual cells.

Cell adhesion to a substrate is another area of interest. The second example is the results published by S. Leporatti and his colleagues in 2009 [6]. They observed that the values of Young's modulus for two cancerous cell lines were affected by the adhesion behavior of cells onto the substrate. The results of their study for MCF\_7 (human breast cancer cell line) and HeLa (human cervical carcinoma cell line) are shown in Table 1.1

Table 1.1: Young's modulus of two different cancerous cell lines [6]

Cell line	Young's modulus (kPa)
MCF_7 living	20–30
MCF_7 fixed	50–150
HeLa living	100–200
HeLa 7 fixed	400–500

Their results show that not only Young's modulus of the fixed cells (for both of the cell lines) have almost two times the magnitude of those of living cell lines, but also there is a



significant difference between Young's modulus of MCF\_7 and HeLa cells. They justified such that despite exhibiting similar phenotypic characteristics, MCF\_7 and HeLa cells have different cytoskeleton structure (see the cell physiology source book [7]), which could induce different stiffness into the cell structures [6].

Another research example is related to the ageing of living cells. A review of the mechanical properties of the living cells with ageing has been carried out by M. N. Starodubtseva in 2009 [4]. Their study showed that the stiffness of living cells increased with ageing, while their abilities to undergo external stress and large deformation decreased [4].

These examples clearly demonstrate the rational reasons for measuring and investigating the properties of living cells. Studying how living cells undergo external stress or respond to a stimulus is being investigated by experimental techniques.

This work aims to measure the Young's modulus of two cancer cell lines, MDA-MB-231 (highly metastatic human breast carcinoma cell line) and MCF-7 (weakly metastatic human breast carcinoma cell line) using a field-induced experimental method. A dielectrophoresis (DEP) microdevice to induce electro-deformations on living cells is designed and fabricated to experimentally measure the deformation of cancer cells in a non-uniform electric field. The Young's modulus of cells then is calculated by matching the deformation of cells obtained experimentally by adjusting the parameters of the simulation in the finite element analysis. The objective is to compare the obtained results with the results presented in the literature to demonstrate the application of the DEP microdevice for measuring the mechanical properties of human cancer cells.

## **1.2 Achieving single cell assessment**

One way to move toward single cell assessment is to measure the properties of a cell, investigating the obtained result, and then evaluating the cells and their states. The important properties of living cells include mechanical/structural, electrical, optical, magnetic, and acoustic properties. There is a special trend to measure the mechanical/structural properties of the living cells due to their key roles in cell physiology. Also, the other properties of the living cells are strongly coupled with their mechanical/structural properties. For example, the mathematical models (e.g. solid/elastic, liquid/viscous) proposed for modeling the acoustic responses of a single cell must be based on the primary investigation of the mechanical/structural properties of that single cell. Otherwise, the models could lead to incorrect evaluations.

Furthermore, most of the living cells have different behaviors against different types and ranges of stimuli (as they are alive). The experimental techniques could partially clarify these behaviors. In this study, during the presentation of the experimental methods, some of these behaviors have been indicated.

## **1.3 Mechanical and structural properties of living cells**

The mechanical and structural properties of living cells alter during the cell cycle (e.g. growth, division, and senescence) as well as when an external condition is applied to the cell structure or cell environment. Although all of the cell components (see the cell physiology source book [7]) influence the cell function, some of them have dominant roles in certain situations. For example, the cytoskeleton network suffers from mechanical loads [4], while the structure of the cell membrane changes following drug

interaction [8]. Thus, measuring Young's modulus of the cytoskeleton or the stiffness of the cell membrane could predict the state of the living cells. However, estimation of the cell state based on the data obtained from the experimental methods is not generally adequate. An appropriate mechanical model (see review paper [9]) must be considered to evaluate the raw data and properly assess the properties of a single cell. Measuring the mechanical and structural properties of the living cells, including mass density, stiffness, Young's modulus, shear modulus, static and dynamic viscosity, natural frequency, cell-cell interaction, and cell adhesion to the substrate is a first step toward cell assessment.

The mass of a single cell is one of the important properties of cells which has a direct role in the synthesis of proteins and the replication of the large molecules and DNA inside the cell during division and growth [10]. Estimating the cell cycle progression is achieved by this fact that through the cell cycle, cell progress occurs only when the cells have sufficient mass and appropriate size [11]. In some of the research, cell volume is used to estimate the mass of the cell simply by multiplying the cell density and the cell volume [12]. It has been proven that this estimation cannot be accurate because the mass densities of cells alter through the cell cycle [13]. Direct measurement of the mass density of cells leads to a more accurate understanding of the cell cycle.

It has been shown that among the various moduli of the living cells (e.g. Young's modulus, shear modulus, and bending modulus [4]), Young's modulus changes more considerably upon applying an external force [14]. It is one of the most important basic elastic properties of the living cells, which could be used for investigations of cell function. For example, Young's modulus of the HUVE cells (human umbilical vein endothelial cells) is increased with exposure to shear stress [14]. This increase is more

significant at the nuclear region, such that the nuclear region of HUVE cells appears to be stiffer [14]. Also, some living cells show considerable variations in elastic properties when they start moving, such that their nuclear region becomes softer [14]. Furthermore, variations of Young's modulus have been demonstrated for cancerous cells and adhered cells compared to normal cells and suspended cells respectively (mentioned before). Thus, almost all experimental methods attempt to measure Young's modulus of different regions of a cell to assess cell behavior. As indicated above, usually Young's modulus of living cells cannot be obtained directly by experimental techniques. An appropriate mechanical model for cells is needed to calculate Young's modulus of living cells using the value of stiffness or deformation of the cell membrane [9]. A simple linear elastic model for living cells, where the single cells are considered as the homogeneous elastic solid, can be used based on the principle of the simplification of viscous materials [15].

There are various experimental techniques used to calculate the elastic and viscoelastic properties of living cells. They can be applied to measure the local mechanical properties of the cell membrane or those of the whole cell. Meanwhile, experimental techniques could investigate cell adhesion to the substrate and also cell-cell interaction.

The natural frequency of the living cells is another important property of the living cell whose measurement is not simple in any way. As the living cells are small particles in the range of ten micrometer, they have a high natural frequency in the range of a few hundred *kHz* to *MHz*. There are some papers that report having measured the natural frequency of a certain living cell, but it is apparent that they have just measured the natural frequency of the coupled system (the cell and the measuring equipment). It

can be suggested that only non-contact methods (such as acoustic microscopy [16]) can overcome this problem, although the excitation of living cells in their physiological environments, which serve as an absorber, yield specific difficulties. The only report of an observation of resonance of living cells in a high-amplitude ultrasonic field, based on the belief of Zinin and his colleagues [17], is that from 1986 carried out by Miller [18].

#### 1.4 Literature review

In 1950, Crick and Huges [19] were among the first researchers who utilized the magnetic particle method to study the mechanical properties of living cells. Since then, several methods and techniques have been developed. In this study, the recent experimental methods applicable to a single cell level are introduced and reviewed based on the techniques employed, as summarized in Table 1.2.

Table 1.2: Experimental methods for single cell assessment

Cantilever based assay			Micro bead based assay	Micro plate/micropipette based assay	Field-induced assay		
Atomic force microscopy (AFM) [20],[14]	Microneedle (MN) [21]	Oscillatory cantilevers [10]	Magnetic twisting cytometry (MTC) [22]	Laser/optical tweezers (OT) [23]	Microplates [24]	Micropipette aspiration [25]	Dielectrophoresis (DEP ) micro-devises [26]

In the following, the detailed discussions regarding these techniques have been provided and a systematic review on the related papers has been conducted and categorized in the following sub-sections.

#### 1.4.1 Atomic force microscopy (AFM)

Atomic force microscopy [20] is an accurate investigative tool for imaging and probing living cells [14] (accuracy of approximately 1nm and pN for imaging techniques and applied forces respectively [27]). AFM is a standard tool for biological application thanks to its ability to operate in the physiological condition of living cells [28]. It consists of a cantilever beam, which can bend using piezoelectric actuators. Laser/optical tools are used to measure the bending of the cantilever and prepare the signal controller feedback for the piezoelectric actuator [27]. Figure 1.1 shows a schematic of the AFM method.

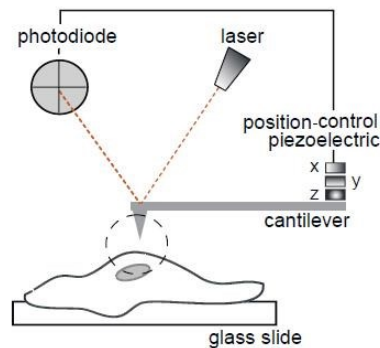


Figure 1.1: Schematic of AFM for living cell probing [29].

The operation of AFM is dependent on the mode of cantilever tip including contact mode, tapping mode, and noncontact mode [30].

In contact mode, the tip of the cantilever is inserted into the cell and the interaction between the tips and cell walls causes bending of the cantilever. The bending value of the cantilever is detected using a focused laser on the cantilever tip [14]. As illustrated in Figure 1.1, a feedback signal from the photodiode makes a position control for the cantilever tip using piezoelectric embedded in the other end of cantilever. The contact mode requires a direct indentation into the samples (typical value of  $10^{-7}$ N for repulsive interatomic force) by the cantilever tip which cannot be applied to living cells [30]. In such a situation, usually a microbead is attached to the tip of the cantilever to make the contact between the tip and sample more gentle [31], or using the noncontact mode of AFM is recommended.

In the noncontact mode of operation, the tip of the cantilever moves a distance of 50–150 Å above the cell surface and the attractive forces between them (typical value of  $10^{-13}$ N) are detected using the same manner as in the contact mode [30]. The only difference between the contact and noncontact modes is that, in the noncontact mode, due to the weakness of attractive forces, the tip–surface force interaction can be measured by changes in the resonance frequency of the cantilever when it is positioned in the proximity of cell surface. The significant problem with the noncontact mode is effects of contamination of cell surface on the cantilever oscillation which leads to the low resolution [30].

The tapping mode of AFM is used for the topographic imaging of living cells. Like the noncontact mode, the tapping mode is a dynamic detection mode. The piezoelectric actuator causes the cantilever to oscillate near its resonant frequency while it is not in contact with the cell surface. Then, the cantilever, while it is oscillating, is

moved toward the cell until it touches the surface of the cell and then is moved horizontally on top of the cell surface. The changes (i.e. the decrease of the oscillation amplitude) of the vertical oscillation of the cantilever tip are used as a feedback signal for the piezoelectric actuator and result in topographic imaging of the cell surface [30].

At the single cell level, Weisenhorn et al. (1993) [32] were among the first ones to measure the elastic modulus of lung cancer cells. In their study, they mentioned that when AFM is used for measuring the mechanical properties of soft samples like living cells, high resolution imaging techniques were needed to achieve the desired accuracy of measured values. Also, they indicated that the problems with soft samples were related to the weak adhesive force between living cells and the hard substrate which could produce the large deflection of the cantilever. To tackle this problem, they corrected the force-versus-indentation curves of soft samples by the force-versus-indentation curves of hard samples obtained by the same cantilever. They reported that an applied force about 1-10  $pN$  was needed to have high resolution images of living cells with approximately 1  $nm$  vertical deformation. They applied this technique to measure Young's modulus of rubber, cartilage, and living cells and obtained the values of 0.013-0.15  $MPa$  for Young's modulus of lung cancer cells. Although they calibrated the micro cantilever for soft samples, the demand for high resolution imaging of soft samples remains a challenge in such experiments.

It seems that the application of atomic force microscopy is limited to only probing the adherent cell. In addition to the difficulties reported by Weisenhorn and his colleagues [32] in recent research, the standard AFM technique cannot be applied on the cells which are not attached to the substrate. One way to overcome this limitation is to



attach the non-adhered cells to a glass surface using Poly-L-lysine solution, which can create a good attachment between the cells and glass surface [14]. There are two limitations to this approach, including the loss of accuracy due to inducing membrane rearrangement and the effect of positively charged Poly-L-lysine solution on the cells with negative electrostatic force (e.g. red blood cells) [14]. Regarding these phenomena, efforts have directed the AFM method toward probing the suspended cells in their physiological environments.

One example of this trend refers to the two-fingered micro-hand as a micro-manipulation system for a single cell level, fabricated and tested by Kenji Inoue and his colleagues (2007) [33]. Their device is comprised of six degree of freedom two-fingered micro-hand, an auto-focusing optical microscope, and a user interface, which has the ability to grasp, move, rotate, and release single living cells. They describe two applications for their device. In the first application, they used four fingers to extract the nucleus of an egg cell of a rat. Two fingers are inserted into the cell while it is being held by two other fingers and then the nucleus is extracted, as illustrated in Fig.6 in the reference paper [33].

In the second application, they measured the stiffness of a normal human leukocyte and a yeast cell using the gradient of the force-deformation curve. Only one hollow finger is used for the second application. The procedure of measuring cell stiffness first involves the single cell being attracted by a hollow finger with  $2\mu\text{m}$  tip radius due to a capillary suction effect and then the finger moves the cell toward the AFM cantilever and presses it against the cantilever tip. The absolute deformation of the cell will be obtained from the difference between the deflection of the cantilever and the

moving distance of the fingertip measured using an optical microscope. The microscope images of the experiment illustrated in Fig.9 in the reference paper [33] shows the application of this technique for measuring the stiffness of a human leukocyte cell.

The combination of micro-finger and AFM sensor in this technique permits the highly accurate point-by-point analysis of a single living cell and also makes using the inexpensive probing technique comparable to the standard AFM probing [33]. One significant drawback of this method is the lack of signal control feedback to control the position of the micro-finger used for tuning the applied force. Also, the misalignment of the applied force via the end-effectors of a micro-finger causes it to bend under high forces or may produce the disconnection between the cell and cantilever tip. Furthermore, there are some limitations in the size and shape of single cells in making use of capillary suction as an attraction force between hollow fingers and cells.

Hiratsuka et al. (2009) [34] investigated the viscoelastic properties of mouse fibroblast NIH3T3 cells in large numbers using atomic force microscopy (AFM) and microarray techniques. As the living cells have individual variance in their properties, statistical estimation has been used in this study. For their experiment, the suspended living cells are deposited on the wells of the microarray within an appropriate medium. An optical microscope measures the total number of cells such that each single cell occupies one well of the microarray [34]. As illustrated in Fig.1.1 in the reference paper [34], the micro cantilever is moved on top of the each well while it operates in dynamic mode. A function generator applies an oscillatory vertical movement (0.5-200 Hz frequency and 10 nm amplitude) to the cantilever. For gentle contact between the cells and cantilever and also for well-defined contact geometry, a micro-bead (colloidal silica

bead of approximately  $2\mu\text{m}$  radius) is attached to the tip of the cantilever using epoxy glue. During indentation of the micro-bead to the cell surface (about 35s.), the phase and amplitude shift of the cantilever are measured by a lock-in amplifier. Finally, the frequency dependent shear modulus of single cells ( $G^*$ ) are measured by measuring the complex loading force ( $F^*$ ) using a Hertz model based on the approximate mathematical relations presented by Mahafy et al. (2004) [35].

Cell adhesion also represents another area of interest when assessing a single cell. Cell adhesion to a substrate and also cell-cell interaction is performed by Actin Cytoskeleton [36] and alters during the cell cycle. For example, the shape of an adherent cell changes at the beginning of mitosis (process of cell division) from spread to round, which causes a reduction in the adhesion force [37]. Characterization of the mechanical properties of Actin stress fibers (SFs) has been considered due to their key role in force transmission [38]. One of the applications of AFM is at the fiber drawing contact mode [39] at which the force between extracellular matrixes (ECM) and Integrin proteins is measurable due to the ability of AFM in the force spectroscopy domain [40].

Weder et al. (2009) [37] applied the fiber drawing contact mode of AFM in their experiment to investigate and measure the focal adhesion force of Saos-2 cells (human osteosarcoma cells) to a glass substrate during the cell cycle. They analyzed 15,000 cells of each cell line and plotted the force-distance curves to investigate the cell cycle phase, as illustrated in Figure 1.2.

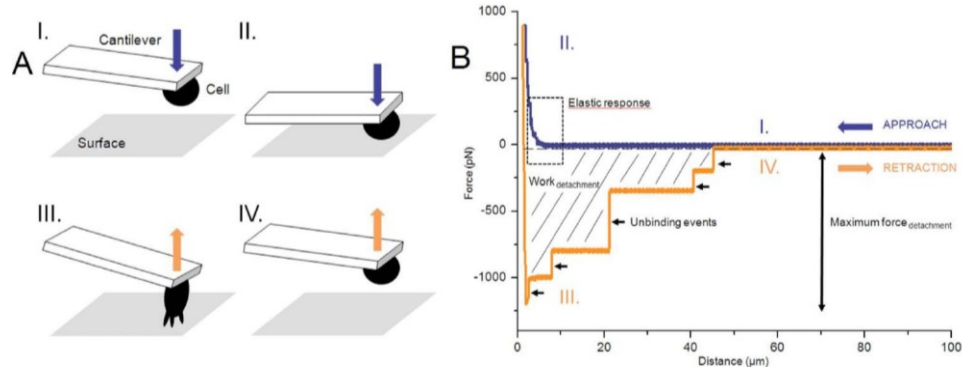


Figure 1.2: A) Single force spectroscopy, B) Force-versus-distance curves [37]

To accomplish the experiment, they first brought a population of each cell line to the same phase using a cell Synchronization [41] process. Then, a single mitotic cell which was detached from the culture dishes was attached to the cantilever using an appropriate solution. The cantilever was moved toward the surface while it carried the cell until the repulsive force between the cell and substrate reached 900 pN. Consequently, the cell was pushed against the surface and then rebounded. The contact time was about one second, after which the retract step was started.

Several features obtained from the force-versus-distance experiment (Figure 1.2.B) have been reported in this study: 1) Maximum force of detachment from Step IV. 2) The displacement which is needed to remove the cell from the substrate from Step III to Step IV. 3) The work done at detachment (the hatched area illustrated in Figure 1.2). 4) Identifying and analyzing the unbinding events from the discrete steps of force-distance curves [37].

Generally, AFM is an expensive method [33] and it is also difficult to determine when the tip of the cantilever touches the samples [31]. Furthermore, force feedback is

needed to decouple the force and displacement intended for direct measurements of the stiffness of the samples [39].

### 1.4.2 Microneedle

The microneedle (MN) technique is another cantilever based approach which is not only used for stiffness measurements, but is also a tool for the delivery of nanoparticles (e.g. a drug) into the living cell without inducing any unwanted biochemical activity within the cell [42].

Felder and Elson (1990) [43] investigated the adhesion of chick embryo heart fibroblast cells to different substrates. Ishijima et al. (1991) [44] measured the attachment and detachment force of actin filaments using the microneedle technique. Like the other methods, the microneedle technique is still being developed with the intention of achieving the highest possible accuracy. Ahmad et al. (2008) [21] used four types of nanoneedles for the characterization of the cellular mechanics of yeast cells. They showed that (Figure 1.3) nanoneedles with different spring constants could be used for measuring the local mechanical properties of a living cell or penetrating the cell membrane in a single cell surgery.

A simple mathematical equation can be used to estimate the stiffness of a single cell by assuming the single cell and nanoneedle as two equivalent springs in series such

that  $k_{cell} = k_{probe} \left( \frac{\Delta_{total} - \Delta_{cell}}{\Delta_{cell}} \right)$  where  $k_{probe}$  is the spring constant of the soft probe,  $\Delta_{total}$  is

the total displacement of two springs, and  $\Delta_{cell}$  is the deformation of the cell observed by the imaging tools [21].

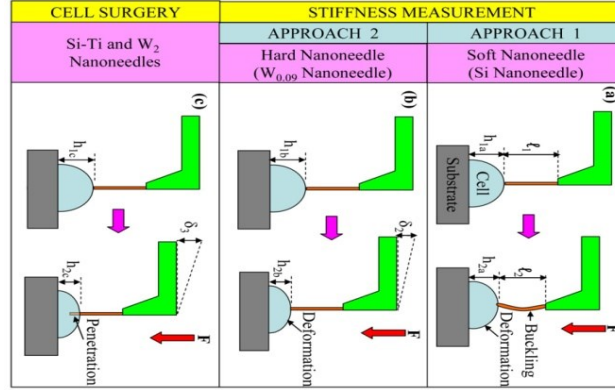


Figure 1.3: Schematic of experiments done by Ahmad et al. [21]

In both AFM and MN, Young's modulus of a single cell can be calculated using Hertz-Sneddon models (i.e., the modified Hertz's mechanics model [45] to estimate Young's modulus of cells based on the shape of tips: conical, spherical, or cylindrical [21]). Ahmad and his colleagues [21], in the recent study described above, measured a value of 3.64MPa and 1.47MPa for global and local stiffness of a W303 yeast cell, respectively (see the relative ESEM images (environmental scanning electron microscope) in the reference paper [21]).

One advantage of the MN technique compared to AFM is its ability to measure both the local and global stiffness of living cells using hard and soft probes, respectively. Although observing the deformation of cells in their environments has become easier and more accurate by ESEM, some difficulties reported in the literature limit its application in wet samples [39]. Furthermore, the accurate calibration of the needles is required before and after each experiment by a cantilever with known stiffness.

### 1.4.3 Oscillatory cantilevers

This is a unique method for the accurate measurement of the mass density of single cells based on the resonance frequency of micro-cantilevers. Park et al. (2008) [10] used a living cantilever array to measure the mass of single adherent cells in liquid based on the measurement of a resonance frequency of cantilevers using LDV (Laser Doppler Vibrometer). The basis of their methods is measuring the mass of single cells by extracting the resonance frequency shift of the micro cantilever. HeLa cells have been chosen for the experiment. As illustrated in Fig.1 in the reference paper [10], the suspended HeLa cells are injected into the microfluidic channels, comprised of silicon micro cantilevers with dimensions 25-40  $\mu m$  long, 240  $nm$  thick and 10  $\mu m$  wide. Positive dielectrophoresis is used to capture the cells on top of the micro cantilevers. The resonance frequencies of micro-cantilevers are measured by LDV. The mass of living cells is inversely proportional to the difference between the resonance frequency of cantilevers with and without the cells, as given by

$$\Delta m = \frac{k}{4\pi^2} \left( \frac{1}{f_1^2} - \frac{1}{f_0^2} \right), \text{ where } \Delta m \text{ is the mass of living cells, } k \text{ is the spring constant of}$$

the cantilevers,  $f_1$  and  $f_0$  are the resonance frequency of the cantilever with and without the cells, respectively.

Godin et al. (2007) [46] and Burg et al. (2007) [47] have also used the shift in the resonance frequency to measure the mass density of living cells. Although this approach is an effective technique for the direct measurement of the mass density of cells, some difficulties and deficits have been observed. This method can be applied only on the

adherent cell and attaching the cell to the cantilevers may induce membrane rearrangement [14], resulting in an incomplete growth of cells. As is indicated above, the mass of the living cell is a variable property depending on the cell cycle, thus the misunderstanding about the state of the cell leads to wrong values of cell density. Furthermore, controlling the number of cells attached to the cantilevers is almost impossible and thus the measured frequency is not related only to one single cell. There is also some mismatching with the theoretical approaches, which is related to the error of measurement devices and resolution limits of confocal microscopy [10].

#### **1.4.4 Magnetic twisting cytometry (MTC)**

Magnetic twisting cytometry is an effective technique for measuring the rheological properties of the living cell membrane. Comparing with the other non-magnetic cytometry techniques, such as laser/optical techniques, it will not produce destructive heat even in high levels of generated forces [48]. Wang et al. (1993) [22] were the first researchers who used MTC to investigate the function of transmembrane cell adhesion molecules (e.g. Integrin proteins) without producing large-scale changes in the cell shape. Fabry et al. (1999) [49] simultaneously measured the rotation of 50,000 beads bounded to 20,000-40,000 bovine capillary endothelial cells (BCE) and human airway smooth muscle cells (HASM) using magnetic twisting cytometry. In the MTC technique, first the surface of living cells is incubated with ferromagnetic microbeads coated with a synthetic RGD peptide (a specific ligand for integrin receptors [49]) or full-length ECM proteins, and then a strong magnetic field (over a very short period of time)



applies a force to the beads along the orthogonal direction to induce the twisting deformation into the cell membrane [50].

Overby et al. (2005) [51] investigated the focal adhesion behavior of bovine capillary endothelial cells (BCE) by applying a dynamic tensional force to the cell surface integrin receptors, via bounded ligand-coated magnetic beads, using a combination of MTC, a permanent electromagnetic microneedle, and magnetic tweezers. They applied the electromagnetic force waveform to the microbeads bound to a single cell (10-20 beads/cell) using a magnetic needle. An amplifier supplies and controls the current to generate any arbitrary force regime. The displacement of beads is recorded by a microscope and a CCD camera as illustrated in Figure 1.4.

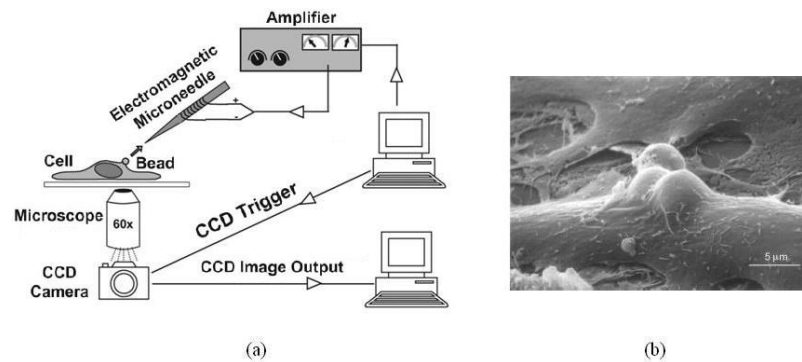


Figure 1.4: a) Experimental setup for pulling cytometry of a BCE cell [51], b) SEM image of beads embedded in the cell surface [49].

Several results have been reported by Overby et al. [51] as follow: 1) The induced magnetic pulling force into the micro bead is linearly proportional to the applied current; 2) Up to a 10 nN force can be applied to the magnetic beads using a microneedle, and for applied forces in the range of 100pN to 1nN, the change of bead displacement is linearly proportional to the applied force; 3) Stress-induced displacement of microbeads

is measured using MATLAB image processing by computing the dynamic displacement versus time; 4) Various mechanical stimuli including sinusoidal, rapid, and prolonged magnetic pulses are applied to the beads and their displacements are measured; 5) The investigation of viscoelastic creep behavior of living cells showed that only 48% of focal adhesions (induced into the cytoskeleton network by microbeads bound to the cell surface) obey the power-law relationship ( $at^b$ ). The advantage of this method (electromagnetic pulling cytometry) compared to the standard magnetic twisting cytometry (which can produce only a uniform perpendicular magnetic field) is its ability to generate various strong tensional forces and use the interchangeable electromagnetic microneedle, although like the standard MTC, it has no ability to apply non-attractive forces [51].

#### **1.4.5 Laser/optical tweezers**

The laser/optical tweezers method is another experimental technique for manipulating and assessing single living cells. In this method, the embedded dielectric microbeads transmit the external force into the living cells and the desired changes (e.g. frequency dependent deformation) can be detected using a laser beam and a microscope. In this method, the controlled force generated using laser power results to produce the force in range of pico-Newton with a resolution as accurate as 100 aN [23].

For the first time, at the single cell level, Ashkin et al. (1989) [52] used the optical trap method to manipulate the individual bacteria cells and single red blood cells in a sample medium. For this purpose, the cells have to be located within a medium whose refractive index is lower than the cells [27]. After laser exposure, the gradient force

pushes the dielectric particle toward a highly focused light beam [52]. This is a noncontact manipulation technique which can be used to move the cells in their medium [23].

Lim et al. (2004) [53] used optical tweezers (OT) for large deformations of the red blood cells. They stretched the cell using two embedded silica microbeads as illustrated in Figure 1.5.

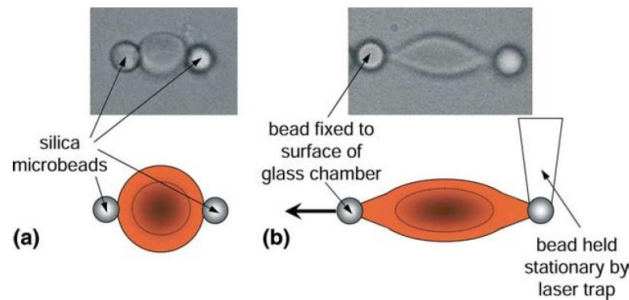


Figure 1.5: Stretching a single human red blood cell using the optical tweezers method [53]

The methodology of their experiment was such that the left hand side bead was fixed to the surface of a glass chamber and the right hand side bead was trapped using a laser beam. The deformation was observed via a microscope and recorded on videotape. They obtained the deformation of the cell versus the stretching force and also the viscoelastic properties of the red blood cells by characterization of relaxation response [53].

Directly measuring the living cell deformation is one of the significant advantages of the optical tweezers method, but the heat generated by the laser exposure, which can induce thermal shock into the living cells, limits its application in cell membrane stretching. An optical trap can induce a force of up to a few hundred pico-Newtons, while

up to 400 pN is possible in optical tweezers (which uses the dielectric beads attached to the sample) [53]. Using the embedded beads facilitated the mechanical probing of the living cell membrane [27].

#### 1.4.6 Microplates

Binding the living cell between two plates (one thick and rigid and the other thin and flexible) is also another experimental technique to investigate the deformation of living cells. In this technique, the rigid plate serves as an actuator and the flexible, calibrated plate as a force sensing sensor. Thoumine and Ott (1997) [24] measured the overall mechanical properties (i.e. elastic and viscoelastic responses) of a single suspended fibroblast cell on a time scale using the microplate technique. They investigated the time dependent deformation of several single cells on the compression, traction, and oscillatory perturbation experiments. During the experiments, the vertical displacements of the rigid microplate were being controlled using a piezoelectric actuator and the deflection of the flexible plate was being observed using a CCD camera. Figure 1.6 shows the step-by-step traction experiment applied to a single fibroblast cell by Thoumine and Ott [24].

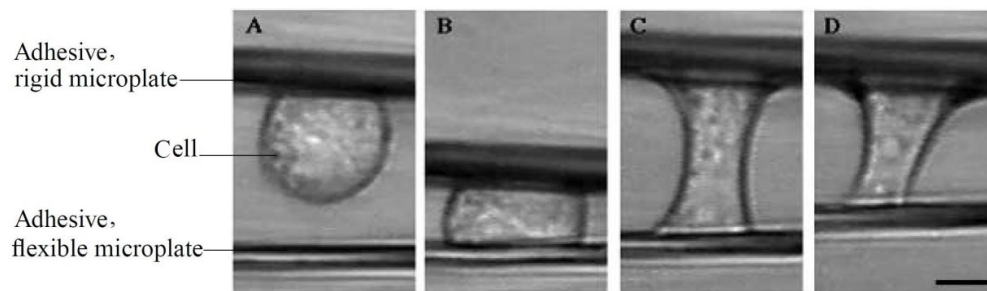


Figure 1.6: Stretching a single fibroblast cell using microplates technique [24]

The uniaxial force applied on the single cell (in this manner) was in the range of  $10^{-8}$  N and the sensitivity of the flexible microplate was accurate to  $10^{-9}$ - $10^{-8}$  N/ $\mu$ m. The measured deflection of the flexible plate (with known stiffness) was used to calculate the applied force. Thoumine and Ott [24] also showed that the cell deformation behavior during the traction-relaxation experiment could be modeled mathematically using a three-element Kelvin viscoelastic model (a serial combination of a spring and a dashpot in parallel with the second spring) [24]. This suggestion has not been accepted by Desprat et al. (2005) [54]. They believed that the creep behavior of a living cell as a complex material could not be modeled simply by a finite number of springs and dashpots. They believed that the power law could describe the creep behavior of such materials. They showed that the complex modulus  $G^*(\omega) = G'(\omega) + iG''(\omega)$  derived by creep function  $J(t) = Ae^{\alpha t}$  (using Laplace Transform such that  $G^*(s) = \frac{1}{J^*(s)}$ ) had an excellent agreement with those obtained by the other experimental techniques [54].

The microplates method is a simple geometric tool to investigate the compressive responses of a single cell, as well as its tensile responses [24]. Although it seems that the technique used in microplates is the same as atomic force microscopy such that the rigid plate serves as substrate and the flexible plate as the cantilever, there is a very important difference that must be considered. In microplates methods, the stress and strain are coupled but in AFM, as feedback makes the stress constant, the stress and the strain are decoupled [55].

#### 1.4.7 Micropipette aspiration

Unlike atomic force microscopy (AFM), magnetic twisting cytometry (MTC) and laser/optical tweezers which are used to measure the local mechanical properties of single living cells, micropipette aspiration is an experimental technique which can be applied for whole cell deformation [49].

In the micropipette aspiration technique, a deformation of the living cell membrane is investigated using the portion of the cell membrane which is aspirated into a glass pipette by applying a pressure difference. Investigations of the cell membrane can indicate if the cell behaves as a solid or as a liquid. Young's modulus, surface tension, and viscosity of the cell are among the properties of a living cell which can be measured using micropipette aspiration [25].

Rand (1964) [56] and Rand and Burton (1964) [57] studied the required pressure difference to aspire a single red blood cell into a micropipette. They found that the required pressure difference is inversely proportional to the pipette radius. They also found that when the length of the aspirated tongue ( $L_p$ ) was equal to the radius of the micropipette ( $R_p$ ), no additional pressure difference was needed. They measured the elastic and viscoelastic properties of the red blood cell membrane based on the theory of liquid drop analogy (Laplace Law). Evans (1973) [58] showed that when the outside portion of a single red blood cell became spherical, no more cell surfaces can be drawn into the pipette and increasing the pressure difference could only induce an elongation into the inside portion of the cell [58]. He also measured the shear modulus of red blood cells using micropipette aspiration, based on the rheological model of the cell membrane.

Micropipette aspiration is also an effective technique to investigate how certain cells flow through the smallest vessels or tissues [25]. Hochmuth (2000) [25] studied the behavior of two cell lines (neutrophils and chondrocytes) intending to measure their elastic and viscous properties using micropipette aspiration. Also, he showed that the soft cells, such as red cells, behaved as a liquid drop in a glass pipette while the more rigid cells such as endothelial cells behaved as a solid. Figure 1.7 shows a single neutrophil cell and a single chondrocyte cell completely aspirated into a glass pipette.

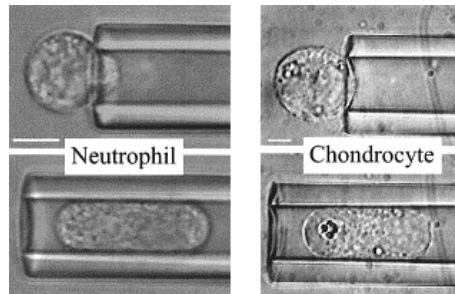


Figure 1.7: The aspirated neutrophil and chondrocyte cells into glass pipettes [25]

From the shape of the cells inside the glass pipette, one cannot completely say which one behaves as a solid, but it can be possible from the behavior of the cell after a critical point where the length of the aspirated tongue ( $L_p$ ) was equal to the radius of the micropipette ( $R_p$ ). Hochmuth [25] showed that (based on his experiments and also previous work done by the other researchers) when  $L_p / R_p < 1$ , both the soft and rigid cells behave as solids. But when the suction pressure exceeded the critical pressure (where  $L_p / R_p = 1$ ), the soft cells behaved as liquid drops and flowed smoothly into the micropipette, while the more rigid cells behaved as solids and the aspiration length of cells increased linearly with applied pressure difference. He also proposed that Young's

modulus of solid-like cells could be measured by  $\Delta P = 4.4 E L_p / R_p$ , where  $\Delta P$  and  $E$  are the suction pressure and Young's modulus, respectively.

Micropipette aspiration is also used to investigate cell adhesion to the substrate. Moussy et al. (1994) [59] aspirated adhered endothelial cells which were attached to different solid substrates into a glass pipette and showed that the force of detachment is a function of the surface tension of the substrate. Chu et al. (2004) [60] used a dual micropipette assay to investigate cell-cell adhesion strength. They showed that the required force for the separation of two cadherin-dependent cells was a function of the duration of contact and cadherin levels. Also, they found that the adhesion between cadherin (Calcium-dependent adhesion molecules) and the actin cytoskeleton (the protein for maintenance of cell junction and cell shape) initially did not have a significant effect on the separation force, but for more contact times it could induce stronger attachment [60]. Although the micropipette aspiration method is an effective experimental technique in single cell and tissue levels, controlling the suction pressure especially near the critical point is a serious issue.

#### **1.4.8 Dielectrophoresis (DEP ) micro-devices**

When a biological cell is exposed to a non-uniform electric field (either AC or DC since DEP phenomena does not depend on the polarity of the electric field), the electric charges accumulate in boundaries, as Figure 1.8 shows, and the cell experience a net force called dielectrophoretic (DEP) force [26]. In a certain frequency range, some neutral cells are more polarizable than the surrounding medium and experience positive DEP forces and are attracted toward the region where the gradient of electric field is



higher. Cells that are less polarizable than the surrounding medium are directed away from the high electric field region.

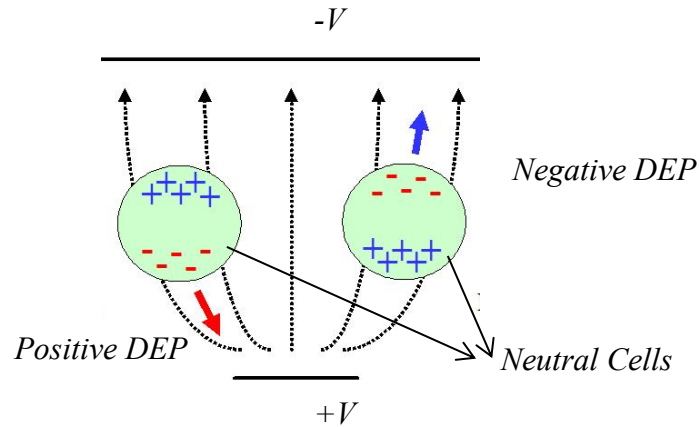


Figure 1.8: Schematic drawing of DEP phenomena

The ability of dielectrophoretic MEMS devices as field-induced based techniques to manipulate and characterize biological cells have attracted more attention (e.g. Zimmermann et al. (1982) [61], Engelhardt et al. (1988) [62], Minerick et al. (2003) [63], and Salipante et al. (2012) [64]). Depends on the configuration of electrical parts (electrodes) and shape of the cells, the distribution of the DEP forces leads to electro-rotation or/and cell elongation.

Among several analytical approaches to study the effect of electric field in dielectric particles, Maxwell stress tensor is regarded as the most general approach to calculate the field-induced forces, specifically, when the field is highly non-uniform. For instance, Engelhardt et al. (1988) [62] measured the shear elastic moduli and viscosities of red blood cell membranes using a dielectrophoretic based device in a high-frequency electric field. They obtained the elastic constants of cells by evaluating the electro-

deformation of cells based on an approximate function of electric Maxwell tension. Wang et al. (1997) [65] derived a general expression for dielectrophoretic force using the Maxwell stress tensor method. Since then, their general expression has been widely used by other researchers. Among biological samples, red blood cells are mostly used regarding the ease of preparation. (e.g. Sukhorukov et. al (1998) [66], Minerick et al. (2003) [63], and Hua et al. (2011) [67]).

Recently, the use of dielectrophoresis phenomena to characterize cancerous cells and compare their behavior with those of normal cells is of upmost interest. For instance, Jian et al. (2011) [68] developed a dielectrophoresis microdevice for mechanical characterization of SiHa and ME180 cells (two cervical cancer cell lines). Also, Guido et al. (2011) [69] compared, experimentally, the elongations of cancerous origin (MCF-7) cells with those of noncancerous tissue (MCF-10A) using a dielectrophoretic device. Application of Dielectrophoresis microdevices in cell electro-deformations is presented, more in detail, in the entire thesis.

## **1.5 Mechanical models for single cell assessment**

As mentioned before, beside experimental approaches, different mechanical models have been proposed to characterize mechanical properties of living cells based on type and general shape of the cells. A comprehensive review on the appropriate mechanical models for living cells has been carried out by Lim et al. (2006) [9]. They summarized the mechanical models in three categories as: 1) Cortical shell-liquid, used for suspended cells and applicable in micropipette aspiration and optical/laser tweezers, 2) Solid model, used for adherent cells and applicable in micropipette aspiration,

magnetic twisting cytometry (MTC), and atomic force microscopy (AFM), 3) Power-law structural damping model used for adherent cells and applicable in MTC and AFM.

A popular cortical shell-liquid model used to characterize large deformation of cell membrane is Newtonian liquid drop model proposed by Yeung and Evans (1989) [70]. They considered the cell wall as a thin fluid layer with constant tension  $T_0$  and cytoplasm as a Newtonian liquid droplet. Their solution for a single cell aspirated into a micropipette leads to a relationship between the rate of change of the aspirated tongue length ( $\dot{L}_r$ ) and applied pressure that is modified by Needham et al. (1990) [71] as:

$$\frac{(\Delta P - P_{cr})}{\mu(\dot{L}_r)} = m \left( 1 - \frac{R_p}{R_C} \right) \quad \text{for } 0.5 \leq \frac{R_p}{R_C} \leq 1.0$$

Where  $R_p$  is the radius of the micropipette,  $R_C$  is the radius of the cell,  $\Delta P$  is the total suction pressure,  $P_{cr}$  is critical pressure such that  $P_{cr} = 2T_0(1/R_p - 1/R_C)$ ,  $T_0$  is constant tension of cortical layer,  $\mu$  is the shear viscosity, and  $m$  is a coefficient, approximately set at 6.

Unlike the cortical shell-liquid model, solid model considers the whole cell as a homogeneous incompressible elastic or viscoelastic solid [9]. Table 1.3 shows how the simplified elastic solid model, depending on the experimental techniques, is used to characterize the mechanical properties of living cells.

Table 1.3: Linear elastic solid model used for single cell level

Technique	Formula	source
Atomic force microscopy	$F = 1.4906G\delta^2 / (1-\nu) \tan \theta$	Bilodeau (1992) [72]
Micropipette aspiration	$L_p / R_p = (2.0 - 2.1)\Delta P / 2\pi G$	Therer et al. (1988) [73]
Magnetic twisting cytometry	$T / \phi = 0.3G \text{ and } T / d = 0.33G / R$	Mijailovich et al. (2002) [74]

Where, in Atomic force microscopy (AFM),  $F$  is the force of indentation,  $\delta$  is the depth of indentation,  $G$  is the shear modulus,  $\nu$  is the Poisson's ratio, and  $\theta$  is the inclination angle of triangular faces and, in Magnetic twisting cytometry (MTC),  $T$  (Pa) is the applied mechanical load per unit bead volume,  $\phi$  and  $d$  are the measured bead rotation and laterally translation respectively, and  $R$  is the radius of the bead [9].

Power-law structural damping model is also a popular model to characterize dynamic behavior of living cells. In AFM, an oscillatory force,  $F(t) = \text{real}[A_F e^{i(\omega t)}]$ , induces oscillatory indentations,  $\delta(t) = \text{real}[A_\delta e^{i(\omega t - \varphi)}]$ , into the cell surface such that  $F(t)$  is the oscillatory force,  $\delta(t)$  is the oscillatory indentations,  $\omega$  is the angular frequency,  $A_F$  and  $A_\delta$  are the amplitudes, and  $\varphi$  is the phase lag [9]. Alcaraz et al. (2003) [75] applied Taylor expansion to the force-indentation relationship proposed by Bilodeau (1992) [72] and also considered a Power-law structural damping model for cells to derive an equation for complex shear modulus  $G^*(\omega)$  as:

$$G^*(\omega) = \frac{(1-\nu) \tan \theta}{3\delta_0} \left[ \frac{A_F}{A_\delta} e^{i\varphi} - i\omega b(0) \right] \text{ where } i\omega b(0) \text{ is a correction term related to the}$$

viscous friction imposed on the cantilever by surrounding fluid (see the reference paper [9] for supplementary information).

Sound and light scattering by living cells, resonance oscillations of living cells at their natural frequencies, and quality factor of these oscillations are among the mechanical behaviors of living cells which could be estimated using the analytical analysis of appropriate theoretical models as well as experimental approaches. Many researchers propose a theoretical model based on the theory of spherical shells because the analytical solutions of spherical shells have been well derived and it can be assumed that cancer cells and bacteria have spherical shapes [76]. Research shows that theoretical results based on the theory of spherical shells are in very good agreement with experimental results (e.g. Baddour et al. (2005) [77]).

Ackerman (1951) [78], for the first time, proposed the resonance in mechanical oscillation of living cells. He derived simplified relationships for frequencies of resonance vibrations of two different cell models (cell with an interfacial tension in membrane and a rigid cell wall) based on the theory of spherical shells filled with and surrounded by an ideal incompressible liquid [78]. In his further studies, Ackerman (1954) [79] mathematically investigated the effects of viscosity and compressibility of fluids on the resonance of living cells. Based on early works of researchers (Ackerman (1954) [79], Rayleigh and Lamb (1959) [80] , and Zinin et al. (1987) [81] ), Zinin et al. (2005) [17] proposed a more rigorous theory of the natural oscillation of bacteria cells. They proposed a shell model to estimate the quality of the natural vibration of different type of bacteria as well as to determine their natural frequencies. In the shell model, the cell is assumed having an elastic cortex with constant tension  $T_0$  and the internal fluid and

the surrounding fluid are considered to be viscous and incompressible [17]. The analytical solution is achieved based on the equation of motion of an elastic spherical shell, the wave equations, and the boundary condition on the cell surface due to fluid-structure interaction.

Experiments have shown that ultrasound has biological effects on living cells. Many researches aim to investigate the therapeutic and destructive effects of ultrasound on living cells. Ilyukhina (2008) [82] used a shell model to study the deformation of cell membrane under shock pulse treatment. Like the previous researches in this regard, he considered a single cell as an isotropic homogeneous elastic spherical shell and studied the effect of a shock pulse on a cell at different times from the moment the shock front reached the cell [82]. Zinin et al. (2009) [76] developed a theoretical framework based on their earlier work (Zinin et al. (2005) [17]) and an assumption proposed by Ackerman (1957) [83] (i.e. mechanical resonances of cells could be excited in the presence of micro-bubbles). They mathematically modeled the interactions of micro-bubbles with different type of bacteria based on the natural oscillations of viscous drops [84] and the theory of spherical shells. They predicted that oscillation of micro-bubbles at the natural frequencies of cells could rupture bacteria with low quality factor of natural vibration (less than 1) and would not have sufficient mechanical effects on bacteria with high quality factor [76].

## **1.6 Thesis organizations**

Mechanical properties of living cells could be used as biomarkers to distinguish between normal and abnormal cells in a population. Measuring the mechanical properties of living cells could be achieved using various experimental methods addressed in the first chapter of this thesis. A comprehensive literature review about the recent experimental methods for single cell assessments is presented in the chapter.

In this thesis, among several experimental methods introduced in chapter one, dielectrophoresis (DEP) based devices has been chosen for in depth study. Regarding the ability of DEP to directly measuring the electro-deformations of living cells, the experimental setup of DEP micro-devices is almost easy and cost effective comparing the other experimental methods such as Magnetic twisting cytometry and optical tweezers.

Electrical-neutral charged living cells subjected to a non-uniform external electric field experience dielectrophoretic (DEP) forces which could lead to cell elongations. The fundamental theories of electro-deformation of living cells based on DEP phenomena and two mostly used methods for calculation the DEP forces on the cell surfaces are presented in the second chapter. To calculate the DEP forces on the cells, numerical techniques (e.g. FEM) should be used to obtain the actual electrical field distribution around the cells. In chapter two a finite element simulation of the electro-mechanical analysis of a shelled-spherical cell in a non-uniform electric field using COMSOL Multiphysics 4.2a is achieved as well.

In chapter three, parametric studies are performed to investigate the influence of the design parameters of a DEP microdevice on the electro-deformation of neutral

biological cells. Design optimization of a MEMS device to induce maximum electro-deformations on living cells by means of COMSOL- MATLAB (GA toolbox) integration is also performed in the chapter. The optimum design of the microdevice is compared with the initial design to show its ability to induced maximum deformation on the cells.

The results of electro-deformation process of two cancerous cell lines, MDA-MB-231 (highly metastatic human breast carcinoma cell line) and MCF-7 (weakly metastatic human breast carcinoma cell line) using a positive DEP micro-device are presented in chapter four. The electro-deformations of cells are simulated using COMSOL Multiphysics and elastic constants of cells are measured by comparing the finite element results with the experimental results. Concurring with the previous works, it is expected that highly metastatic breast cancer cells (MDA-MB-231) are softer than weakly metastatic breast cancer cells (MCF-7) and have more elongations upon applying a given electro-mechanical force.

To induce symmetric elongation on cells, an improved design to trap the suspended living cells in the middle of electrodes is designed and presented in the chapter. Holding and stretching the cells between electrodes could improve the accuracy of calculated elastic constant of cells.

The last chapter of the thesis includes the summary and possible future works to improve the efficiency and accuracy of the DEP method for cell deformations.



## **1.7 Concluding remarks on the experimental methods**

The new possibility to fabricate nano-scale equipment (e.g. nanoneedles), emerging new imaging approaches (e.g. environmental scanning electron microscopy), and modification of appropriate mathematical models for extracting results (e.g. Hertz-Sneddon) have made the experimental methods to assess the living cells in their physiological environments more powerful, accurate, and efficient. The investigation of the outcomes of recently published papers is a traditional approach toward finding new methods and improving older ones. This study addressed the recent experimental methods and equipment for single cell assessment while indicating their advantages and disadvantages.

It cannot be said which method is better simply by comparing them. Also, as is indicated in this review, all methods are in progress and there is a good opportunity of modifying them depending on the problem. The efficiency of each method is strongly dependent on what that method is used for. For example, atomic force microscopy (AFM) is an accurate method of assessing an adhered cell, but it is not applicable for a suspended cell. Also, atomic force microscopy is an expensive, due to using laser light, and complicated method. Although the microplates method, which uses the same approach as atomic force microscopy but is applicable for suspended cells, is more simple and cost effective, there is no feedback to control the applied force based on the desired deformation. For another example, it is possible to have the applied pressure hold a single cell in the micropipette aspiration method, which is difficult to control, but this method is a simple way to displace a single cell in a medium compared with the laser/optical tweezers method.

The efficiency of each experimental method can also be estimated using analytical analysis of an appropriate mechanical model of living cells. This study also addressed some of the mechanical models proposed in literature to mathematically investigate the interaction of living cells with their environment and predict cell behavior upon external excitations.

Not only must the problem definition be considered to choose a method, but also the possibility of performing experiments, including the accessible equipment and the time needed must all be considered.

## Chapter 2: ELECTRO-DEFORMATION OF LIVING CELLS IN A NON-UNIFORM ELECTRIC FIELD

### 2.1 Introduction

Electrical-neutral charged living cells subjected to a non-uniform external electric field experience a dielectrophoretic force whose magnitude and direction depends on the electric field conditions, electrical properties of cells and their surrounding medium, and the structural properties of cells. Total forces acting on a cell bilayer membrane (see Figure 2.1) suspended in a medium include the dielectrophoretic force, gravitational force, bouncy force, drag force. In the absence of fluid flow, the drag force could be neglected. Furthermore, the gravitational force and the bouncy force, in the equilibrium position of the cells, are eliminated. The only force, a cell membrane resists to, is the dielectrophoretic (DEP) force.

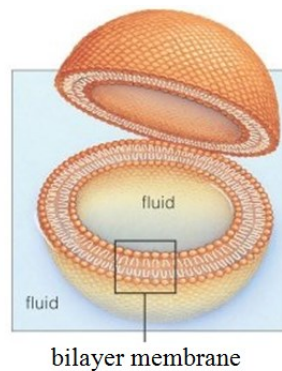


Figure 2.1: Lipid bilayer forming a microsphere

In this chapter, fundamental theories of electro-deformation of living cells and two mostly used methods for calculation of electric field intensities and dielectrophoretic forces are presented. Furthermore, an electro-mechanical finite element model of a

shelled-spherical cell in a non-uniform electric field has been developed using COMSOL Multiphysics 4.2a and the simulation results have been discussed.

### 2.1.1 Electromechanical model of a living cell

The mechanical model considered for a living cell is an elastic homogeneous spherical shell. The electromechanical model of cell represents a lossy spherical shell surround by (external medium) and filled with (cytoplasm) lossy mediums and exposed to a non-uniform electric field. The electric parameters of the cells are considered to be independent of the shape deformation of the cell. The surface charge based on the Maxwell-Wagner polarization is neglected. The magnetic and electric filed are decoupled such that there is no induced magnetic field due to application of the external electric field. The surrounding medium is chosen to have a permittivity less than the cell to enable the maximum positive dielectrophoretic forces.

### 2.1.2 Governing equations

In a frequency domain, the governing equation can be expressed in a time-varying differential equation as [85]

$$\nabla \times H = J + i\omega D \quad (1)$$

Where  $H$  is the magnetic field,  $J$  is the current density,  $\omega$  is the angular frequency, and  $D$  is the electric field flux density.

In the current case, the applied electric field is in a frequency range less than 100 MHz. Thus the corresponding wavelength is several orders of magnitude larger than the largest

dimension of a DEP experimental setup (including electrodes dimensions and cell diameter). When such a situation is applied, the electric field satisfies the quasi-static assumption and the so-called near field approximation can be considered and the effects of magnetic field could be ignored [65] such that,

$$J + i\omega D = 0 \quad (2)$$

Considering that  $J = \sigma E$  and  $D = \epsilon_0 \epsilon_r E$ , where  $\sigma$  is the electrical conductivity,  $\epsilon_0$  and  $\epsilon_r$  are vacuum permittivity and relative permittivity, respectively, and taking the divergence of the equation, then the Eq.2 becomes

$$\nabla \cdot \sigma E + i\omega \nabla \cdot (\epsilon E) = 0 \quad (3)$$

Considering the complex conductivity as  $\sigma^* = \sigma + i\omega \epsilon$  and  $E = -\nabla \Phi$ , where  $\Phi$  is the electric potential in (3), gives the complex form of Laplace equation as

$$\nabla \cdot (\sigma^* \nabla \Phi) = 0 \quad (4)$$

$$\text{Or } \nabla^2 \Phi = 0$$

Solving the Eq.4 and considering  $E = -\nabla \Phi$ , lead to evaluation of the electric field intensity around the cell surface.

## 2.2 Dielectrophoresis phenomena

When a biological cell is exposed to a non-uniform electric field (either AC or DC since DEP phenomena does not depend on the polarity of the electric field), the electric charges accumulate in boundaries, as Figure 2.2 shows, and the cell experience a net force called dielectrophoretic (DEP) force [26]. In a certain frequency range, some neutral cells are more polarizable than the surrounding medium and experience positive

DEP forces and are attracted toward the region where the gradient of electric field is higher. Cells that are less polarizable than the surrounding medium are directed away from the high electric field region.

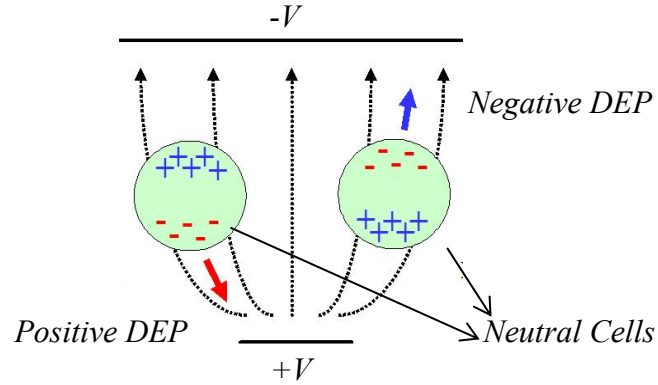


Figure 2.2: Schematic drawing of DEP phenomena

Depending on the configuration of electrical parts (electrodes) and shape of the cells, the distribution of the DEP forces leads to electrorotation or/and cell elongation. There are several analytical approaches to study the effect of electric field in dielectric particles. The most developed approaches to express the dielectrophoretic force induced in biological cells include Maxwell stress tensor and effective dipole moment approximation. While Maxwell stress tensor method is regarded as the most general approach to calculate the field induced forces, there are some limitations for using dipole moment approximation indicated in following sections.

### 2.3 Maxwell stress tensor (MST) approach

For a general conductive dielectric medium, the Maxwell stress tensor,  $\vec{\vec{T}}$ , in an electric field is given by [65]

$$\vec{\vec{T}} = Re(\varepsilon^*) \left( \vec{\vec{E}}\vec{\vec{E}} - \frac{1}{2} E^2 \vec{\vec{I}} \right) \quad (5)$$

Where  $\varepsilon^* = \varepsilon - \frac{\sigma}{i\omega}$  is the complex permittivity,  $\vec{\vec{I}}$  is the unit tensor, and  $\vec{E}$  is the real part of the harmonic electric field.

Considering  $\vec{E} = Re \left( \vec{E}(r, t) \right) = Re(\vec{E}(r) e^{i\omega t})$ , then  $\vec{E}$  can be written as

$$\vec{E} = \frac{1}{2} (\vec{E}(r, t) + \vec{E}^*(r, t)) \quad (6)$$

Where  $\vec{E}^*(r, t)$  is the conjugate complex of electric field. Then Eq. (5) becomes,

$$\begin{aligned} \vec{\vec{T}} = \vec{\vec{T}}_1 + \vec{\vec{T}}_2 = \frac{1}{4} Re(\varepsilon^*) \left[ \left( (\vec{E}\vec{E}^* + \vec{E}^*\vec{E}) - |E|^2 \vec{\vec{I}} \right) \right] \\ + \frac{1}{4} Re(\varepsilon^*) \left[ \left( \vec{E}\vec{E} + \vec{E}^*\vec{E}^* - \frac{1}{2} (\vec{E} \cdot \vec{E} + \vec{E}^* \cdot \vec{E}^*) \vec{\vec{I}} \right) \right] \end{aligned} \quad (7)$$

Where  $\vec{\vec{T}}_1$  is the time-average stress tensor and  $\vec{\vec{T}}_2$  is an instantaneous term of stress tensor [65]. As  $\vec{\vec{T}}_2$  vanishes under time average, the DEP force could be calculated based on the time-average Maxwell stress tensor derived in the next section.

## 2.4 DEP force calculation on the living cell membrane using MST approach

A homogeneous spherical dielectric cell immersed in a homogeneous dielectric medium and subjected to a harmonic electric field experiences a time-averaged net DEP force given by Wang [65](1997) as

$$\langle \vec{f}_{DEF} \rangle = \frac{1}{4} Re(\varepsilon_k^*) \oint ((\vec{E}_k \vec{E}_k^* + \vec{E}_k^* \vec{E}_k) - |E_k|^2 \vec{I}) \cdot \vec{n} dA \quad (8)$$

Where  $A$  is the surface enclosing the particle,  $\vec{n}$  is the outward unit vector normal to the cell surface, and  $k$  stands for inside or outside the particle.

Considering that  $\vec{\bar{T}}$  is the time-average Maxwell stress tensor, the DEP force acting on the cell membrane is derived based on Eq.7 and Eq.8 as:

$$\begin{aligned} \langle \vec{f}_{DEF} \rangle &= \oint (\vec{\bar{T}}_{out} - \vec{\bar{T}}_{in}) \cdot \vec{n} dA = \frac{1}{4} \oint \left\{ Re(\varepsilon_m^*) \left[ (\vec{E}_m \vec{E}_m^* + \vec{E}_m^* \vec{E}_m) - |E_m|^2 \vec{I} \right] - \right. \\ &\left. Re(\varepsilon_c^*) \left[ (\vec{E}_c \vec{E}_c^* + \vec{E}_c^* \vec{E}_c) - |E_c|^2 \vec{I} \right] \right\} \cdot \vec{n} dA \end{aligned} \quad (9)$$

Where subscribes  $m$  and  $c$  stand for medium and cell properties, respectively. Equation (9) explains that the net DEP force on a cell membrane is the difference between integration of normal component of upward Maxwell stress tensor,  $\vec{\bar{T}}_{out}$ , and that of downward Maxwell stress tensor,  $\vec{\bar{T}}_{in}$  over the surface enclosing the cell.

## 2.5 Electro-deformation of living cells in a non-uniform DC electric field

In the following section the theoretical founding of living cell deformation is presented.

### 2.5.1 Problem description

A shelled spherical cell surrounded in a medium is exposed to a non-uniform DC electric field as Figure 2.3 shows. When an electric potential is applied, the cell is polarized more than the surrounding medium and experiences a positive DEP force



(when the permittivity of the cell is higher than that of the surrounding medium). As the field is non-uniform, the DEP forces acting on each half-sphere of the cell are different and cell will move toward higher electric field and settles down at its equilibrium position. By keeping or increasing the applied electric potential, the distribution of forces cause the cell to elongate along the electric field direction called electro-deformation.

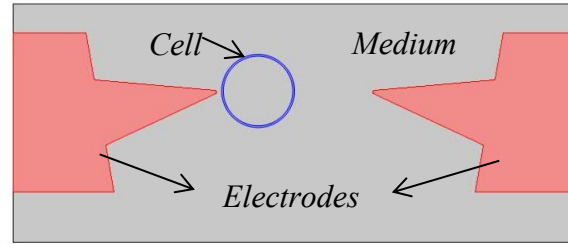


Figure 2. 3: Schematic drawing of a spherical cell in a non-uniform electric field

The Maxwell stress tensor, based on Eq.5, is

$$\vec{\vec{T}} = \varepsilon \left( \vec{E}\vec{E} - \frac{1}{2} \vec{E}^2 \vec{I} \right) \quad (10)$$

Expanding Eq.10 in matrix format yields to:

$$\vec{\vec{T}} = \frac{1}{2} \varepsilon \begin{bmatrix} E_x^2 - E_y^2 - E_z^2 & 2E_x E_y & 2E_x E_z \\ 2E_x E_y & E_y^2 - E_x^2 - E_z^2 & 2E_y E_z \\ 2E_x E_z & 2E_y E_z & E_z^2 - E_y^2 - E_x^2 \end{bmatrix}$$

This is a symmetrical tensor whose diagonal elements represent pressure and off-diagonal elements represent shear [68].

Considering Figure 2.4, the DEP force per unit area is derived by:

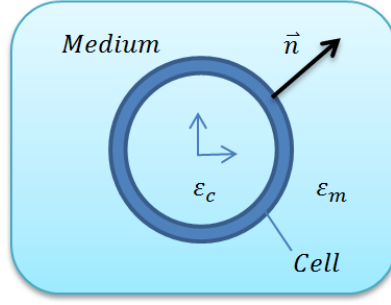


Figure 2.4: Electromechanical model of a living cell

Where  $\vec{n}$  is outward unit-vector normal to the cell surface,  $\vec{\vec{T}}_{out}$  and  $\vec{\vec{T}}_{in}$  are the Maxwell stress tensor outside and inside the cell, respectively.  $\vec{\vec{T}}_{out} \cdot \vec{n}$  and  $\vec{\vec{T}}_{in} \cdot \vec{n}$  could be written as:

$$\vec{\vec{T}}_{out} \cdot \vec{n} = \epsilon_m \left( (\vec{E}_{out} \cdot \vec{n}) \vec{E}_{out} - \frac{1}{2} |\vec{E}_{out}|^2 \vec{n} \right)$$

$$\vec{\vec{T}}_{in} \cdot \vec{n} = \epsilon_c \left( (\vec{E}_{in} \cdot \vec{n}) \vec{E}_{in} - \frac{1}{2} |\vec{E}_{in}|^2 \vec{n} \right)$$

Finding the electrical field distribution is a complex problem. Regarding the configuration of electrodes, as shown in Figure2.3, as well as the presence of the cell , numerical techniques (e.g. FEM method) should be used to obtain the actual electrical field distribution [65]. The electrical field distribution could be derived based on the Laplace equation (i.e.  $\nabla^2 \Phi = 0$ ), Maxwell equation (i.e.  $E = -\nabla \Phi$ ), and the set of boundary conditions as:

$$\begin{cases} \Phi_{electrode} = \Phi_0 \\ \epsilon_m \frac{\partial \Phi_{out}}{\partial n} = \epsilon_c \frac{\partial \Phi_{in}}{\partial n} \\ \vec{E}_{out} \times \vec{n} = \vec{E}_{in} \times \vec{n} \end{cases} \quad or \quad \epsilon_m \vec{E}_{out} \cdot \vec{n} = \epsilon_c \vec{E}_{in} \cdot \vec{n} \quad (12)$$

Where  $\Phi_0$  is the applied electric potential,  $\varepsilon_m$  is medium permittivity,  $\varepsilon_c$  is cytoplasm permittivity,  $\Phi_{out}$  and  $\Phi_{in}$  are the electric potential outside and inside the cell, respectively. The last two boundary conditions refer to the conservation of electric charge and the continuity of the potential function in the interface boundary (i.e cell membrane), respectively [65]. It should be noted that in the Maxwell-Wagner frequency range, as the present case, the considerable part of applied potential drops across the cell membrane such that the cell membrane could be considered as a nonconductive interface. The potential difference between external and internal space of the cell (surrounding medium and cytoplasm) is called transmembrane potential [86].

For a shelled spherical cell, the DEP force per unit area based on Eq.11 is defined by

$$\vec{f}_{DEF}^s = \varepsilon_m \left( (\vec{E}_{out} \cdot \vec{n}) \vec{E}_{out} - \frac{1}{2} |\vec{E}_{out}|^2 \vec{n} \right) - \varepsilon_c \left( (\vec{E}_{in} \cdot \vec{n}) \vec{E}_{in} - \frac{1}{2} |\vec{E}_{in}|^2 \vec{n} \right) \quad (13)$$

Substituting boundary conditions (12) in Eq.13 yields:

$$\vec{f}_{DEF}^s = \frac{\varepsilon_m}{2} \left( \frac{(\varepsilon_c - \varepsilon_m)}{\varepsilon_m} |\vec{E}_{in}|^2 + \frac{\varepsilon_m^2 - \varepsilon_c^2}{\varepsilon_m^2} (\vec{E}_{in} \cdot \vec{n})^2 \right) \vec{n} + \varepsilon_c (\vec{E}_{in} \cdot \vec{n}) (\vec{E}_{out} - \vec{E}_{in})$$

The normal component of DEP force per unit area is defined by

$$(\vec{f}_{DEF}^s \cdot \vec{n}) = \frac{\varepsilon_m}{2} \left( \frac{(\varepsilon_c - \varepsilon_m)}{\varepsilon_m} |\vec{E}_{in}|^2 + \frac{(\varepsilon_c - \varepsilon_m)^2}{\varepsilon_m^2} (\vec{E}_{in} \cdot \vec{n})^2 \right)$$

The tangential component of DEP force per unit area is defined by

$$(\vec{f}_{DEF}^s \cdot \vec{t}) = \varepsilon_c (\vec{E}_{in} \cdot \vec{n}) [(\vec{E}_{out} \cdot \vec{t}) - (\vec{E}_{in} \cdot \vec{t})]$$

The DEP force on the cell membrane could be derived by integration of Maxwell stress tensor over the membrane surface as:

$$\langle \vec{f}_{DEF} \rangle = \oint (\vec{T}_{out} \cdot \vec{n} - \vec{T}_{in} \cdot \vec{n}) dA = \begin{cases} \oint (\vec{f}_{DEF}^s \cdot \vec{n}) dA \\ \oint (\vec{f}_{DEF}^s \cdot \vec{t}) dA \end{cases}$$

Living cells, in general, are made of lipid bilayer membranes. In such cases, when an electric field is applied, the cell membrane acts as an insulator and accumulates electric charges on both sides. As accumulated charges are significantly small, cells are considered to be neutral [67]. Regarding this fact that the thickness of lipid membrane is very small compared with the cell diameter (three order of magnitude), the cell membrane could be considered as a zero-thickness capacitor [86].

The total force strength acting on the cell membrane is the sum of the total DEP force per unit area and the membrane mechanical force strength as

$$\vec{f}^s = \vec{f}_{mem}^s + \vec{f}_{DEF}^s$$

Based on the theory of very thin spherical shells, the cell membrane could be considered as a curved two-dimensional shell with finite thickness [67], see Figure 2.5.

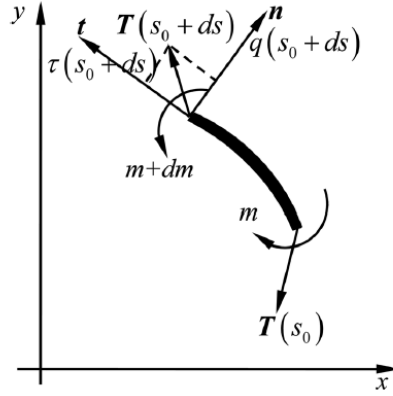


Figure 2.5: A two-dimensional shell with finite thickness

The membrane mechanical strength is a measure of the resistance of the cell membrane against both bending and stretching and is expressed as:

$$\vec{f}_{mem}^s = \left( E_s \frac{d\epsilon}{ds} + k E_B \frac{d(k - k_0)}{ds} \right) \vec{t} + \left( E_B \frac{d^2(k - k_0)}{ds^2} - E_s \epsilon k \right) \vec{n}$$

Where  $E_s$  is the shear modulus,  $E_B$  is the bending stiffness,  $\epsilon$  and  $k$  are the tensile strain and the resting curvature of the membrane, respectively,  $\vec{t}$  is the unit tangent vector, and  $\vec{n}$  is the unit normal vector, as shown in Figure 2.5.

In the present case, where there is no fluid flow, the total force exerted on the cell, in the equilibrium position, is equal to zero such that:

$$\int_{\Gamma} (\vec{f}_{mem}^s + \vec{f}_{DEF}^s) ds = 0 \quad (14)$$

Where  $\Gamma$  denotes cell membrane and  $s$  is the arc length along the cell membrane [67]. By solving Eq.14, one could derive the mechanical properties of cell membrane.

## 2.6 Living cells in a uniform DC electric field

As indicated, when the applied electric field is highly non-uniform due to the configuration of electrodes and the presence of cells, numerical techniques (e.g. FEM method) should be used to obtain the actual electrical field distribution [65]. The ability of FEM method could be validated using a simple problem. For this end a single cell is considered to be placed between two planar electrodes as Figure 2.6 shows.

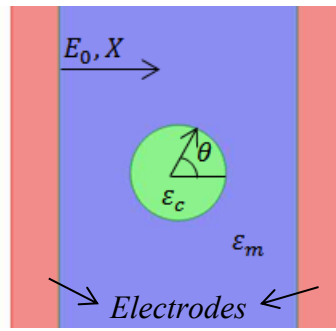


Figure 2.6: Schematic drawing of a spherical cell in a uniform electric field

In the absence of the cell the electric field between the electrodes is uniform and described by

$$E_0 = U/d \quad (15)$$

Where  $E_0$  is the uniform electric field,  $U$  is the applied electric potential, and  $d$  is the distance between electrodes.

It is important to point out that, even if this situation is applied, the presence of a cell in a uniform electric field makes the fields non-uniform and dielectrophoresis could occur. The only point should be considered is that the dimension of the cell should be comparable with the typical length of electrodes as well as the distance between them.

When a spherical cell is placed between two electrodes, Figure 2.6, the electric field inside and outside the cell are different and can be obtained using Laplace equation (i.e.  $\nabla^2\Phi = 0$ ) and the set of boundary conditions (12). In polar coordinate system  $(r, \theta)$ , where the driving electric field is in  $X$  direction,  $\varepsilon_m$  is medium permittivity,  $\varepsilon_c$  is cell permittivity,  $r_c$  is cell radius, the electric field inside,  $E_{in}$ , and outside,  $E_{out}$ , the cell are found in [87] expressed by

$$E_{in} = \frac{3\varepsilon_m}{\varepsilon_c + 2\varepsilon_m} E_0 (\cos\theta \hat{r} - \sin\theta \hat{\theta}) \quad (16)$$

$$E_{out} = E_0 (\cos\theta \hat{r} - \sin\theta \hat{\theta}) + \frac{\varepsilon_c - \varepsilon_m}{\varepsilon_c + 2\varepsilon_m} \frac{r_c^3}{r^3} E_0 (2\cos\theta \hat{r} - \sin\theta \hat{\theta}) \quad (17)$$

Based on Eq.10, the DEP force per unit area of a spherical particle could be defined as

$$\overrightarrow{f}_{DEF}^s = \varepsilon_m \left( (\overrightarrow{E_{out}} \cdot \vec{n}) \overrightarrow{E_{out}} - \frac{1}{2} |\overrightarrow{E_{out}}|^2 \vec{n} \right) \quad (18)$$

The normal component of DEP force per unit area is given by

$$(\overrightarrow{f}_{DEF}^s \cdot \vec{n}) = \varepsilon_m \left( (\overrightarrow{E_{out}} \cdot \vec{n}) (\overrightarrow{E_{out}} \cdot \vec{n}) - \frac{1}{2} |\overrightarrow{E_{out}}|^2 \right) \quad (19)$$

Using the boundary conditions (12), the expression could be defined in terms of the field at the particle's center as

$$(\overrightarrow{f}_{DEF}^s \cdot \vec{n}) = \frac{\varepsilon_m}{2} \left( -|\overrightarrow{E_{in}}|^2 + \frac{\varepsilon_m^2 + \varepsilon_c^2}{\varepsilon_m^2} (\overrightarrow{E_{in}} \cdot \vec{n})^2 \right) \quad (20)$$

Substituting Eq.16 in recent expression leads to

$$(\overrightarrow{f}_{DEF}^s \cdot \vec{n}) = \frac{\varepsilon_m}{2} \left( \frac{3\varepsilon_m}{\varepsilon_c + 2\varepsilon_m} \right)^2 E_0^2 \left( -1 + \frac{\varepsilon_m^2 + \varepsilon_c^2}{\varepsilon_m^2} \cos^2 \theta \right) \quad (21)$$

If the cell permittivity is two times larger than the medium permittivity then,

$$(\vec{f}_{DEF}^s, \vec{n}) = \frac{\epsilon_m}{2} \left(\frac{3}{4}\right)^2 E_0^2 (-1 + 5 \cos^2 \theta) \quad (22)$$

Based on the Eq.22, the maximum traction (DEP force per unit area) occurs at the cell's poles (where  $\theta = 0$ ) and its minimum occurs at the cell's equator (where  $\theta = \pi/2$ ).

Numerical analysis of the above problem was carried out using COMSOL multiphysics. A potential difference ( $U=10V$ ) is applied between electrodes. A spherical cell is placed in the center of the electrodes with distance of  $50 \mu m$ . The medium relative permittivity is considered to have a value of 40 while the cell relative permittivity is set to 80. Although the initial electric field between planar electrodes is uniform ( $E_0=U/d$ ), the presence of the cell makes the field non-uniform as Figure 2.7 shows.

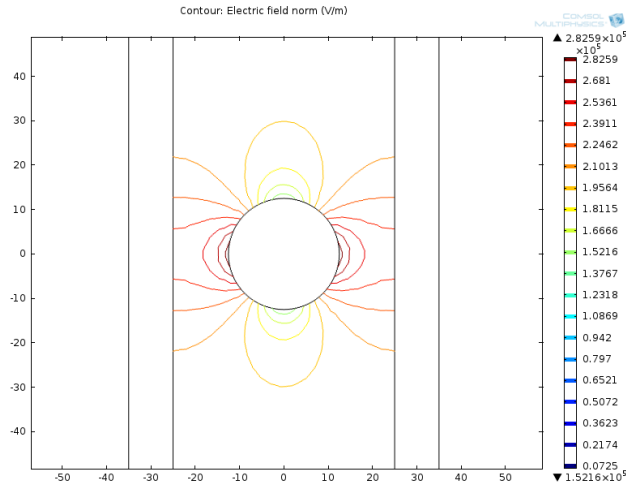


Figure 2.7: Contour plot of the electric field intensity around the cell

Figure 2.8 illustrates the outward Maxwell stress tensor (electrical tractions) over the boundary of the cell. The simulation results show that radial component of tractions has a maximum value of  $14.84 Pa$  in cell's poles and a minimum value of  $-3.56 Pa$  in



cell's equator which are in good agreement with those obtained analytically using Eq. 22. Based on the analytical approach, Eq. 22, the radial component of tractions has a maximum value of  $15.93 \text{ Pa}$  in cell's poles and a minimum value of  $-3.98 \text{ Pa}$  in cell's equator.

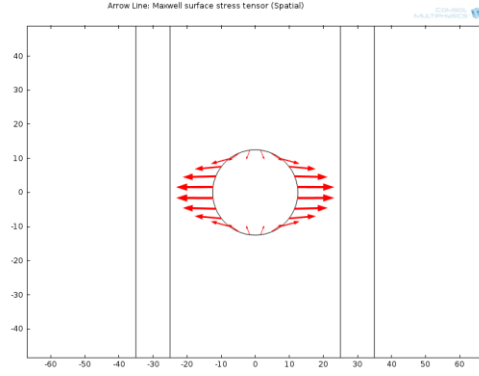


Figure 2.8: Outward Maxwell stress tensor over the boundary of the cell

Table 2.1 compares the values of maximum and minimum tractions over the cell boundary based on FEM analysis (COMSOL) and theoretical analysis (Eq.22).

Table 2.1: Comparing the maximum and minimum tractions over the cell boundary based on FEM analysis (COMSOL) and theoretical analysis (Eq.22).

Method	Maximum traction ( $\text{Pa}$ )	Minimum traction ( $\text{Pa}$ )
FEM analysis (COMSOL)	14.84	-3.56
Theoretical analysis (Eq.22)	15.93	-3.98
Error	6.84 %	10.55 %

## 2.7 Effective dipole moment approximation

Another method to obtain DEP force on particles, in an electric field, is the effective dipole moment approximation.

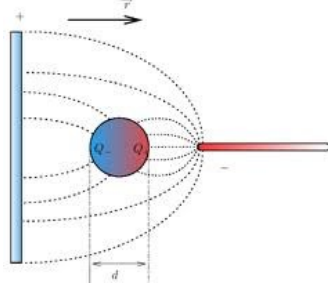


Figure 2.9: Schematic drawing of a cell as a dipole particle in a non-uniform electric field

Based on this approximation, living cells are considered as polarizable dipole particles, as shown in Figure 2.9. The net DEP force is derived and given everywhere as:

$$\langle \bar{F}_{DEF} \rangle = 2\pi\epsilon_m r^3 \text{Re}(K(\omega)) \nabla E_{rms}^2 \quad (23)$$

Where  $r$  is the radius of the particle,  $E_{rms}$  is the root-mean-square of the applied electrical field, and  $K(\omega)$  is the complex Clausius-Mossotti function expressed as:

$$K(\omega) = \frac{\epsilon_p - \epsilon_m - i(\sigma_p - \sigma_m)/\omega}{\epsilon_p + 2\epsilon_m - i(\sigma_p + 2\sigma_m)/\omega} \quad (24)$$

Where  $\epsilon_p$  and  $\sigma_p$  are the permittivity and conductivity of the particle, respectively [88]. Dipole moment approximation measures the DEP force exerted in the center mass of particles and cannot provide the additional information about the distribution of DEP force over the surface of particles. Thus this method is effective when particles are small compared to the characteristic length of electrodes and medium. This method also does not take into account the non-uniformity of electric field due to the presence of particles and fail to calculate accurately the DEP force on particles very close to the electrodes [89]. In such cases, as the present study, where dimensions of particles are comparable with the characteristic length of electrodes, the higher-order multipole assumption is

needed. The overall time-average DEP force based on multipole assumption has a form of [90]:

$$\langle \bar{F}_{DEF} \rangle^n = \frac{1}{2} \sum_{n=1}^{\infty} \frac{4\pi}{n!(2n-1)!!} \varepsilon_m r^{2n+1} \text{Re}(K(\omega)_n) (\nabla)^{n-1} E[.]^n (\nabla)^n E \quad (25)$$

Where  $(\nabla)^n E$  is a symmetric tensor of rank  $n$ ,  $[.]^n$  is  $n$  dot product operations, and  $K(\omega)_n$  is the general multipole form of Clausius-Mossotti function expressed as:

$$K(\omega)_n = \frac{\varepsilon_p - \varepsilon_m - i(\sigma_p - \sigma_m)/\omega}{n\varepsilon_p + (n+1)\varepsilon_m - i(n\sigma_p + (n+1)\sigma_m)/\omega} \quad (26)$$

In the case, when the electrical field is axially symmetric and the particle is spherical, considering only the dipole term ( $n=1$ ) and the quadrupole ( $n=2$ ) leads to a good agreement with MST approach [89]. The DEP could be expressed as [90]:

$$\langle \bar{F}_{DEF} \rangle^2 = 2\pi\varepsilon_m r^3 \text{Re}(K(\omega)) \nabla E^2 + \frac{2}{3}\pi\varepsilon_m r^5 \text{Re}(K(\omega)_2) \nabla \cdot \nabla E^2 \quad (27)$$

Although using the higher order of multipole assumption leads to the more accuracy in DEP calculation, this method, however, is unable to predict the DEP force distributions over the surface of particles.

## 2.8 Finite Element simulation of the cell deformation using COMSOL

The below section presents the numerical solution of the deformation of the model presented in 2.4 - 2.7.

### 2.8.1 Theoretical background

FEM analysis of electro-deformation of a single spherical shell in a non-uniform electric field is an electrostatic problem coupled with a linear-elastic mechanical problem. To do so, first a steady-state electrostatic analysis is achieved to calculate the electric field intensity inside and outside the sphere and then the DEP force is exerted on the boundary of the sphere based on the components of Maxwell stress tensor in a steady-state mechanical analysis.

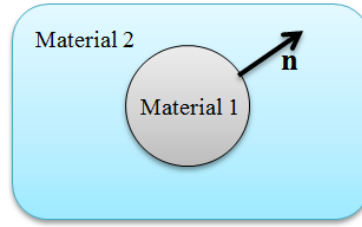


Figure 2.10: Schematics of a linear elastic material (Material 1) placed in a medium (Material 2)

Consider a linear elastic material placed in a medium (Material 2) and subjected to an external electric field as shown in Figure 2.10. The electrostatic equilibrium equation of motion is given by [91]

$$\nabla \cdot T^T + f_{ext} = 0 \quad (28)$$

Where  $T^T$  is the total stress tensor and  $f_{ext}$  is an external volume force. The stress tensor must be continuous across the interface [91] such that

$$T^T_1 \cdot \vec{n}_1 + T^T_2 \cdot \vec{n}_2 = 0 \quad \text{or} \quad (T^T_2 - T^T_1) \cdot \vec{n} = 0 \quad (29)$$

Where  $\vec{n}_1 = -\vec{n}$  and  $\vec{n}_2 = \vec{n}$ . The total stress tensor in the elastic material ( $T^T_1$ ) is comprised of the downward Maxwell stress tensor ( $T_{down}$ ) and mechanical stress ( $\sigma_M$ ).

The total stress tensor in the medium ( $T^T_2$ ) is comprised of the upward Maxwell stress tensor ( $T_{up}$ ) and the pressure due to the medium ( $P$ ) [91] such that

$$T^T_1 \cdot \vec{n}_1 = T_{down} + \sigma_M \cdot \vec{n}_1 \quad (30)$$

$$T^T_2 \cdot \vec{n}_2 = T_{up} + P \quad (31)$$

Assume that the pressure,  $P$ , is eliminated by the internal pressure of the material 1, then the surface force applied on the mechanical body (i.e. Dielectrophoretic force in this study) is given by Eq.18 and rewritten as

$$\vec{f}_{DEF}^s = T^T_2 \cdot \vec{n}_2 = T_{up} = \epsilon_2 \left( (\vec{E}_2 \cdot \vec{n}) \vec{E}_2 - \frac{1}{2} |\vec{E}_2|^2 \vec{n} \right) \quad (32)$$

Where  $\vec{f}_{DEF}^s$  is the Dielectrophoretic tractions which will be calculated from the steady-state electrostatic module of COMSOL multiphysics. Traction then will be applied as surface forces on the cell membrane in a steady-state mechanical analysis to calculate the electromechanical deformation of the cell. The mechanical stresses could be derived by substituting Eq.(30), (31) in Eq.(29) as

$$\sigma_M \cdot \vec{n} = T_{up} + T_{down} \quad (33)$$

### 2.8.2 Problem formulation

A single shelled-spherical cell surrounded by a dielectric medium is exposed to a non-uniform DC electric field as shown in Figure 2.11. First, a potential difference of 10  $V$  is applied between two electrodes to achieve a steady-state electrostatic analysis. Then, the surface traction forces, based on the component of Maxwell stress tensor, are applied

on the cell boundary to calculate mechanical stresses and deformations in a steady-state mechanical analysis.

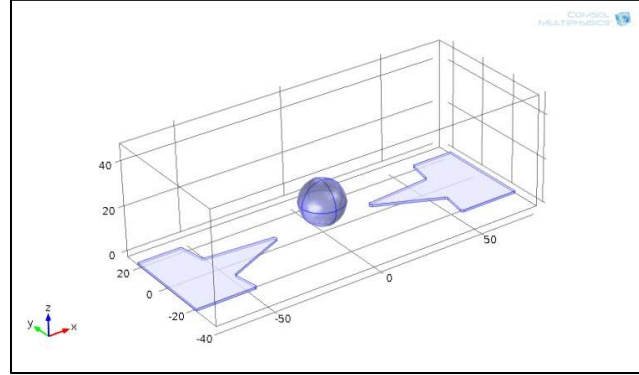


Figure 2.11: 3D representation of a single shelled spherical cell surrounded in a non-uniform DC electric field

Both cell and medium are considered as dielectric materials. The problem is coupled as electrostatic - mechanical analysis but, only the cell is considered as the mechanical part of the model. The input parameters of the model are defined in Table 2.2.

Table 2.2: Input parameters of the 3D electrostatic-mechanical analysis

Description	Unit
Cell radius	10 $\mu\text{m}$
Cell relative permittivity	80 [92]
Cell density	1150 $\text{kg/m}^2$
Cell Young's modulus	600 Pa
Cell poison ratio	0.37
Medium relative permittivity	40 [92]
Medium density	1150 $\text{kg/m}^2$
Cytoplasm relative permittivity	60 [92]
Electrodes thickness	1 $\mu\text{m}$
Cell positioning in Z	9 $\mu\text{m}$
Model length in X	154 $\mu\text{m}$
Model length in Y	65 $\mu\text{m}$
Model length in Z	50 $\mu\text{m}$
Electrodes distance	40 $\mu\text{m}$

As clear from Figure 2.11, the special configuration of the electrodes produces non-uniform electric field intensity everywhere. The non-uniformity of the electric field will be higher in electrode's tips. In a real situation (e.g. an experimental observation) the cells motion toward an electrode tip depends on the spatial proximity of the cell. When the cells are close to the electrodes, the electric field would be more non-uniform. As indicated before, when an electric potential is applied, the cell membrane acts as a capacitor and the applied potential jumps over the cell. A jump in applied potential is called transmembrane potential [86]. For the given parameters in Table 2.2, Figs. 2.12a and 2.12b shows the contour of electric field intensity with and without the cell, respectively. As clear in Figure 2.12a, the electric field inside and outside the cell are different.

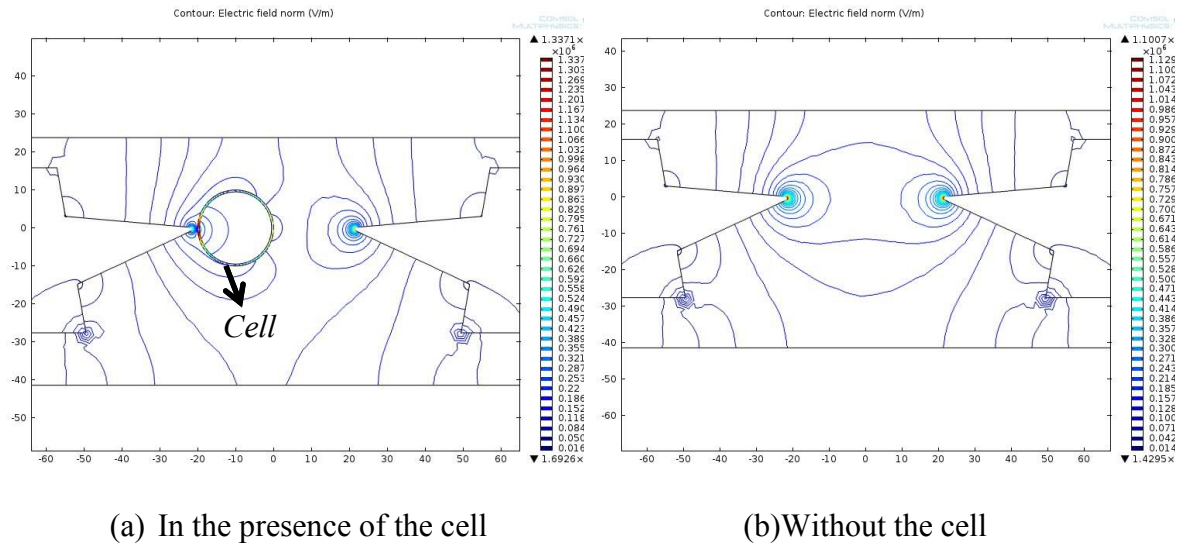


Figure 2.12: Contour plot of electric field (a) when the cell is present, (b) no cell is present

Figure 2.13 shows the 3D finite element model of the problem. The analysis is carried out based on the input parameters in Table 2.2 and following assumptions as:

- 1- The cell is considered as a linear elastic material
- 2- The cell permittivity is more than that of surrounding medium
- 3- The cell, electrodes, and medium are all considered in electrostatic analysis
- 4- Only the cell is considered as a mechanical part in the mechanical analysis
- 5- The cell is fixed at the bottom and all degrees of freedom are set to zero around a circular boundary on the bottom of the cell.
- 6- The total volume of the cell is considered to be constant during analysis.

The final dimensions of the simulation model to minimize the number of elements were determined by starting with a larger size and then finishing with the current size without losing the accuracy of the results. The element type is Tetrahedral with the predefined fine size ( $0.5\text{-}7\mu\text{m}$ ). The mesh independency was achieved at 120,000 elements.

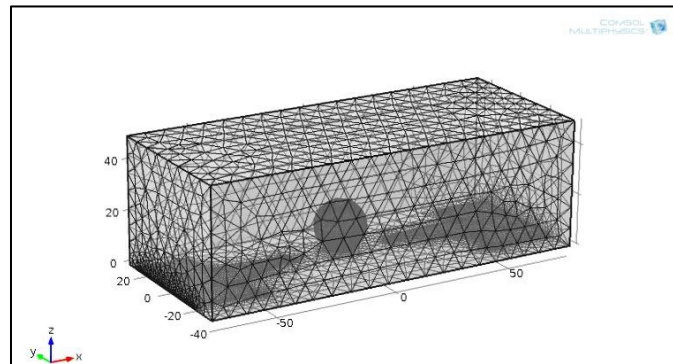


Figure 2.13: 3D finite element model of the problem

As indicated, the surface boundary loads applied on the cell membrane are based on the components of Maxwell stress tensor on the cell membrane. As cytoplasm is also considered as a medium with certain permittivity, the total electrical tractions on the cell



membrane are calculated based on the components of Maxwell stress tensor in cell interior as well. Figure 2.14 shows the electric tractions inside and outside the cell.

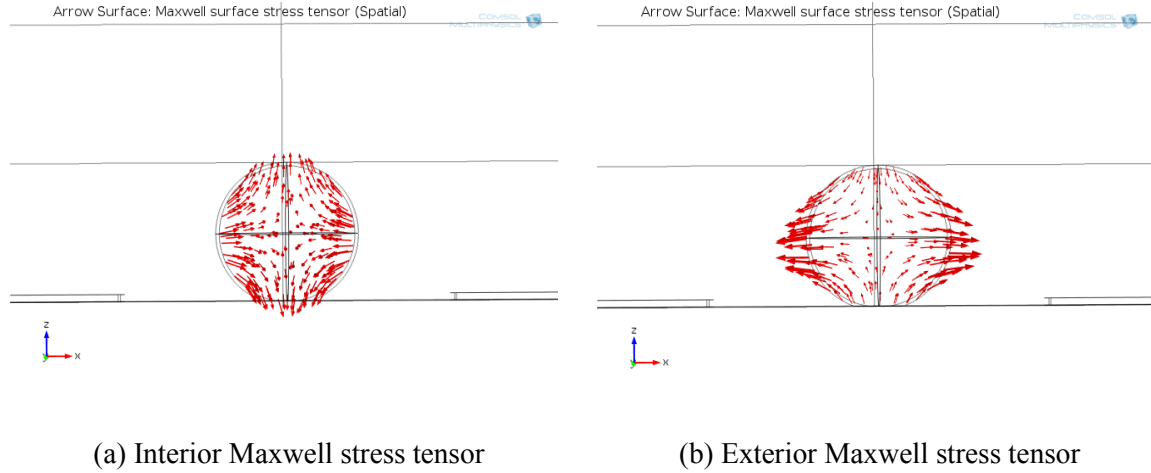


Figure 2.14: Electric tractions inside (a) and outside (b) the cell

The cell is placed in the center line between electrodes where the net force in  $X$  and  $Y$  direction is approximately zero and the cell is considered to be in its equilibrium position. The distribution of DEP forces in cell's boundaries, while the cell is fixed in the bottom, leads to an elongation in  $X$  direction as shown in Figure 2.15.

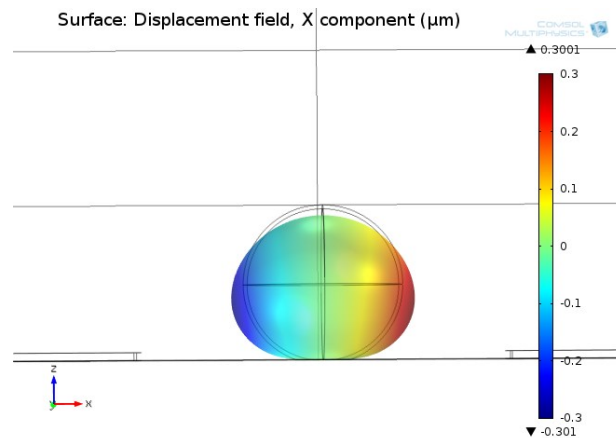


Figure 2.15: Electro deformation of the cell in a non-uniform electric field

As clear in Figure 2.15, the total elongation of the cell in  $X$  direction is  $0.6011 \mu m$ .

## 2.9 Summary

Electro-static formulation of electrically neutral living cells subjected in a non-uniform electric field has been presented in this chapter. Electro-deformation of biological cells as dielectric particles could be studied based on two mostly used approaches, Maxwell stress tensor (MST) and effective dipole moment approximation. When the sizes of cells are comparable with the typical length of electrodes, using dipole moment approximation approach leads to wrong result. In such cases, only Maxwell stress tensor approach could be able to predict the distribution of dielectrophoretic tractions over the cell's boundaries. As indicated, when the applied electric field is highly non-uniform, numerical techniques (e.g. FEM) should be used to obtain the actual electric field distribution [65]. A simple 2D example showed that results of FEM analysis using COMSOL Multiphysics are in good agreements with those of theoretical analysis presented in 2.6. A 3D finite element analysis of a shelled-spherical cell in a non-uniform electric field was achieved. FEM simulations showed that for an applied electric field of  $250 \text{ V/mm}$  a spherical cell with properties presented in Table 2.2 had  $0.6 \text{ }\mu\text{m}$  of elongation in direction of applied electric field.

## **Chapter 3: PARAMETRIC STUDY AND OPTIMIZATION OF THE ELECTRO-DEFORMATION MEMS DEVICE TO INCREASE DEP FORCES ON BIOLOGICAL CELLS**

### **3.1 Introduction**

Influence of the design parameters of a DEP microdevice on the electro-deformation of neutral biological cells are presented in this chapter. The aim is to induce maximum electro-deformation on living cells without applying undesirable physiological effects on cells including Joule heating (i.e. thermal side effect associated with high voltage) and electrolysis (i.e. breaking down of a cell to release the subcellular materials).

Also, design optimization of the DEP microdevice is performed using the integration of COMSOL Multiphysics and Genetic Algorithms (GAs) optimization technique. The optimum design of the model is presented based on the above method and compared to the results of the parametric study. Several parametric studies are performed to compare the results of GA with those found by parametric sweep feature-node of COMSOL Multiphysics. Furthermore, the best design configuration of the model has been compared with the initial design which showed an increase of more than two times in the maximum induced deformation on the cell in *X*-direction (see Figure 3.15).

### **3.2 Parametric study**

The scope of the parametric study is to investigate the influence of design parameters to the ability of the DEP method to induce electro-deformation on the living cells.

Figure 3.1 shows the schematic of a spherical cell in a non-uniform electric field and the parameters of the model. Cell is considered to have a spherical shape. The mechanical model of the cell is a homogeneous isotropic spherical shell with a given Young modulus. Before applying the electric potential difference, the cell is assumed to be in an equilibrium position where the total force on the cell is balanced out.

When applying the electric potential, the distributed DEP forces on the cell surface lead to an elongation on the cell membrane. It is assumed that the volume of the cell is conservative and there is no liquid transformation between cytoplasm and medium. The cell is placed in the center line between electrodes where the total DEP forces on the two cell halves are equal.

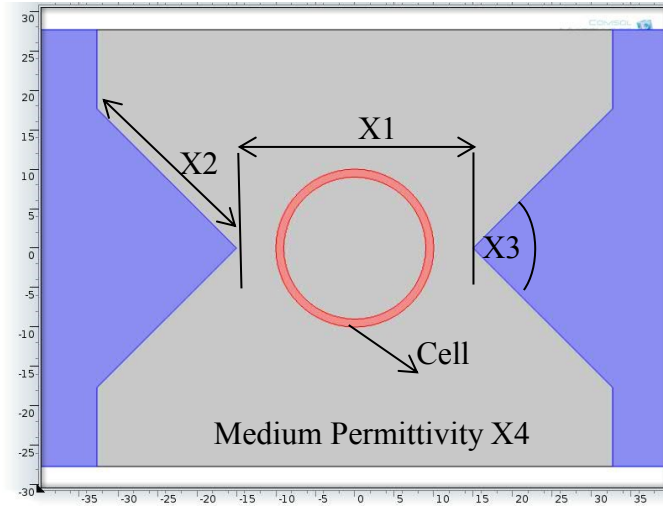


Figure 3.1: Schematic of a spherical cell in a non-uniform electric field and the input parameters of the model

The effects of different parameters including cell radius,  $r$  ( $\mu m$ ), distance between electrodes,  $X1(\mu m)$ , length of electrodes,  $X2(\mu m)$ , relative permittivity of the medium,  $X4$ , and tip angle of electrodes,  $X3(\text{degree})$ , are studied by the means of the parametric

study feature node of COMSOL 4.2a. Other input parameters are constant during the parametric study and defined in Table 3.1.

The model size is chosen to reduce the number of mesh elements in the model and to be large enough such that the change of the cell deformation versus the model size would not be significant. It should be noted that the model length and width are variable based on the geometrical parameter of the model. Based on several simulations, the model height is set to  $60\ \mu m$ .

Table 3.1: Input parameters of the parametric study

Description	Unit
Cell relative permittivity	80 [92]
Cell density	$1150\text{ kg/m}^2$
Cell Young's modulus	600 Pa
Cell poisson ratio	0.37
Medium density	$1150\text{ kg/m}^2$
Cytoplasm relative permittivity	60
Model height	$60\ \mu m$
Electrodes length	$30\ \mu m$
Electrodes distance	$25\ \mu m$
Tip angle	$90^\circ$
Medium relative permittivity	40

### 3.2.1 Influence of distance between electrodes on cell elongation

Figure 3.2 shows the maximum deformation of the cell, calculated in the cell pole in a direction parallel to the electric field, versus distance between electrodes. The simulation is performed for different size of the cell. As clear, for all cases, the

deformation decreases when the distance between electrodes increases. Figure 3.2 also shows that for a given electrodes distance, larger cells have more deformations.

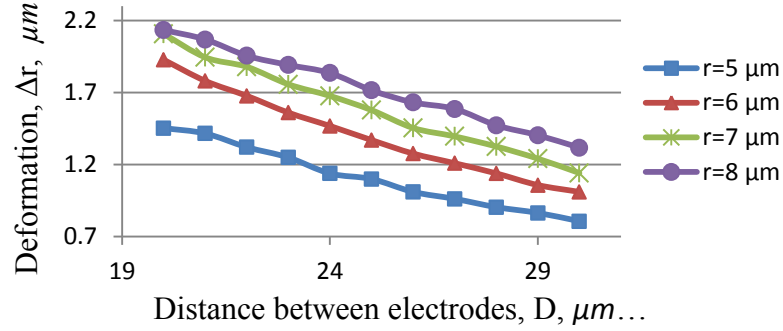


Figure 3.2: Deformation of the cell versus distance between electrodes for different size of the cell

Non-dimensional study has also been performed to investigate the cell deformation ratio versus size ratio (i.e. distance between electrodes ( $D$ ) to the cell radius ( $r$ )).

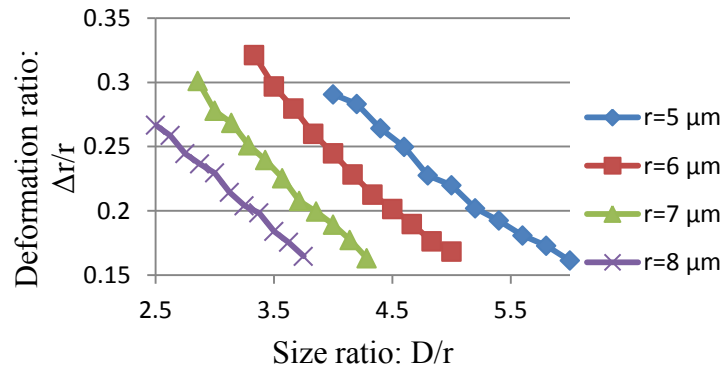


Figure 3.3: Deformation ratio ( $\Delta r/r$ ) of the cells versus size ratio ( $D/r$ )

Figure 3.3 demonstrates the maximum deformation ratio of the cells versus size ratio. Also it shows that for a given cell radius, increasing the size ratio leads to the less deformation for all cell sizes. As is clear from Figure 3.3, for a given size ratio, smaller

cells have larger deformations. To verify the results, two cases have been considered for a size ratio of 3. Case number one is a spherical cell with the radius of  $5\ \mu m$ ,  $r$ , placed between two electrodes with  $15\ \mu m$  of distance,  $D$ , and case number two is a spherical cell with the radius of  $6\ \mu m$  placed between two electrodes with  $18\ \mu m$  of distance. The geometrical and material properties of the models are same as defined in Table 2-1. The component of DEP force in the direction of electric field ( $X$  component) is calculated by the integration of the  $X$  component of the Maxwell surface stress tensor over half surface of the sphere. Figure 3.4 demonstrates the results. As it can be realized, for case.1,  $F_x=4.6\ nN$  and for case.2,  $F_x=4.47\ nN$  which shows the force exerted on the surface of the bigger cell is less.

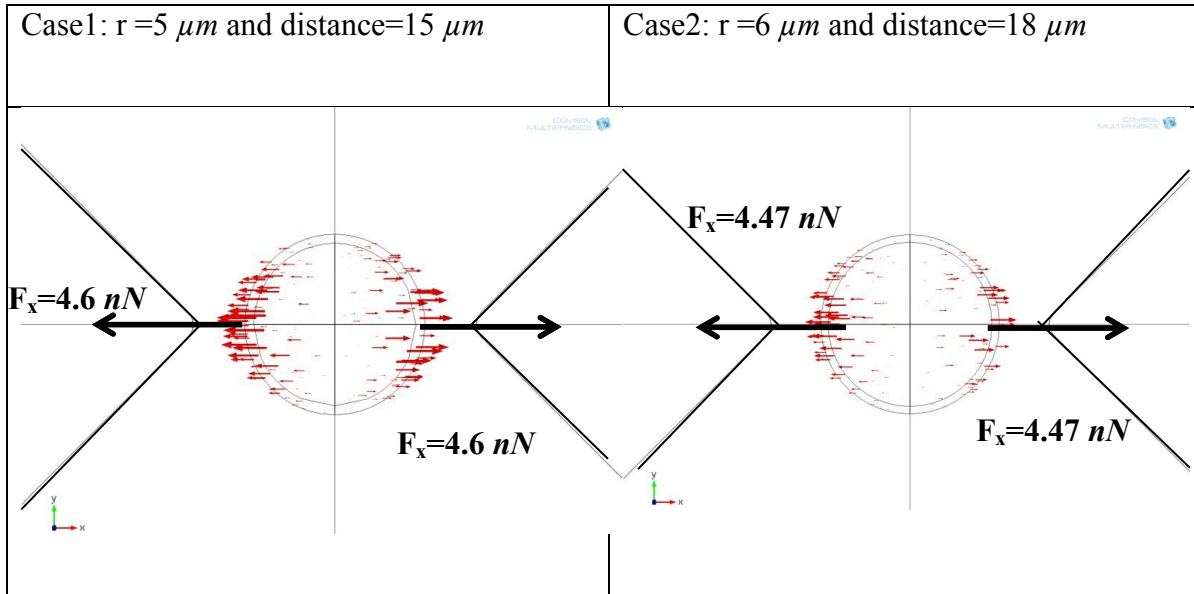


Figure 3.4: Comparing the  $X$  component of dielectrophoretic force on cell surfaces

### 3.2.2 Influence of tip angle of electrodes on cell elongation

Figure 3.5 shows the maximum deformation of the cell, calculated in the cell pole in a direction parallel to the electric field, versus tip angle of electrodes. The results show

that sharper electrodes induce less deformation on cell membrane. This happens because of the distribution of the DEP force components in the direction of electric field.

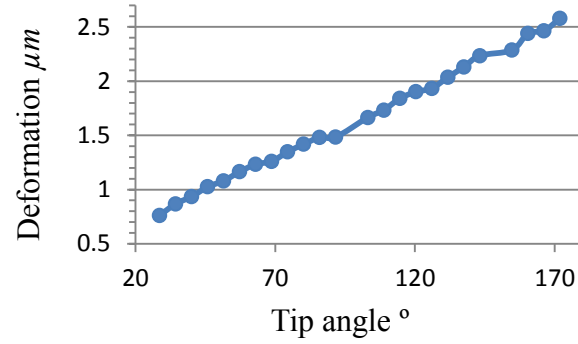


Figure 3.5: Comparison of the  $X$  component of dielectrophoretic force on cell surfaces

Figure 3.6 compares the electric tractions (Maxwell stress tensor components) on the cell membrane, for tip angles of  $90^\circ$  and  $170^\circ$  respectively while other parameters are kept constant.

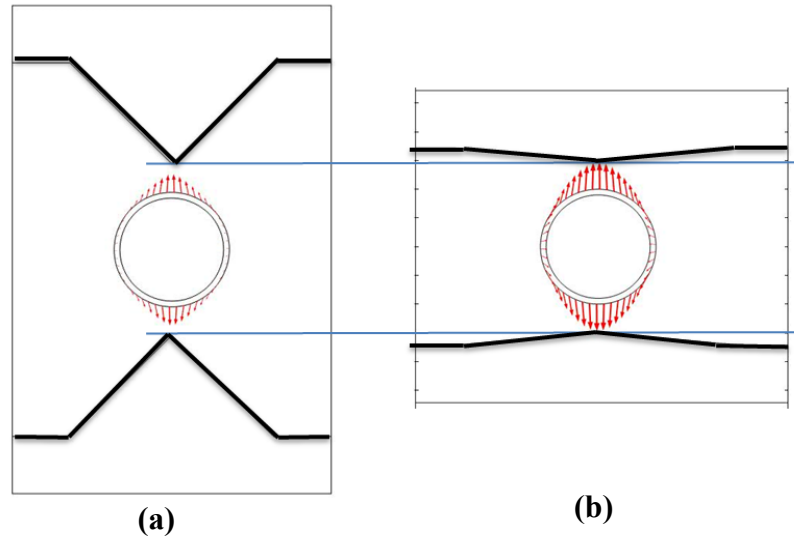


Figure 3.6: Comparison of the electric tractions on the cell surfaces regarding the tip angle of electrodes. (a) A cell placed between sharp electrodes. (b) A cell placed between flat electrodes. Arrows indicate the electric tractions on the cell membrane



As clear from Figure 3.6, when the tip angle of electrodes is more flat, the electric tractions on the cell poles are larger than those on the quadruples that induce more electro-deformation on the cell membrane in direction of applied electric field.

### 3.2.3 Influence of relative permittivity of the medium on cell elongation

As discussed in chapter 2, the relative permittivity of surrounding medium should be chosen to have a value less than that of the cell to enable the maximum positive dielectrophoretic forces. Figure 3.7 shows the maximum deformation of the cell versus the medium permittivity. Here the relative permittivity of cell is set to 80. As Figure 3.7 reveals, more difference between permittivity of the medium with that of the cell leads to more deformation on the cell membrane. This is because cells are much more polarizable than the surrounding medium and experience larger DEP forces.

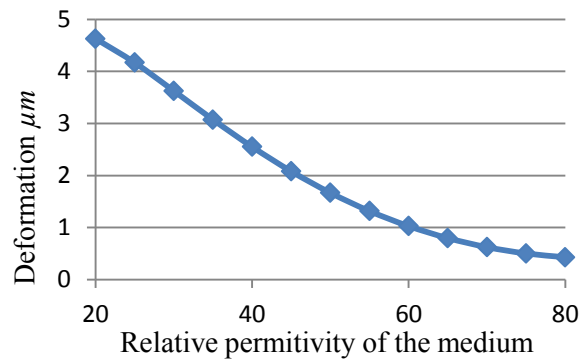


Figure 3.7: Maximum deformation of the cell versus the medium permittivity

### 3.2.4 Influence of length of electrodes on cell elongation

Figure 3.8 shows the curve of the maximum deformation of the cell versus the length of electrodes.

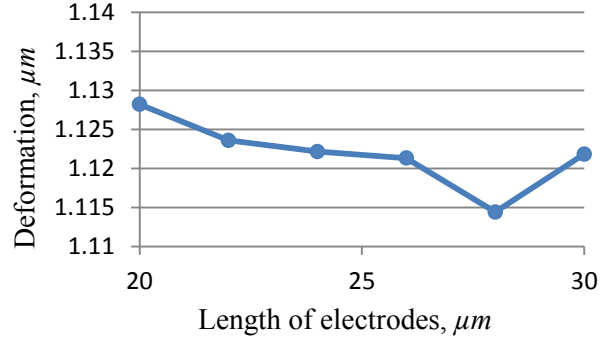


Figure 3.8: Maximum deformation of the cell versus the length of electrodes

As clear from Figure 3.8, when the radius of the cell is  $10 \mu m$  and the applied potential difference is  $10 V$ , different electrode lengths between  $20 \mu m$  to  $30 \mu m$  will induce a change in cell deformation less than  $0.1 \mu m$  that is not significant. This happens because the distributed DEP forces on cell halves are such that the total force does not show significant changes regarding different lengths of electrodes. For instance, the DEP force on each cell halve varies from  $1.18$  to  $1.22 nN$  for a distance range of  $20$  to  $30 \mu m$ .

### 3.3 Optimization study

When dealing with human cells, viability of cells during experiments and experimental limitations should be considered. Optimization of DEP devices is a way to overcome the limitation of fabrication and experimental tools. An appropriate optimization method must be able to address linear and nonlinear functions. Also, it must be applicable for a number of discrete design variables (parameters). Genetic Algorithms (GAs) has demonstrated the ability to optimize complex problems. In most of the complex problem, as the current case, there is no closed form of objective function and numerical techniques must be used to calculate the objective function. For instance,

Muñoz et al. (2008) [93] demonstrated the integration of Genetic Algorithms technique and finite elements method to find the best geometric configuration of a heat exchanger device. Also, Pelster et al. (2011 COMSOL conference in Stuttgart) [94] presented the ability of COMSOL multiphysics to perform an optimization procedure by means of LiveLink for MATLAB module [95] based on Genetic Algorithms (GAs) technique.

The aim of optimization study is to find the most suitable geometric configuration of electrode parts of the dielectrophoretic MEMS device used for electro-deformation of biological cells. The optimization procedure consists of finding the optimal geometry and configuration of the set of electrodes for a given potential difference to maximize electro-deformation of cells with respect to the geometrical boundaries and experimental limitations. Parametric studies, performed in the previous section, are useful as they prepare some ideas on how to choose the upper and lower bounds of the parameters for an optimization algorithm. Genetics Algorithm has been chosen as the optimization technique. The optimization procedure is performed based on integration of COMSOL Multiphysics and MATLAB GA optimization toolbox. Results of the GA optimization are validated using a sweep in each design parameter while others are constant.

### 3.3.1 General formulation of the optimization problem

The optimization problem can be formulated as:

$$\text{Min } F(\vec{X}) = -f(\vec{X})$$

$$\text{Where } \vec{X} = (X_1, X_2, X_3, X_4)^T \in \mathcal{S}$$

$$\text{S.t } lb \leq \vec{X} \leq ub$$

Where  $\mathcal{S}$  is the solution space and  $f(\vec{X})$  is the displacement of a specific point on the cell membrane in direction of applied electric field. The point is chosen such that it demonstrates the maximum deformation on the cell membrane. Also  $lb$  and  $ub$  are the lower and upper bounds of the vector  $\vec{X}$  that is comprised of the following design variables:

$$\vec{X} = (X_1, X_2, X_3, X_4)^T$$

Where,  $X_1$  is the length of electrodes,  $X_2$  is the distance between electrodes,  $X_3$  is the tip angle of electrodes, and  $X_4$  is the medium relative permittivity. The lower and upper bound are chosen such that the distance between electrodes must be larger than the cell diameter ( $X_2 \geq 1.25D_c$ ), the tip angle of electrodes could be very sharp up to flat, and the medium relative permittivity must be less than the cell relative permittivity to achieve the positive Dielectrophoresis ( $X_4 \leq \epsilon_c$ ).

### 3.3.2 Optimization algorithm

First, a finite-element model consisting parametric geometries, material types, meshing, and physics interfaces is performed using COMSOL. Then, an optimization code based on Genetic Algorithms (GAs) is written in MATLAB which is linked with COMSOL. The optimization procedure will stop when the maximum generation is exceeded. The flow chart of the optimization process is shown in Figure 3.9 [94].

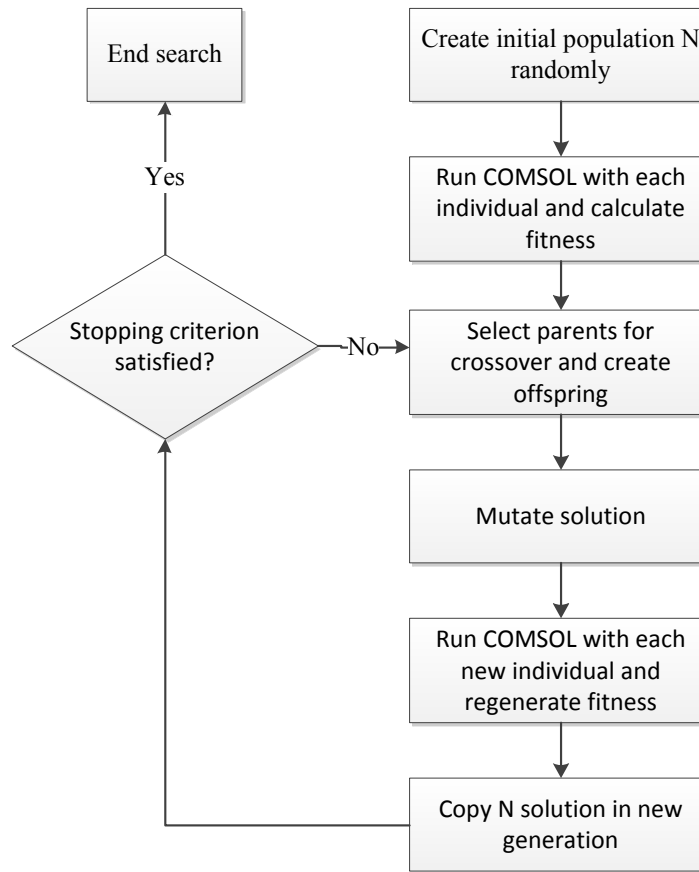


Figure 3.9: Flow chart of optimization process [94]

### 3.3.3 General concepts of the genetic algorithm optimization method

The genetic algorithm is a method for solving optimization problems that is based on natural selection, the process that drives biological evolution. The genetic algorithm repeatedly modifies a population of individual solutions. At each step, the genetic algorithm selects individuals at random from the current population to be parents and uses them to produce the children for the next generation. Over successive generations, the population evolves toward an optimal solution. You can apply the genetic algorithm to solve a variety of optimization problems that are not well suited for standard optimization

algorithms, including problems in which the objective function is discontinuous, non-differentiable, stochastic, or highly nonlinear.

The genetic algorithm uses three main types of rules at each step to create the next generation from the current population:

- Selection rules select the individuals, called parents that contribute to the population at the next generation.
- Crossover rules combine two parents to form children for the next generation.
- Mutation rules apply random changes to individual parents to form children.

### **3.3.4 Terminology of the genetic algorithm [96]**

Fitness Functions: The fitness function or objective function is the function that should be optimized. During the optimization procedure, the GA code attempts to find the minimum value for the fitness function.

Individuals: Any point comprising the vector of design variables  $\vec{X}$ , is an individual.

Populations and Generations: A population is an array of individuals in each generation.

Parents and Children: To create the next generation, first the best individuals in the current population are selected which are named parents. Children are individuals created from parents based on the value of Elite, Crossover, and Mutation fractions.

Elite, Crossover, and Mutation: The default for Elite is 2. It means that two of the best individuals in each generation will be transferred to the next generation. The crossover fraction defines the number of children created by parents while the mutation fraction defines the number of children created by a random change in an individual.

### **3.3.5 Optimization procedure**

The optimization procedure, in this study, is summarized in 4 steps as follow:

Step 1. Define the initial population.

Step 2. Create Elite, Crossover, and Mutation children from the initial population based on the defined options.

Step 3. Calculate the fitness value for each individual.

Step 4. If stopping criteria is satisfied, then introduce the individual associated with the minimum fitness value as an optimum design otherwise go to step.2

### **3.3.6 Optimum design of the problem**

Figure 3.1 shows a schematic drawing of a spherical cell in a non-uniform electric field. The input parameters of the model are defined in Table 3.2 and the design variables are shown in Fig 2.1.

Table 3.2: Input parameters for 3D optimization analysis

Description	Value
Cell radius	$10\ \mu m$
Cell relative permittivity	80 [92]
Cell density	$1150\ kg/m^2$
Cell Young's modulus	$600\ Pa$
Cell poisson ratio	0.37
Medium density	$1150\ kg/m^2$
Cytoplasm relative permittivity	60
Electrodes length	$X_1$
Electrodes distance	$X_2$
Tip angle	$X_3$
Medium relative permittivity	$X_4$
Model height	$60\ \mu m$

The problem is to find optimum geometries of electrodes to achieve maximum force and deformation on cell membrane. The fitness value in GA algorithm is calculated in every generation for each individual using a live-link to the COMSOL structural-electrostatic analysis. To better demonstrate the optimization procedure, the GA-COMSOL code is divided in four sub-codes in MATLAB including *run\_it.m*, *fun.m*, *model.m*, and *fl.m*. The code *run\_it.m* will call the genetic algorithm function, *ga*, at the command line of the MATLAB workspace as,

1) *run\_it.m*

```
nvars = 4; % Number of variables
```



```

gen=60;
pop_size=10;
lb=[15 25 1.57 10];
ub=[35 35 3 40];
%opts = gaoptimset;
rand('state', 71); % These two commands are only included to
randn('state', 59); %make the results reproducible
load opt % opt is pre-defined options that could be modified here
AA=[15 30 1.57 18;30 30 2 24;30 25 3 18];
options.InitialPopulation=AA;
options.Generations=gen;
options.StallGenLimit=gen;
options.PopulationSize=pop_size;
options.EliteCount=2;
options.CrossoverFraction=0.9;
options = gaoptimset(options,'Display', 'iter');
options = gaoptimset(options,'PlotFcns', { @gaplotbestf @gaplotdistance });
[answer,fitness] = ga(@fun, nvars,[],[],[],lb,ub,[],[1 2 4],options);

```

Where *nvars* is the number of variables, *gen* is the number of generation and stall generation as well, *pop\_size* is the number of population in each generation, *lb* and *ub* are the lower and upper bounds of design variables, respectively, *AA* is a matrix whose rows represent the initial population. The last line asks GA function to find the fitness value using a function defining the fitness function. It should be noted that the geometrical variables are integer values. To introduce them as integer, one should set the *IntCon* of the *ga* function to [1 2 4]. It means that  $X_1$ ,  $X_2$ , and  $X_4$  have integer values. The

parameters *rand* and *randn* are defined to make the result reproducible. The fitness function is defined in *fun.m* function code as,

2) *fun.m*

```
function y=fun(x)
assignin('base','x',x);
mymodel=model;
y = fl(mymodel)
```

The *fun* function defines the fitness function as a function of vector *X*, the design variables. Consequently *fl.m* will calculate the value of fitness function as:

3) *fl.m*

```
function U = fl(model)
1) x=evalin('base','x');
2) model.param.set('x1',x(1));
3) model.param.set('x2',x(2));
4) model.param.set('x3',x(3));
5) model.param.set('x4',x(4));
6) model.sol('sol1').run;
7) maxop1 = model.cpl.create('maxop1','Maximum','geom1');
8) maxop1.selection.set(3);
9) model.sol('sol1').updateSolution;
10) U = -1*mphglobal(model,'maxop1(u));
```

When a finite-element simulation is performed in COMSOL Desktop, one can save the model *M.file* for transferring the model to MATLAB. The model object contains all the information about a model, from the geometry to the results. The model object is

defined on the COMSOL server and can be accessed at the MATLAB command line using a live-link in MATLAB. LiveLink for MATLAB packages contains several functions to make it easy to access results directly from the MATLAB command line. For the present problem, line 7-10 will calculate the maximum deformations of the cell membrane in x-direction using *mphglobal* function. For transferring the result and edited parameters to COMSOL Desktop, it just needs to call the last function names *model.m* presented in the Appendix A.1.

### 3.3.7 Results

Figure 3.10 shows the result of the optimization algorithm for Crossover fraction of 0.9 where the population size is 10 and the stopping criteria is based on the maximum generation of 30.

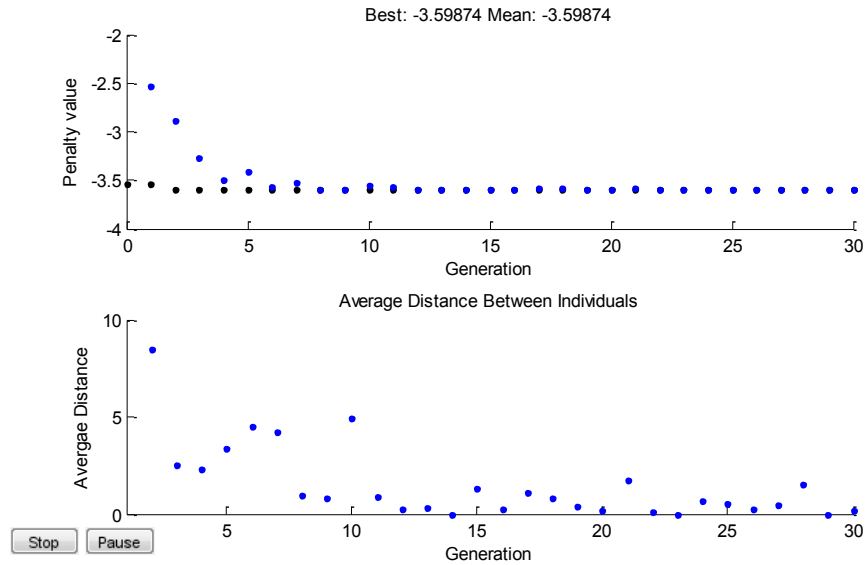


Figure 3.10: Result of the optimization algorithm for Crossover fraction of 0.9

Figure 3.10 also shows the average distance between individuals in each generation. The average distance between individuals is important as it shows the possibility to find the global optimal. If the distance is very high, the problem will need more generation to find the optimal point. On the other hand, if it is small, the algorithm is unable to find the global optimal point and may stop in a local minimal point. Several parameters influence the diversity of the population including the initial range, crossover fraction, and mutation fraction. Table 3.3 compares the results of optimization study based on different crossover fractions.

Table 3.3: Comparing different optimum points found by optimization algorithms associated with the different crossover fractions

Crossover fraction	Objective value ( $\mu\text{m}$ )	Optimum point $\mathbf{X}^* = (X_1, X_2, X_3, X_4)^T$
0.9	-3.59	(27, 25, 3, 16)
0.8	-3.56	(29, 25, 3, 16)
0.6	-3.56	(29, 25, 3, 16)

### 3.3.8 Validation of the genetic algorithm based optimization results

To validate the results found by GA optimization method and to investigate if the optimal points are global or local, several parametric sweep studies are performed by means of COMSOL Multiphysics. The procedure is such that in each parametric study one element of the optimum points  $\mathbf{X}^*$  in Table 3.3 sweeps along its bound (*lb-ub*) while the others are kept constant.

- Case 1. Sweep of the parameter  $X_1$

Figure 3.11 shows the curve of maximum deformation of the cell membrane in x-direction versus parameter  $X_1$ .

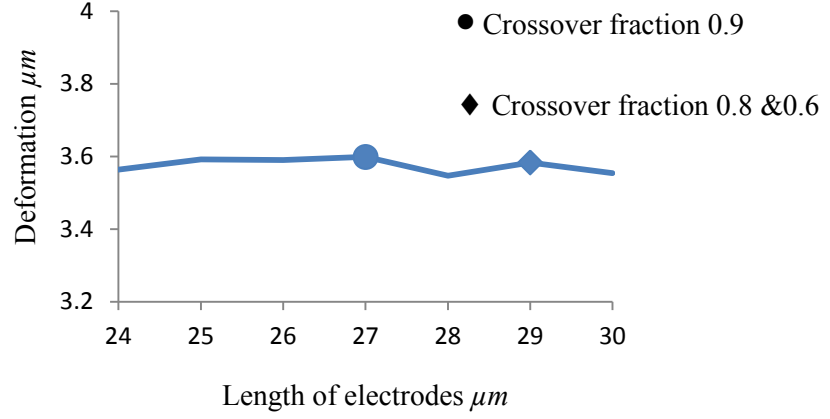


Figure 3.11: Maximum deformation of the cell membrane versus parameter  $X_1$

As is clear from Figure 3.11, the optimum points found using parametric sweep analysis by COMSOL are exactly those found by the GA code. Here, the point marked by a circle is the optimum point that the GA code found for crossover of 0.9 which is a global maximum point. This verification shows how the diversity of the population in a GA algorithm leads to the different results.

- Case2. Sweep of the parameter  $X_2$

Figure 3.12 shows the curve of maximum deformation of the cell membrane in X-direction versus parameter  $X_2$ .

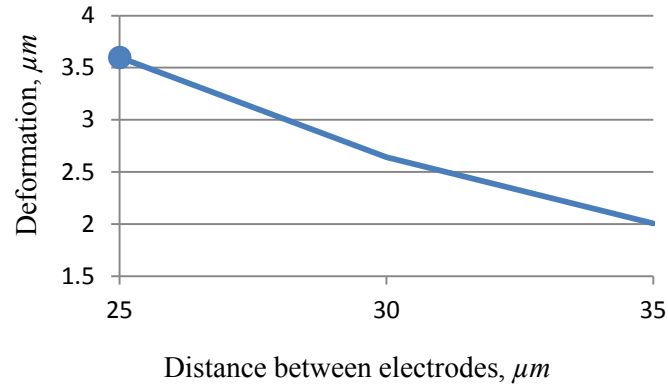


Figure 3.12: Maximum deformation of the cell membrane versus parameter  $X_2$

As Figure 3.12 shows, the maximum deformation occurs when the distance between electrodes is 25  $\mu m$  (in the lower bound). Also GA found the same point for all values of crossover fractions.

- Case 3. Sweep of the parameter  $X_2$

Figure 3.13 shows the curve of maximum deformation of the cell membrane in  $X$ -direction versus parameter  $X_3$ . The result shows that when the electrodes are sharp, the deformation of the cell is less. The maximum deformation occurs when the tip angle is 170° approximately.

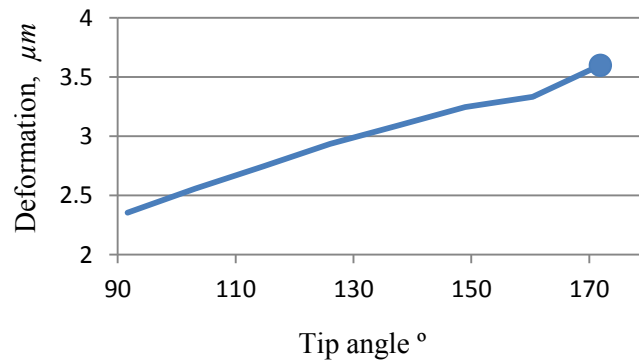


Figure 3.13: Maximum deformation of the cell membrane versus parameter  $X_3$

- Case 4. Sweep of the parameter  $X_4$

The last case is to study the influence of medium permittivity on cell deformation. As mentioned before, the electro-deformation occurs when the permittivity of the medium is less than that of the cell. Figure 3.14 shows the curve of maximum deformation of the cell membrane in x-direction versus parameter  $X_4$ . As is clear, the maximum deformation is related to medium permittivity of 16. The point associated with permittivity of 16 is also found by GA optimization method for all values of crossover fractions (see Table 3.3)

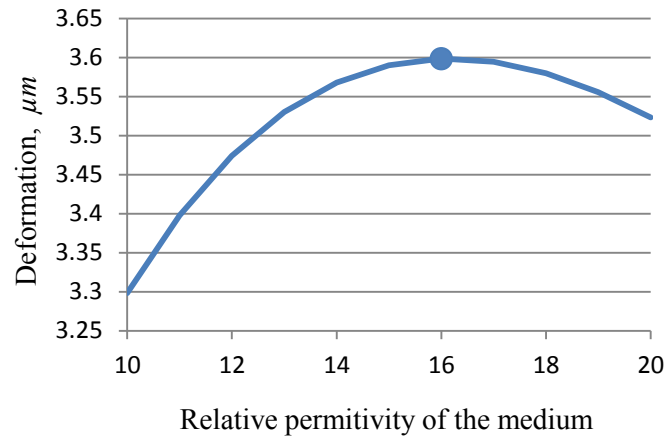
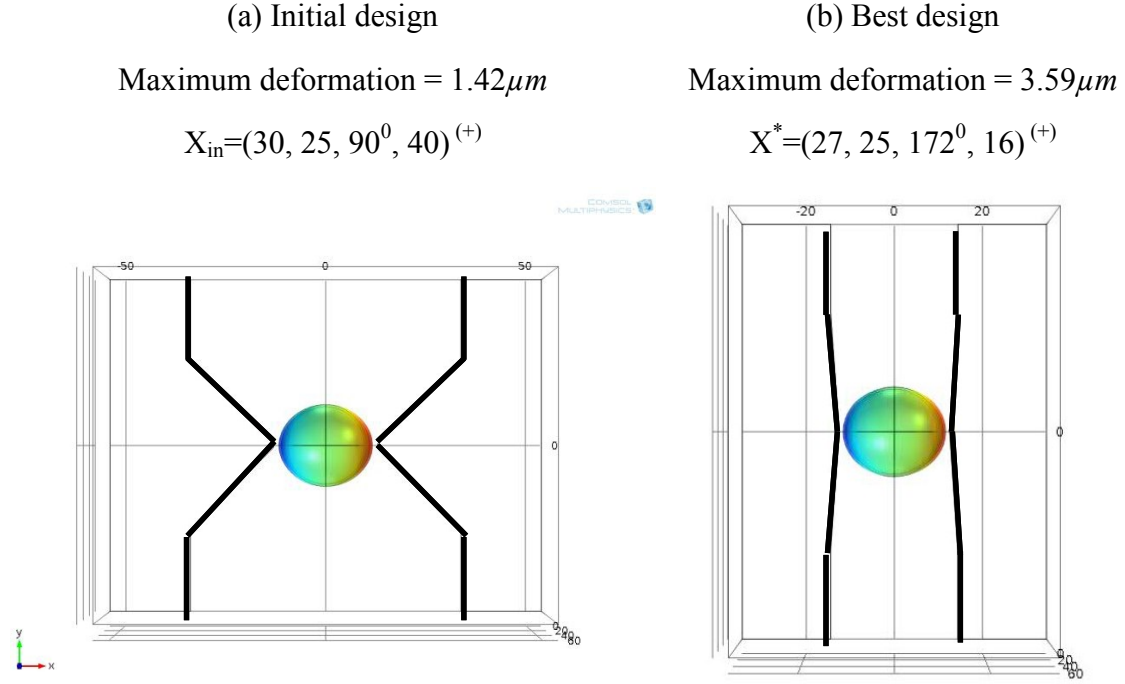


Figure 3.14: Maximum deformation of the cell membrane versus parameter  $X_4$

Based on Figure 3.14, results of optimization study restricted the maximum difference between permittivity of the medium with that of the cell. Despite the first assumption of electro-deformation of living cells that revealed more difference between permittivity of the medium with that of the cell led to more deformation on the cell membrane, optimization study showed that there is an optimum point where the induced deformation of the cell is maximum.

### 3.3.9 Best Design

Based on the input parameters given in Table 3.2, Figure 3.15 compares the electro-deformation of the cell in the initial design of microdevice chip with the best design found by optimization technique.




---

<sup>(+)</sup> $X=(X_1, X_2, X_3, X_4)$  where  $X_1 (\mu\text{m})$  is the length of electrodes,  $X_2 (\mu\text{m})$  is the distance between electrodes,  $X_3$  (degree) is the tip angle of electrodes, and  $X_4$  is the medium relative permittivity

---

Figure 3.15: Comparison of the maximum deformation of the cell in the initial design (a) and the best design (b)

The results show that, for a given potential difference, cells placed between flat electrodes exhibit more deformation. Also, more difference between cell permittivity and medium permittivity increases DEP forces and induced electro-deformation on neutral living cells. There is always some limitations and uncertainty about medium permittivity. For instance, adding a small amount of Glycerol oil in the prepared solution decrease the



permittivity of the medium but, as the media becomes very viscous and adherent, it limits the movement of the suspended cells. Also, to avoid thermal effects, the electrical conductivity of the medium should be kept very low that restricts the possibility of using different solution.

### **3.4 Conclusion**

Results of the above parametric study showed that the maximum deformation of a cell significantly depends on the geometrical properties of the model. It should be noted that, any change in the cell deformation less than  $0.1\text{ }\mu\text{m}$  has not been taken into account because it is not measurable with the imaging techniques used during the experimental studies. Based on this assumption, among different parameters, the distance between electrodes and the tip angle of electrodes have more influence on the cell deformation comparing with the length of electrodes. On the other hand, the limitations of preparing a medium for suspending the living cells lead to discounting the medium permittivity as a significant parameter. For choosing the best geometrical model, to achieve a maximum deformation, an optimization study has been performed and described in this chapter.

Design optimization of a MEMS device to induce maximum electro-deformations on living cells was performed by means of COMSOL- MATLAB (GA toolbox) integration. Crossover fraction influences directly the diversity of the individuals during optimization. Very high or low diversity leads to increasing the iteration number or stopping in a local minimum, respectively. As GA is based on random selection and modification of individuals, it might be unable to catch all the points in a feasible set. To validate the ability of GA algorithm, several parametric studies

have been performed to compare the results of GA with those found by parametric sweep feature-node of COMSOL Multiphysics. As discussed, the points found as local or global optimums are compatible with optimum points found by GA for different crossover fractions. As noted, in this study, the design variables are mixed integer. With the best knowledge of the author, among different optimization toolboxes of MATLAB 2012a, only GA has the ability to accept mixed integer variables. Furthermore, the best design configuration of the problem was compared with the initial design which showed an increase of more than two times in the maximum induced deformation on the cell in  $X$ -direction (see Figure 3.15).

## **Chapter 4: EXPERIMENTAL ANALYSIS OF ELECTRO-DEFORMATIONS OF SINGLE LIVING CELLS AND VALIDATION OF THE MODEL**

### **4.1 Introduction**

The results of electro-deformation process of two cancer cell lines, MDA-MB-231 (highly metastatic human breast carcinoma cell line) and MCF-7 (weakly metastatic human breast carcinoma cell line) using a positive DEP microdevice are presented in this chapter. The detailed process of cell preparation and suspension medium, experimental setup, and microdevice design are also briefly described. The electro-deformations of cells are simulated using COMSOL Multiphysics and elastic constants of cells are measured by comparing the finite element results with the experimental results. Furthermore, deformations of two cell lines are compared and the conclusion is presented.

### **4.2 Cell preparation protocol**

MDA-MB-231 and MCF-7, human breast cancer cell lines, have been obtained from the Center of Experimental Therapeutics in Cancer, (lady Davis Institute for Medical Research of the Sir Mortimer B. Davis-Jewish General Hospital, McGill University, Montreal, Canada).

Cells were cultured in 75  $cm^2$  tissue culture flask (Falcon) and fed every 48h with RPMI-1640 medium with 10% fetal bovine serum FBS and 1% penicillin. At 80-90% confluence, the cells were washed with phosphate buffered saline PBS, trypsinized with 0.05% Trypsin in 0.53  $mM$  EDTA and reseeded at a ratio of 1:4.

### **4.3 Suspension medium**

A medium solution with low conductivity was used in the experiments to prevent the thermal effects of Joule heating on the living cells. The medium has been prepared in the laboratory by adding 8.5% (w/v) sucrose plus 0.3% (w/v) dextrose to distilled water. The medium was filtered and then sterilized in order to avoid any contamination of the living cells during the experiments. The electrical conductivity of the medium was adjusted to the desired conductivity (5 to 10  $mS/m$ ) by adding a small quantity of trypsin. Addition of 700 $\mu L$  of Trypsin to 100  $mL$  of sucrose/dextrose provides a medium with conductivity of 10  $mS/m$ .

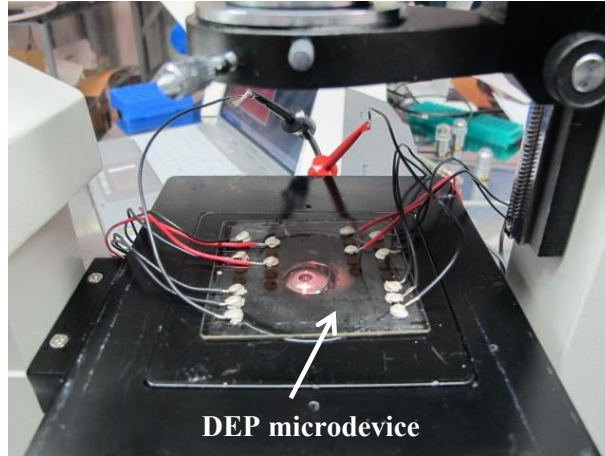
### **4.4 Specimen preparation**

Two different specimens of living breast cancer cells were used in the experiments. The procedure of preparation of the specimens is given below:

- a. Liquid media covering cells were removed using the aspirator.
- b. Cells were washed with 5  $ml$  of phosphate buffered saline (PBS) for a 30  $s$  and then PBS was removed from the flask using the aspirator.
- c. Cells were trypsinized by adding 3  $ml$  of 0.05% Trypsin in 0.53  $mM$  EDTA to the flask and incubated for 5 minutes until they detached from the flask.
- d. Cells were removed from the incubator and checked under the microscope to ensure detaching of cells from the walls of flask.
- e. 5  $ml$  of RPMI-1640 was added to the flask and then the solution was mixed consistency to prevent any cluster of cells.
- f. Cells were counted using the hemocytometer.

- g. The solution were transferred into 15 *ml* centrifuge tubes and centrifuged for 4 min at 500*g*.
- h. After centrifugation, cells pellet would settle down at the bottom of the tube and liquid medium could be removed using the aspirator.
- i. Cells were suspended in the sucrose/dextrose medium with adjusted electrical conductivity made by Trypsin as described earlier. Cells pellet has been suspended carefully to avoid any cluster of cells.
- j. For MCF-7 specimen a ratio of 2:1 of sucrose/dextrose medium to distilled water is needed. It has been observed that adding this quantity of water is needed to prevent the cells membrane of absorbing too much of sucrose/dextrose and keep the shape of cells spherical. For MDA-MB-231 the step (i) is enough for having spherical cells.
- k. A droplet of the specimens was placed on the P-DEP device shown in Figure 4.1.
- l. A difference of potential of 2 Volts, peak-to-peak, with frequency of 1*MHz* was applied to the cells in order to achieve P-DEP phenomenon and trap the cells at the tips of the electrodes where the electric field is higher as illustrated in figure 4.3.
- m. The applied voltage was increased by small steps to 20 Volts peak-to-peak in five minutes at same frequency of 1*MHz*.
- n. The process was performed in the clean room to prevent any contamination and cells were kept under 20 Volts peak-to-peak applied voltage for 10 minutes for achieving electro-deformation as shown in Figure 4.4.

(a)



(b)

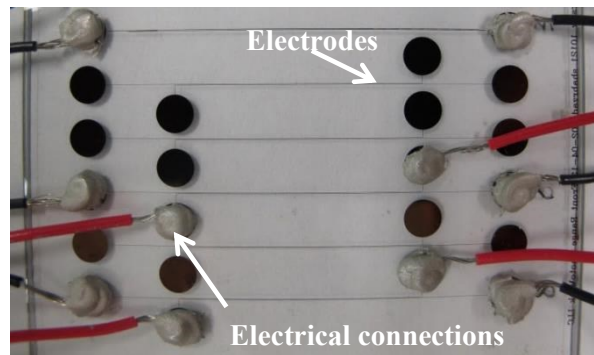


Figure 4.1: (a) The P-DEP microdevice for trapping and stretching the living cells, (b) Electrode lines and electrical connections

#### 4.5 Experimental setup

The experimental setup shown in Figure 4.2 consists of the followings:

- 1- A function generator source to supply potential difference to the microdevice with the required  $AC$  signal.
- 2- The electro-deformation P-DEP microdevice (shown in Figure 4.1)
- 3- Inverted microscope for observation
- 4- Digital camera to record the images of the electro-deformation process.
- 5- Computer to visualize the electro-deformation of living cells.

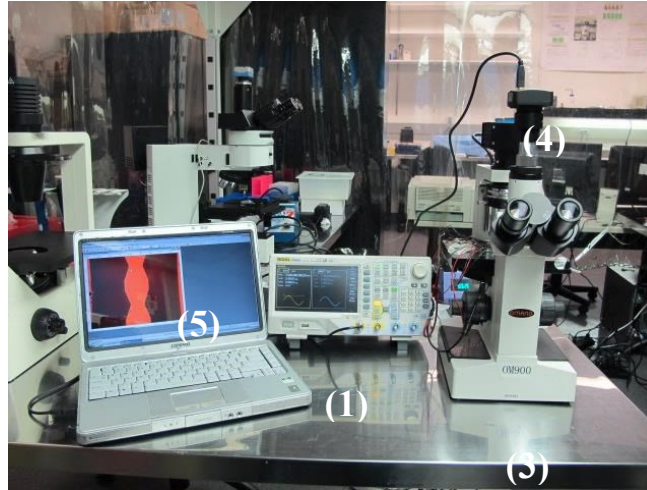


Figure 4.2: Experimental setup for trapping and stretching the living cells

#### 4.6 Microdevice design and fabrication (P-DEP device)

The experimental electro-deformation microdevice was designed to be capable to stretch cells with the diameters of 8 to 20  $\mu m$ . The configuration of the device was established based on the simulations prior described. The device consists of different structures with a variety of electrodes positioned at variable distances and of various shapes. The distance between electrodes was ranged from 15 to 45  $\mu m$ . Triangle shaped electrodes with different tip angles and also parallel electrodes have been designed to induce maximum deformation on the cells in a given voltage. As discussed in chapter 3, the results based on modeling indicate the maximum deformation of cells is expected when placed between parallel electrodes.

Fabrication of the microdevice was carried out by Fineline Imaging Company based on the design provided by the candidate. Very thin layer electrodes (100-250  $nm$ ) are etched on a Ni coated glass substrate. Electrical connections have been installed in the laboratory by means of a conductive epoxy and copper wires as shown in Figure 4.1b.

## 4.7 Experimental analysis of cancer living cell lines

Experimental procedure of electro-deformations of two breast cancer cell lines and the method of estimating the Young's modulus of cells are described in the following sub-sections.

### 4.7.1 Electro-deformation of MDA-MB-231 and MCF-7 cell lines

As described earlier, first an AC potential difference of 2 Volts peak-to-peak with 1 MHz of frequency is applied between electrodes. The applied voltage induces a net positive dielectrophoretic force on the cells that directs the cell toward the tip of electrodes or where the intensity of the electric field is higher, as shown in Figure 4.3.

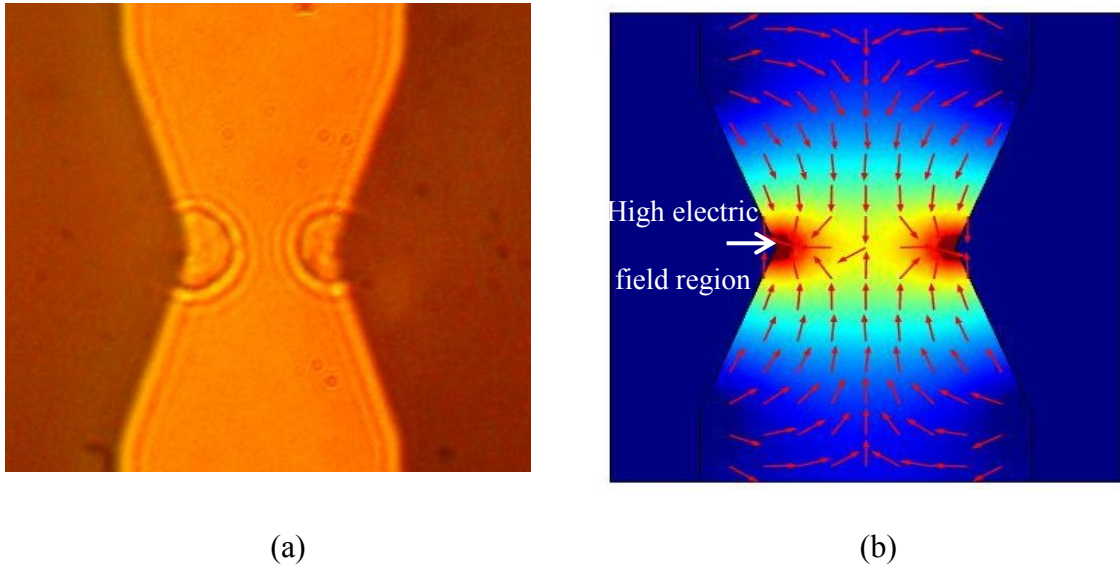


Figure 4.3: (a) MCF-7 cells are attached to the tips of electrodes, (b) Finite element simulation of electric field between the electrodes using COMSOL. The arrows indicate the direction of the dielectrophoretic force. The background contours indicate the electric field strength

To induce electro-deformation on cells, the applied voltage was increased up to 20 Volts peak-to-peak and kept in this voltage for 10 to 15 minutes. Figure 4.4 shows two MDA-MB-231 cells before and after 10 minutes of exposure of 20 Volts voltage. Figure



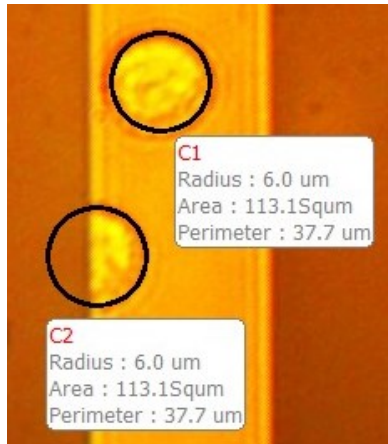
A.2 in the appendix shows more captured images of the trapping-stretching procedure of the sample cells.



(a-1) Captured image of trapping the cells upon applying 2 Volts



(b-1) Captured image of stretching the cells after 10 minutes of exposure of 20 Volts



(a-2) Calibrated image of trapping the cells upon applying 2 Volts



(b-2) Calibrated image of stretching cells after 10 minutes of exposure of 20 Volts

Figure 4.4: MDA-MB-231 trapping- stretching-procedure (a) Trapping the cells upon applying 2 Volts(b) Stretching the cells after 10 minutes of exposure of 20 Volts

Several attempts have been performed for different samples. The detailed procedure of increasing the applied voltage is such that first an AC potential difference of 2 Volts is applied between electrodes. After trapping the cells, the applied voltage is

suddenly increased to 5 Volts. After making sure that no more cells are around the high electric field region (about 2 minutes), the applied voltage is increased to 10 Volts and then, after 2 minutes, to 20 Volts. The applied voltage will be kept at this voltage for 10 minutes. To prevent the negative thermal effects of Joule heating on the cells, the applied potential difference should be always less than 40 Volts peak-to-peak.

The range of cells radius and results of experimental deformations for both cell lines are listed in Table 4.1. Measurements have been performed using Motic Images plus 2 Digital Microscopy Software Suite.

Table 4.1: Statistical results of the experimental electro-deformations of MDA-MB-231 and MCF-7 cells

Cell line	Radius ( $\mu m$ )	Deformation ( $\mu m$ )	Deformation ratio
MDA-MB-231, 20 cells	5.97 $\pm$ 0.88	1.153 $\pm$ 0.49	0.19 $\pm$ 0.08
MCF-7, 15 cells	5.88 $\pm$ 0.72	0.69 $\pm$ 0.33	0.11 $\pm$ 0.05

Here, the deformation is the elongation of cell radius parallel to the applied electric field and deformation ratio is the ratio between the total elongation of the cell and the original diameter of the cell. Statistical results are presented in the form of “mean values  $\pm$  standard deviations” although the number of experiments reported to the population is relatively small. Comparing the experimental results demonstrates that invasive MDA-MB-231 cells are softer than non-invasive MCF-7 cells. Although the sizes of the two cell lines are almost same, elongations of MDA-MB-231 cells are almost twice higher than those of MCF-7 cells that might help cancer cells to migrate through the capillary vessels to other organs and thus being highly metastatic. Figure 4.5 shows and compares the electro-deformation of two different cell lines.

Cell line	Trapping the cells upon applying 2 Volts	Stretching the cells after 10 minutes of exposure of 20 Volts
(a) Captured images of trapping –stretching procedure of MDA-MB-231		
(b) Calibrated images of trapping –stretching procedure of MDA-MB-231	<div data-bbox="781 611 948 705"> <b>C1</b>  Radius : 6.0 <math>\mu\text{m}</math>  Area : 113.1S<math>\mu\text{m}^2</math>  Perimeter : 37.7 <math>\mu\text{m}</math> </div> <div data-bbox="690 768 857 863"> <b>C2</b>  Radius : 4.8 <math>\mu\text{m}</math>  Area : 72.4S<math>\mu\text{m}^2</math>  Perimeter : 30.2 <math>\mu\text{m}</math> </div>	<div data-bbox="1219 642 1414 758"> <b>E1</b>  Major half axis : 7.2 <math>\mu\text{m}</math>  Minor half axis : 5.4 <math>\mu\text{m}</math>  Area : 122.1S<math>\mu\text{m}^2</math>  Perimeter : 40.0 <math>\mu\text{m}</math> </div> <div data-bbox="1219 852 1414 915"> <b>E2</b>  Major half axis : 5.6 <math>\mu\text{m}</math>  Minor half axis : 4.6 <math>\mu\text{m}</math> </div>
(c) Captured images of trapping –stretching procedure of MCF-7		
(d) Calibrated images of trapping –stretching procedure of MCF-7	<div data-bbox="690 1367 857 1461"> <b>C1</b>  Radius : 5.0 <math>\mu\text{m}</math>  Area : 78.5S<math>\mu\text{m}^2</math>  Perimeter : 31.4 <math>\mu\text{m}</math> </div> <div data-bbox="690 1535 857 1629"> <b>C2</b>  Radius : 5.6 <math>\mu\text{m}</math>  Area : 98.5S<math>\mu\text{m}^2</math>  Perimeter : 35.2 <math>\mu\text{m}</math> </div>	<div data-bbox="1073 1272 1268 1388"> <b>E1</b>  Major half axis : 5.6 <math>\mu\text{m}</math>  Minor half axis : 4.8 <math>\mu\text{m}</math>  Area : 84.4S<math>\mu\text{m}^2</math>  Perimeter : 32.8 <math>\mu\text{m}</math> </div> <div data-bbox="1073 1524 1268 1629"> <b>E2</b>  Major half axis : 6.6 <math>\mu\text{m}</math>  Minor half axis : 5.2 <math>\mu\text{m}</math>  Area : 107.8S<math>\mu\text{m}^2</math>  Perimeter : 37.3 <math>\mu\text{m}</math> </div>

Figure 4.5: (a) & (c) Captured images of trapping - stretching of breast cancer cell lines

(b) & (d) Calibrated images using Motic Images Digital Microscopy Software Suite

#### 4.7.2 Estimation of Young's modulus for the two cell lines

The Young's modulus of cells is calculated by matching the deformation of cells obtained experimentally by adjusting the parameters of the simulation in the finite element analysis. Finite element analysis is performed by means of COMSOL Multiphysics (details have been presented in chapter two). For this end, a value for the Young's modulus of the cell is assumed (collected from the published literatures) for given input parameters presented in Table 4.2. Second, the calculated elongation of cell is compared with the experimental results. Then, by sweeping the value of Young's modulus using parametric study feature node of COMSOL Multiphysics, approximate suitable value of the Young's modulus of the cell is extracted such that the deformation of cells from the simulation coincides with the value obtained from the experiments.

Table 4.2: Input parameters of the electro-deformation model of cells

Description	Value
Cell radius	$5.8 \mu m$
Membrane-specific capacitance (MDA-MB-231)	$26 \text{ mF/m}^2$ [97]
Membrane-specific capacitance (MCF-7)	$13 \text{ mF/m}^2$ [92]
Cell density	$1150 \text{ kg/m}^3$
Cell Young's modulus	$500 \text{ Pa}$
Cell poisson ratio	$0.37$
Medium density	$1150 \text{ kg/m}^3$
Cytoplasm relative permittivity	$57$ [97]
Medium relative permittivity	$40$ [87]

Given the uncertainty in the relative permittivity of the medium a value that would yield the closest matching with the experiments was selected from the literature [87], and [98]. Hence, the deformation of cells in the simulation could mimic the actual

deformation of cells observed during experiments. It should be noted that the permittivity of medium should be less than that of the cells to achieve positive dielectrophoresis.

As described in chapter 2, when a cell is placed between electrodes, the positive dielectrophoretic forces cause the cell to move and settles down on one electrode boundary such that the total force on the cell is balanced out (i.e. cell equilibrium position). By increasing the applied electric field, the distributed DEP forces on the two cell halves lead to an elongation of cell which is observable in the plane of motion. To find out the equilibrium position of the cell during the simulation, cells are placed in vicinity of one electrode where the net DEP forces (i.e. integration of the Maxwell stress tensor over each-half of the cell surface in the direction of applied field) will cancel out. Figure 4.6 shows the deformation of the cell after applying a potential difference of 20 Volts peak-to-peak between electrodes as resulted from the simulation.

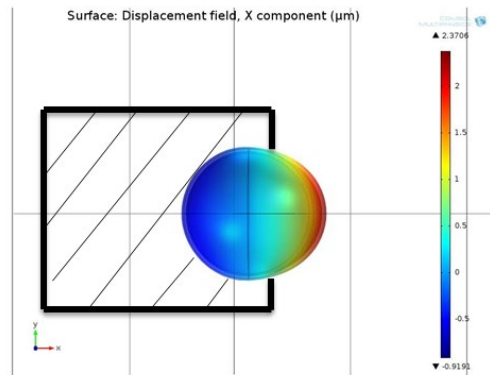


Figure 4.6: Deformation of the cell near one electrode in equilibrium position

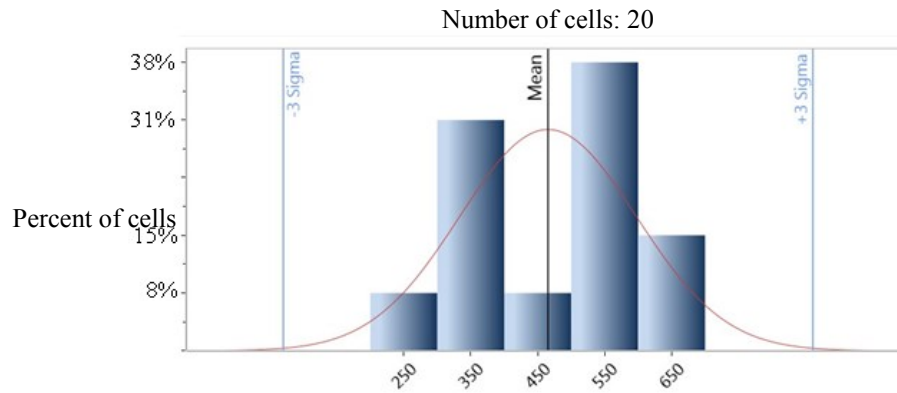
Since the equilibrium position depends on the electrical properties of the components in the model as well as the radius of the cell, the value changes for each size of the cell.

By modifying the calculated deformations obtained from simulation based on measured deformation obtained from the experiments, Table 4.3 shows the calculated Young's modulus for both cell lines. The calculations of Young's modulus were performed based on the control limits approach.

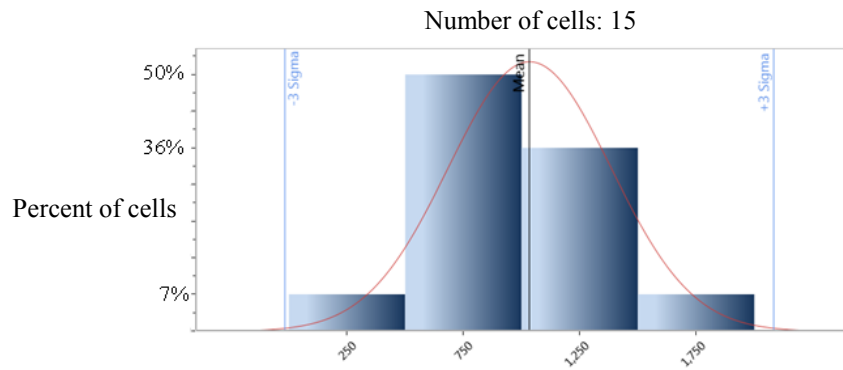
Table 4.3: Calculated values of Young's modulus of MDA-MB-231 and MCF-7 cells

Cell line	Radius ( $\mu m$ )	Young's modulus ( $Pa$ )
MDA-MB-231 20 cells	$5.97 \pm 0.88$	$478 \pm 45.36$
MCF-7, 15 cells	$5.88 \pm 0.72$	$1046 \pm 149.16$

Figure 4.7 shows the histogram of calculated Young's modulus of the two cell line.



(a) Young's modulus of MDA-MB-231 ( $Pa$ )



(b) Young's modulus of MCF-7 ( $Pa$ )

Figure 4.7: Histogram of calculated Young's modulus of MDA-MB-231(a), and MCF7 (b)

In order to examine the sensitivity of the calculated Young's modulus to the number of individual cells, the total measurements of cell properties were divided into five subgroups randomly and the average value of each subgroup was calculated. Figure 4.8 shows the mean control chart of Young's modulus to monitor changes in the mean of total process. The standard error of the mean,  $S.E$ , is defined as:

$$S.E = Z\sigma_{\bar{x}} = 3 \times \frac{\sigma}{\sqrt{n}}$$

Where  $\sigma$  is the population standard deviation and  $n$  is the number of observation per sample. The standard normal variable,  $Z$ , is set to 3 for 99.74% confidence.

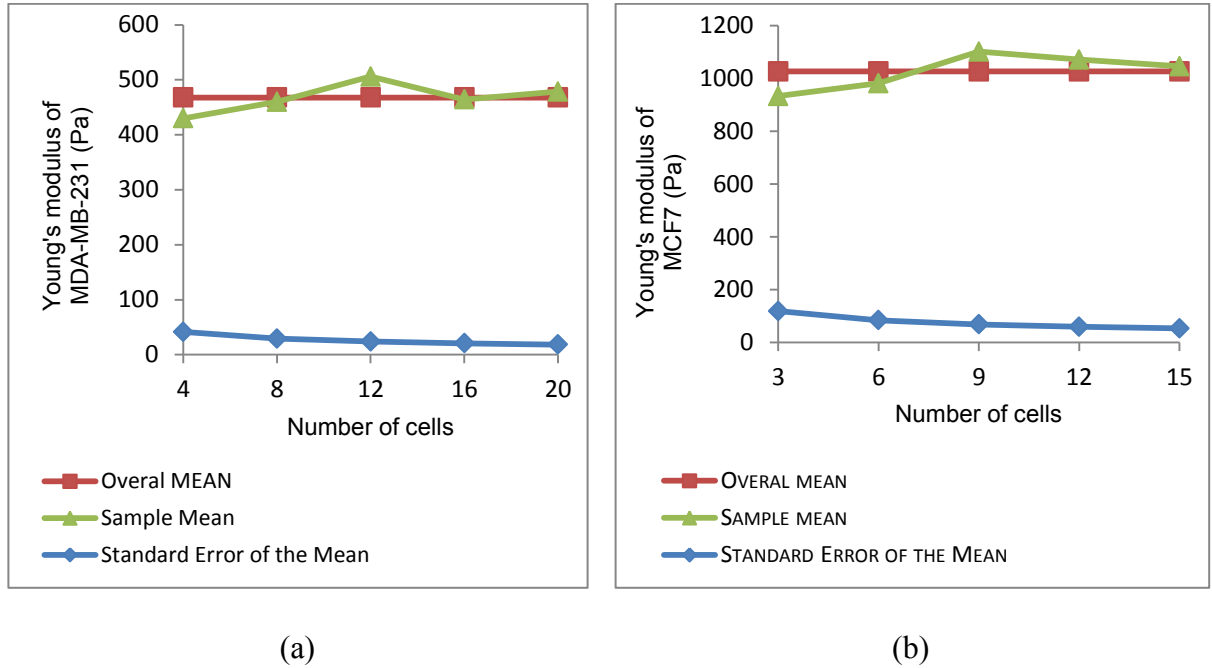


Figure 4.8: Mean control chart of Young's modulus of MDA-MB-231 (a), and MCF-7 (b)

As expected, the standard error of the mean of Young's modulus of cells is decreased with increasing the number of samples cells. As clear from Figure 4.8, the change of Young's modulus versus number of cells is not linear. Since the observed

samples have been randomly selected, more individual cells should be examined to conclude the total needed of cells for achieving maximum accuracy of calculated Young's modulus of cells.

#### 4.8 An improved design to trap the cells in the middle of electrodes

One of the challenges encountered in the experimental work was positioning of the cells between two electrodes. This is clearly illustrated by Figures 4.3, 4.4 and 4.5. This challenge led to a new improved design of the P-DEP device.

One way to induce symmetric deformation on a cell is to hold the cell between two electrodes where the net forces on the cell surface become zero and also the distributed DEP forces on the cell lead to a symmetric deformation on the cell as shown in Figure 4.9.

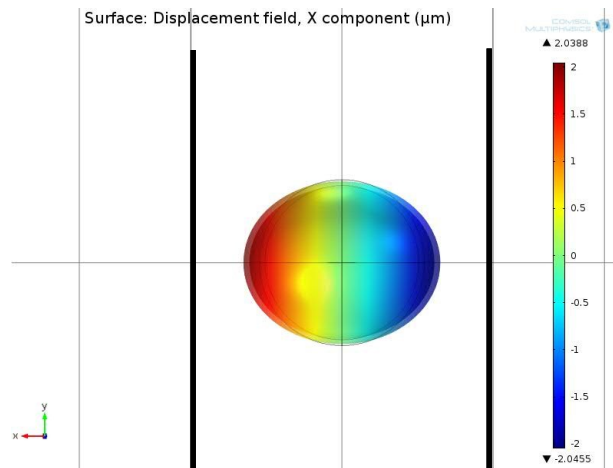


Figure 4.9: Symmetric deformation of a cell positioned at the center line between electrodes

Performing this positioning during experiments would be possible just by using two pairs of electrodes as shown in Figure 4.10.



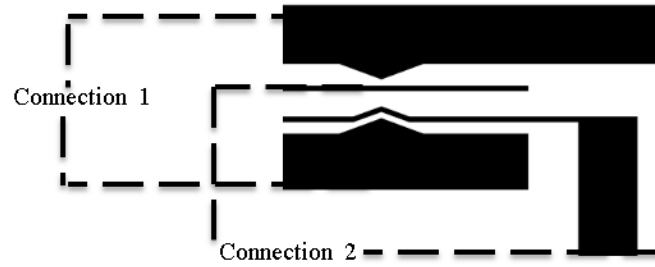
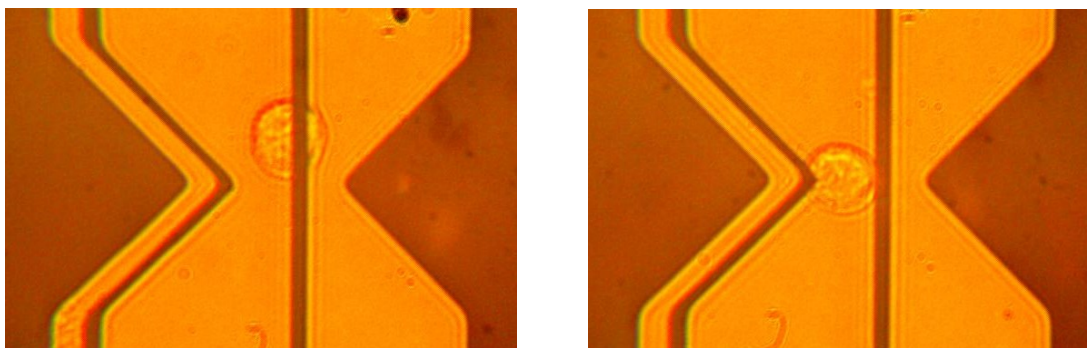


Figure 4.10: Configuration of two electrode circuits to apply symmetric deformations on cells

The procedure of inducing the symmetric deformation on a cell is given below:

- a. Deposit a droplet of suspended cells in media on the chip
- b. Applying a potential difference of 2 Volts p-p, 1 MHz between the positioning (thin) electrodes via connections No.2
- c. Increase the voltage of connections No.2 up to 5 Volts p-p, 1 MHz to fully hold the cells near the tips of left electrode
- d. Apply a potential difference of 5 Volts p-p , 1 MHz between deformation (thick) electrodes via connections No.1
- e. Increasing the voltage of connections No.1 up to 20 Volts p-p, 1MHz to induce a symmetric electro-deformation on the cell.

Figure 4.11 shows the symmetric elongation of a MDA-MB-231 cell performed by two set of electrodes. It should be noted that, depending on the cell size, the applied potential difference between thin electrodes should be tuned to prevent the cell deflecting from the center.



(a) Cell is approaching to highest electric field

(b) Cell is held by thin electrodes and stretched by thick electrodes in the middle

Figure 4.11: Trapping and stretching a MDA-MB-231 cell in the middle of thick electrodes

It should be noted that, since the applied voltage to the positioning (thin) electrodes is not cut during cell stretching, the total deformation of cells could be due to total forces applied by both set of electrodes. Furthermore, due to proximity of electrodes and high frequency of applied voltage, the possibility of induced current should be considered. More investigation is needed to study the influence of electrodes shape and arrangement on the electro-deformation of cells in the improved design. Here the electric field is different. Figure 4.12 shows the finite element simulation of electric field around the electrodes using COMSOL Multiphysics.

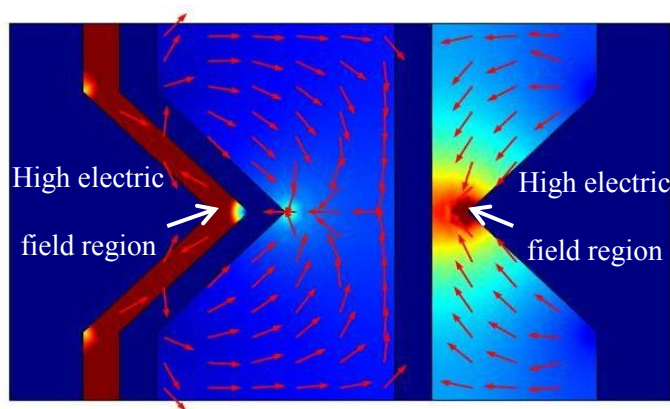


Figure 4.12: Finite element simulation of electric field. The arrows indicate the direction of the dielectrophoretic force. The background contours indicate the electric field strength

#### **4.9 Comparison of the obtained results with the results presented in the literature**

The experimental results of the present study demonstrate that invasive MDA-MB-231 cells are softer than non-invasive MCF-7 cells. Also, the results confirm that metastatic cells are mechanically softer than non-metastatic and weakly metastatic cells of the same type, as reported in other works. To the best knowledge of the candidate, few studies have been carried out to compare the deformability of human breast cells of different lines. For instance, Lee et al. (2012) [99] demonstrated that malignant and metastatic breast cells showed low resistance to deformation. They used atomic force microscopy to measure the Young's modulus of adherent human breast cells at the different states. They reported average amounts of 800 *Pa* for MDA-MB-231, 1300 *Pa* for MCF-7, and 1700 *Pa* for MCF10A (normal human breast epithelial cells) in the cytoplasm region. The results of their study are higher than the values of Young's modulus measured in the present study because; the cells that are adherent and attached to the substrate respond more elastic comparing to those that are suspended in the medium and deform due to cytoskeletal changes [100].

Among different techniques measuring mechanical properties of living cells, as discussed in chapter one, optical stretchers, micropipette aspiration, microfluidic channels, and DEP based devices are applicable for suspended cells. For instance, Guck et al. (2005) [101] measured deformation ratios of  $0.21 \pm 0.011$  for MCF-7 cells, and  $0.33 \pm 0.014$  for MDA-MB-231 using a microfluidic optical stretcher with an incident light power of 600 *mW*.

Microfluidic channels have also the ability to mimic the *in vivo* movement of living cells flowing through capillaries. Hence, in the recent years, investigations of cell deformability flowing through microfluidic channels have attracted much attention. For instance, Hou et al. [102] (2009) observed that MCF-7 cells generally have higher elongation indices compared with MCF-10A cells for the same cell sizes. As the elongation index provides information on the elasticity of the cell, this indicates that cancerous MCF-7 cells compress and elongate more in the microchannel compared to benign MCF-10A cells. This result is also consistent with findings by Lincoln et al. [103] (2004) who have used the optical stretcher to stretch both MCF-7 and MCF-10A cell lines. They have found that MCF-7 cells can stretch five times more than normal cells.

Cell elastic properties, as demonstrated in the present study, could be used as a biomarker to discriminate between normal and cancerous cells and could be practical in cancer diagnostic application. The problem that might restrict such investigations is that, there are several reasons demonstrating that single living cells do not have a unique value of Young's modulus, including:

- 1) When an external mechanical load is applied to the cell structure, most living cells (except the rigid cells such as bone cells) suffer large deformations.

- 2) In some cases, cell deformation is a function of both the magnitude of the external load and the loading rate [104].

- 3) Different regions of a single living cell (i.e. nuclear region or rest of the cell body) have different values of Young's modulus [99].

4) For the cells with very thin membranes, such as bilayer human cells, the different experimental methods (due to the technique used to indent the cell surface) lead to different values of elastic properties of a cell surface [14].

5) Elastic properties of the living cells alter during the cell life [4]. This evidence could be seen as a support of various values of Young's modulus for a single living cell (see Table (1) in the reference paper [14]).

6) The medium composition affects the elasticity of living cells. For instance, Nikkhah et al. (2011) [105] considered the influence of the growth medium in mechanical properties of human breast cells. They measured the Young's modulus of MDA-MB-231 cell line ranging from  $500 \pm 350$  (Pa) to  $370 \pm 250$  (Pa) based on different medium solutions (see Table 2 in appendix A-2 [105]).

#### **4.10 Conclusion**

The ability of a positive DEP based microdevice to trap and stretch living cells was demonstrated in this chapter. The electro-deformations of invasive MDA-MB-231 cells were measured and compared with that of non-invasive MCF-7 cells. Concurring with the previous works, the results of this study showed that highly metastatic breast cancer cells (MDA-MB-231) were much softer than weakly metastatic breast cancer cells (MCF-7), such that they could squeeze easier and migrate into human tissue through capillary blood vessels. The significant difference between mechanical properties of different cancerous cell lines, as demonstrated in Table 4.1 and Table 4.3, could be used as a label free biomarker to distinguish between invasive and non-invasive carcinoma

cells whose shapes and sizes are roughly the same. The author could not find any published study investigating the electro-deformability of human carcinoma breast cells using DEP based devices. However, the results of this study, by its very nature, are in good agreement with those published in the literature as discussed in section 4.9.

## **Chapter 5: SUMMARY AND FUTURE WORK**

### **5.1 Summary of the research study**

Many diseases such as cancers start with single living cell that induce certain biological activities in the adjacent normal cells, and consequently make permanent changes in the mechanical properties of normal cells. The difference between the mechanical and structural properties of normal and abnormal cells, which in most cases is significant, can be the starting point toward recognizing the abnormal cells which generally live beside the normal cells. In the last three decades, experimental methods have proven their ability to measure the mechanical properties of living cells, but their limitations have also been reported.

Some of the experimental methods, such as atomic force microscopy (AFM), despite their high accuracy, can be used only for adhered cell assessment and some of them which are applicable for suspended cells, such as micropipette aspiration, cannot measure the frequency-dependent responses of the living cells. It can be said that the efficiency of each method is strongly dependent on what that method is used for.

The first chapter of the thesis provided a critical review of the recent experimental methods and equipment for single cell assessments. Among recent experimental methods, dielectrophoresis (DEP) based devices have been introduced as novel techniques to directly measuring the living cell deformations. Dielectrophoretic forces are field-induced forces exerted to electrical-neutral charged living cells subjected to a non-uniform external electric field and could leads to cell elongations. The second chapter of the thesis

presented the fundamental theories of electro-deformation of living cells based on DEP phenomena and two mostly used methods for calculation dielectrophoretic forces were introduced. Furthermore, a finite element simulation of electro-mechanical analysis of a shelled-spherical cell in a non-uniform electric field using COMSOL Multiphysics 4.2a was achieved as well.

In the chapter three, parametric studies were performed to investigate the influence of the design parameters of a DEP microdevice on the electro-deformation of neutral biological cells. For choosing the best geometrical model, to induce maximum deformations on cells, an optimization study was performed and described as well. Design optimization of a MEMS device to induce maximum electro-deformations on living cells was performed by means of COMSOL- MATLAB (GA toolbox) integration. Comparing the initial design with optimum design showed an increase of more than two times in the maximum induced deformation on the cell in X-direction (see Figure 3.15).

The results of electro-deformation process of two cancerous cell lines, MDA-MB-231 (highly metastatic human breast carcinoma cell line) and MCF-7 (weakly metastatic human breast carcinoma cell line) using a positive DEP micro-device were presented in chapter four. The electro-deformations of cells were simulated using COMSOL Multiphysics and elastic constants of cells were measured by comparing the finite element results with the experimental results. Concurring with the previous works (regarding this fact that few studies have been carried out to compare the deformability of human breast cells of different lines), the results of this study showed that highly metastatic breast cancer cells (MDA-MB-231) were much softer than weakly metastatic breast cancer cells (MCF-7), such that they could squeeze easier and migrate into human



tissue through capillary blood vessels. The significant difference between mechanical properties of different cancerous cell lines, as demonstrated in Table 4.1 and Table 4.3, could be used as a label free biomarker to distinguish between invasive and non-invasive carcinoma cells whose shapes and sizes are roughly the same.

An improved design to trap the suspended living cells in the middle of electrodes was presented and experimentally tested in the present work. Inducing symmetric elongation on cells could improve the accuracy of calculated elastic constant of cells. Also, as the cells are positioning between electrodes (in the transparent zone), the visibility of captured images and accuracy of calibrated images could be improved. However, holding the cells between electrodes for several minutes to apply maximum electro-deformations is another challenge that needs more investigations.

## **5.2 Areas of further study**

DEP based devices apply minimum permanent biological effects on living cells but, due to this fact that the individual cells have to be positioned near the electrodes, measurement are low throughput. Also, after each experiment, the droplet of cells should be removed and the chip should be cleaned carefully for the next experiment. To increase the speed of manipulation and assessment of living cells, integration of a microfluidic device with the presented DEP device needs to be studied. Cells passing through a micro-channel could also experience electro-deformations by cutting the fluid flow and applying a non-uniform electric field. The process could be repeated for rest of the cells.

As discussed in 4.8, one way to induce symmetric deformation on a cell is to hold the cell between two electrodes where the net forces on the cell surface become zero and also the distributed DEP forces on the cell lead to a symmetric deformation on the cell as shown in Figures 4.9 and 4.11. Since the applied voltage to the positioning (thin) electrodes is not cut during cell stretching, the total deformation of cells could be due to total forces applied by both set of electrodes. Furthermore, due to proximity of electrodes and high frequency of applied voltage, the possibility of induced current should be considered. More investigation is needed to study the influence of electrodes shape and arrangement on the electro-deformation of cells in the improved design. The experimental procedure of using two different electrode circuits could be developed such that the movements of the cells would be completely under control.

Generally, statistical approaches are used to present the calculated Young's modulus of living cells. The mostly used form is based on standard deviation. However, when the number of experiments reported to the population is relatively small, other approaches such as control limits are more appropriate. As the change of Young's modulus versus number of cells is not linear (see Figure 4.8), not always more examined cells leads to more accuracies in calculated results. The total needed of cells for achieving maximum accuracy while considering time consuming is an area of interest and could be studied. Also, different cell lines might be examined in order to clarify the resistance of different cells against mechanical deformations.

## References

1. Linnemeyer, P., *The immune system—an overview*. The Body: The Complete HIV/AIDS Resource. Retrieved November, 1993. **13**: p. 2006.
2. Byers, T., *Two Decades of Declining Cancer Mortality: Progress with Disparity*. Annual Review of Public Health, 2010. **31**(1): p. 121-132.
3. van Baak, M.A. and T.L. Visscher, *Public health success in recent decades may be in danger if lifestyles of the elderly are neglected*. Am J Clin Nutr, 2006. **84**(6): p. 1257-1258.
4. Starodubtseva, M., *Mechanical properties of cells and ageing*. Ageing Research Reviews, 2009.
5. Lekka, M., et al., *Local elastic properties of cells studied by SFM*. Applied Surface Science, 1999. **141**(3-4): p. 345-349.
6. Leporatti, S., Vergara, D., Zacheo, A., Vergaro, V., Maruccio, G., Cingolani, R., and Rinaldi, R., *Cytomechanical and topological investigation of MCF-7 cells by scanning force microscopy*. Nanotechnology, 2009. **20**(Copyright 2009, The Institution of Engineering and Technology): p. 055103 (6 pp.).
7. Sperelakis, N. and W. Tomé, *Cell physiology source book*. Medical Physics, 1999. **26**: p. 664.
8. Wang, J., Wan, Zongfang, Liu, Wenming, Li, Li, Ren, Li, Wang, Xueqin, Sun, Peng, Ren, Lili, Zhao, Huiying, Tu, Qin, Zhang, Zhiyun, Song, Na, and Zhang, Lei, *Atomic force microscope study of tumor cell membranes following treatment with anti-cancer drugs*. Biosensors and Bioelectronics, 2009. **25**(4): p. 721-727.
9. Lim, C.T., Zhou, E. H., Quek, S. T., , *Mechanical models for living cells--a review*. Journal of Biomechanics, 2006. **39**(2): p. 195-216.
10. Park, K., Jang, J., Irimia, D., Sturgis, J., Lee, J., Robinson, JP., Toner, M., and Bashir, R., *'Living cantilever arrays' for characterization of mass of single live cells in fluids*. Lab on a Chip, 2008. **8**(7): p. 1034-1041.
11. Fingar, D., Salama, S., Tsou, C., Harlow, E., and Blenis, J., *Mammalian cell size is controlled by mTOR and its downstream targets S6K1 and 4EBP1/eIF4E*. Genes & development, 2002. **16**(12): p. 1472.
12. Dolznig, H., Grebien, Florian, Sauer, Thomas, Beug, Hartmut, and Mullner, Ernst W., *Evidence for a size-sensing mechanism in animal cells*. Nat Cell Biol, 2004. **6**(9): p. 899-905.
13. Wolff, D. and H. Pertoft, *Separation of HeLa Cells by Colloidal Silica Density Gradient Centrifugation: I. Separation and Partial Synchrony of Mitotic Cells*. Journal of Cell Biology, 1972. **55**(3): p. 579.
14. Kuznetsova, T.G., Starodubtseva, Maria N., Yegorenkov, Nicolai I., Chizhik, Sergey A., and Zhdanov, Renat I., *Atomic force microscopy probing of cell elasticity*. Micron, 2007. **38**(8): p. 824-833.
15. Fung, Y., *Foundations of solid mechanics*. 1965: Prentice Hall.
16. Weiss, E., Anastasiadis, P., Pilarczyk, G., Lerner, RM., and Zinin, PV., *Mechanical properties of single cells by high-frequency time-resolved acoustic microscopy*. IEEE Transactions on Ultrasonics, Ferroelectrics and Frequency Control, 2007. **54**(11): p. 2257-2271.

17. Zinin, P.V., J.S. Allen, and V.M. Levin, *Mechanical resonances of bacteria cells*. Physical Review E, 2005. **72**(6): p. 061907.
18. Miller, D.L., *Effects of a High-Amplitude 1-MHz Standing Ultrasonic Field on the Algae Hydrodictyon*. Ultrasonics, Ferroelectrics and Frequency Control, IEEE Transactions on, 1986. **33**(2): p. 165-170.
19. Crick, F. and A. Hughes, *The physical properties of cytoplasm.: A study by means of the magnetic particle method Part I. Experimental*. Experimental Cell Research, 1950. **1**(1): p. 37-80.
20. Binnig, G., C.F. Quate, and C. Gerber, *Atomic Force Microscope*. Physical Review Letters, 1986. **56**(9): p. 930.
21. Ahmad, M., Nakajima, M., Kojima, S., Homma, M., and Fukuda, T., *In Situ Single Cell Mechanics Characterization of Yeast Cells Using Nanoneedles Inside Environmental SEM*. IEEE Transactions on Nanotechnology, 2008. **7**(5 Part 0): p. 607-616.
22. Wang, N., J. Butler, and D. Ingber, *Mechanotransduction across the cell surface and through the cytoskeleton*. Science, 1993. **260**(5111): p. 1124.
23. Zhang, H. and K. Liu, *Optical tweezers for single cells*. Journal of the Royal Society Interface, 2008. **5**(24): p. 671.
24. Thoumine, O. and A. Ott, *Time scale dependent viscoelastic and contractile regimes in fibroblasts probed by microplate manipulation*. Journal of cell science, 1997. **110**(17): p. 2109.
25. Hochmuth, R.M., *Micropipette aspiration of living cells*. Journal of Biomechanics, 2000. **33**(1): p. 15-22.
26. Pohl, H.A., *Dielectrophoresis: The Behavior of Neutral Matter in Nonuniform Electric Fields*. 1978: Cambridge University Press.
27. Lim, C., Zhou, EH., Li, A., Vedula, SRK., and Fu, HX., *Experimental techniques for single cell and single molecule biomechanics*. Materials Science and Engineering: C, 2006. **26**(8): p. 1278-1288.
28. Butt, H.-J., B. Cappella, and M. Kappl, *Force measurements with the atomic force microscope: Technique, interpretation and applications*. Surface Science Reports, 2005. **59**(1-6): p. 1-152.
29. Van Vliet, K.J., G. Bao, and S. Suresh, *The biomechanics toolbox: experimental approaches for living cells and biomolecules*. Acta Materialia, 2003. **51**(19): p. 5881-5905.
30. Boussu, K., Van der Bruggen, B., Volodin, A., Snauwaert, J., Van Haesendonck, C., and Vandecasteele, C., *Roughness and hydrophobicity studies of nanofiltration membranes using different modes of AFM*. Journal of Colloid and Interface Science, 2005. **286**(2): p. 632-638.
31. Sánchez, D., Johnson, N.,m Li, C., Novak, P., Rheinlaender, J., Zhang, Y., Anand, U., Anand, P., Gorelik, J., and Frolenkov, GI., *Noncontact measurement of the local mechanical properties of living cells using pressure applied via a pipette*. Biophysical Journal, 2008. **95**(6): p. 3017-3027.
32. Weisenhorn, A., Khorsandi, M., Kasas, S., Gotzos, V., and Butt, H., *Deformation and height anomaly of soft surfaces studied with an AFM*. Nanotechnology, 1993. **4**: p. 106.

33. Inoue, K., T. Tanikawa, and T. Arai, *Micro-manipulation system with a two-fingered micro-hand and its potential application in bioscience*. Journal of Biotechnology, 2008. **133**(2): p. 219-224.
34. Hiratsuka, S., Mizutani, Y., Tsuchiya, M., Kawahara, K., Tokumoto, H., and Okajima, T., *The number distribution of complex shear modulus of single cells measured by atomic force microscopy*. Ultramicroscopy, 2009. **109**(Copyright 2010, The Institution of Engineering and Technology): p. 937-41.
35. Mahaffy, R.E., Park, S., Gerde, E., Käs, J., and Shih, C. K., *Quantitative Analysis of the Viscoelastic Properties of Thin Regions of Fibroblasts Using Atomic Force Microscopy*. Biophysical Journal, 2004. **86**(3): p. 1777-1793.
36. Critchley, D., Holt, MR., Barry, ST., Priddle, H., Hemmings, L., and Norman, J. *Integrin-mediated cell adhesion: the cytoskeletal connection*. 1999.
37. Weder, G., Voros, J., Giazson, M., Matthey, N., Heinzelmann, H., and Liley, M., *Measuring cell adhesion forces during the cell cycle by force spectroscopy*. Biointerphases Journal, 2009. **4**(Copyright 2009, The Institution of Engineering and Technology): p. 27-34.
38. Lu, L., Oswald, SJ., Ngu, H., and Yin, FCP., *Mechanical Properties of Actin Stress Fibers in Living Cells*. Biophysical Journal, 2008. **95**(12): p. 6060-6071.
39. Castillo, J., M. Dimaki, and W. Svendsen, *Manipulation of biological samples using micro and nano techniques*. Integrative Biology, 2009. **1**(1): p. 30-42.
40. Zhe, S., Juriani, A., Meininger, G. A., and Meissner, K. E., *Probing cell surface interactions using atomic force microscope cantilevers functionalized for quantum dot-enabled Forster resonance energy transfer*. Journal of Biomedical Optics, 2009. **14**(Copyright 2009, The Institution of Engineering and Technology): p. 040502 (3 pp.).
41. Merrill, G.F., *Chapter 13 Cell Synchronization*, in *Methods in Cell Biology*, P.M. Jennie and B. David, Editors. 1998, Academic Press. p. 229-249.
42. Bianco, A., K. Kostarelos, and M. Prato, *Applications of carbon nanotubes in drug delivery*. Current Opinion in Chemical Biology, 2005. **9**(6): p. 674-679.
43. Felder, S. and E. Elson, *Mechanics of fibroblast locomotion: quantitative analysis of forces and motions at the leading lamellas of fibroblasts*. The Journal of cell biology, 1990. **111**(6): p. 2513.
44. Ishijima, A., Doi, T., Sakurada, K., and Yanagida, T., *Sub-piconewton force fluctuations of actomyosin in vitro*. 1991.
45. Sneddon, I., *The relation between load and penetration in the axisymmetric Boussinesq problem for a punch of arbitrary profile*. International Journal of Engineering Science, 1965. **3**(1): p. 47-57.
46. Godin, M., Bryan, AK., Burg, TP., Babcock, K., and Manalis, SR., *Measuring the mass, density, and size of particles and cells using a suspended microchannel resonator*. Applied Physics Letters, 2007. **91**: p. 123121.
47. Burg, T.P., Godin, Michel, Knudsen, Scott M., Shen, Wenjiang, Carlson, Greg, Foster, John S., Babcock, Ken, and Manalis, Scott R., *Weighing of biomolecules, single cells and single nanoparticles in fluid*. Nature, 2007. **446**(7139): p. 1066-1069.
48. Peterman, E.J.G., F. Gittes, and C.F. Schmidt, *Laser-Induced Heating in Optical Traps*. Biophysical Journal, 2003. **84**(2): p. 1308-1316.

49. Fabry, B., Maksym, Geoffrey N., Hubmayr, Rolf D., Butler, James P., and Fredberg, Jeffrey J., *Implications of heterogeneous bead behavior on cell mechanical properties measured with magnetic twisting cytometry*. Journal of Magnetism and Magnetic Materials, 1999. **194**(1-3): p. 120-125.
50. Sen, S. and S. Kumar, *Combining mechanical and optical approaches to dissect cellular mechanobiology*. Journal of Biomechanics, 2010. **43**(1): p. 45-54.
51. Overby, D.R., Matthews, Benjamin D., Alsberg, Eben, and Ingber, Donald E., *Novel dynamic rheological behavior of individual focal adhesions measured within single cells using electromagnetic pulling cytometry*. Acta Biomaterialia, 2005. **1**(3): p. 295-303.
52. Ashkin, A. and J. Dziedzic, *Optical trapping and manipulation of single living cells using infra-red laser beams*. Berichte der Bunsengesellschaft für physikalische Chemie, 1989. **93**(3): p. 254-260.
53. Lim, C.T., Dao, M., Suresh, S., Sow, C. H., and Chew, K. T., *Large deformation of living cells using laser traps*. Acta Materialia, 2004. **52**(7): p. 1837-1845.
54. Desprat, N., Richert, A., Simeon, J., and Asnacios, A., *Creep function of a single living cell*. Biophysical Journal, 2005. **88**(3): p. 2224-2233.
55. Desprat, N., A. GUIROY, and A. Asnacios, *Microplates-based rheometer for a single living cell*. Review of Scientific Instruments, 2006. **77**: p. 055111.
56. Rand, R.P., *Mechanical Properties of the Red Cell Membrane: II. Viscoelastic Breakdown of the Membrane*. Biophysical Journal, 1964. **4**(4): p. 303-316.
57. Rand, R.P. and A.C. Burton, *Mechanical Properties of the Red Cell Membrane: I. Membrane Stiffness and Intracellular Pressure*. Biophysical Journal, 1964. **4**(2): p. 115-135.
58. Evans, E., *New membrane concept applied to the analysis of fluid shear-and micropipette-deformed red blood cells*. Biophysical Journal, 1973. **13**(9): p. 941-954.
59. Moussy, F., Lin, F. Y. H., Lahooti, S., Policova, Z., Zingg, W., and Neumann, A. W., *A micropipette aspiration technique to investigate the adhesion of endothelial cells*. Colloids and Surfaces B: Biointerfaces, 1994. **2**(5): p. 493-503.
60. Chu, Y., Thomas, WA., Eder, O., Pincet, F., Perez, E., Thiery, JP., and Dufour, S., *Force measurements in E-cadherin-mediated cell doublets reveal rapid adhesion strengthened by actin cytoskeleton remodeling through Rac and Cdc42*. The Journal of cell biology, 2004. **167**(6): p. 1183.
61. Zimmermann, U. and J. Vienken, *Electric field-induced cell-to-cell fusion*. Journal of Membrane Biology, 1982. **67**(1): p. 165-182.
62. Engelhardt, H. and E. Sackmann, *On the measurement of shear elastic moduli and viscosities of erythrocyte plasma membranes by transient deformation in high frequency electric fields*. Biophysical Journal, 1988. **54**(3): p. 495-508.
63. Minerick, A.R., Zhou, Ronghui, Takhistov, Pavlo, Chang, Hsueh-Chia, *Manipulation and characterization of red blood cells with alternating current fields in microdevices*. ELECTROPHORESIS, 2003. **24**(21): p. 3703-3717.
64. Salipante, P.F., et al., *Electrodeformation method for measuring the capacitance of bilayer membranes*. Soft Matter, 2012. **8**(14): p. 3810-3816.

65. Wang, X., X.-B. Wang, and P.R.C. Gascoyne, *General expressions for dielectrophoretic force and electrorotational torque derived using the Maxwell stress tensor method*. Journal of Electrostatics, 1997. **39**(4): p. 277-295.
66. Sukhorukov, V.L., Mussauer, H., Zimmermann, U., *The Effect of Electrical Deformation Forces on the Electroporation of Erythrocyte Membranes in Low- and High-Conductivity Media*. Journal of Membrane Biology, 1998. **163**(3): p. 235-245.
67. Li, H., T. Ye, and K.Y. Lam, *Qualitative and quantitative analysis of dynamic deformation of a cell in nonuniform alternating electric field*. Journal of Applied Physics, 2011. **110**(10): p. 104701.
68. Jian Chen, Y.Z., Qingyuan Tan, Yan Liang Zhang, Jason Li, William R. Geddie, Michael A. S. Jewett, Yu Sun, et al., *Electrodeformation for single cell mechanical characterization*. Journal of Micromechanics and Microengineering, 2011. **21**(5): p. 054012.
69. Guido Isabella, J.M., Duschl Claus, *Dielectrophoretic stretching of cells allows for characterization of their mechanical properties*. European Biophysics Journal, 2011. **40**(3): p. 281-288.
70. Yeung, A. and E. Evans, *Cortical shell-liquid core model for passive flow of liquid-like spherical cells into micropipets*. Biophysical Journal, 1989. **56**(1): p. 139-149.
71. Needham, D. and R.M. Hochmuth, *Rapid Flow of Passive Neutrophils Into a 4  $\mu$  m Pipet and Measurement of Cytoplasmic Viscosity*. Journal of Biomechanical Engineering, 1990. **112**(3): p. 269-276.
72. Bilodeau, G.G., *Regular Pyramid Punch Problem*. Journal of Applied Mechanics, 1992. **59**(3): p. 519-523.
73. Theret, D.P., Levesque, M. J., Sato, M., Nerem, R. M., Wheeler, L. T., , *The Application of a Homogeneous Half-Space Model in the Analysis of Endothelial Cell Micropipette Measurements*. Journal of Biomechanical Engineering, 1988. **110**(3): p. 190-199.
74. Mijailovich, S.M., Kojic, Milos, Zivkovic, Miroslav, Fabry, Ben, Fredberg, Jeffrey J., , *A finite element model of cell deformation during magnetic bead twisting*. J Appl Physiol, 2002. **93**(4): p. 1429-1436.
75. Alcaraz, J., Buscemi, Lara, Grabulosa, Mireia, Trepas, Xavier, Fabry, Ben, Farré, Ramon, Navajas, Daniel, , *Microrheology of Human Lung Epithelial Cells Measured by Atomic Force Microscopy*. Biophysical Journal, 2003. **84**(3): p. 2071-2079.
76. Zinin, P.V. and J.S. Allen, III, *Deformation of biological cells in the acoustic field of an oscillating bubble*. Physical Review E (Statistical, Nonlinear, and Soft Matter Physics), 2009. **79**(Copyright 2009, The Institution of Engineering and Technology): p. 021910 (12 pp.).
77. Baddour, R., Sherar, MD., Hunt, JW., Czarnota, GJ., and Kolios, MC., *High-frequency ultrasound scattering from microspheres and single cells*. The Journal of the Acoustical Society of America, 2005. **117**: p. 934.
78. Ackerman, E., *Resonances of biological cells at audible frequencies*. Bulletin of Mathematical Biology, 1951. **13**(2): p. 93-106.

79. Ackerman, E., *An extension of the theory of resonances of biological cells: I. Effects of viscosity and compressibility*. Bulletin of Mathematical Biology, 1954. **16**(2): p. 141-150.
80. Landau, L.D., Lifshitz, E. M., *Fluid mechanics* (Pergamon Press, Oxford). 1959. **Vol. 6**.
81. Zinin, P.V., V.M. Levin, and R.G. Mayev, *Natural oscillations of biological microspecimens*. Biophysics, 1987. **32**(1): p. 202-210.
82. Ilyukhina, M., *Cell membrane deformation under shock pulse treatment*. Moscow University Physics Bulletin, 2008. **63**(1): p. 39-43.
83. Ackerman, E., *An extension of the theory of resonances of biological cells: III. Relationship of breakdown curves and mechanical Q*. Bulletin of Mathematical Biology, 1957. **19**(1): p. 1-7.
84. Khismatullin, D.B. and A. Nadim, *Shape oscillations of a viscoelastic drop*. Physical Review E, 2001. **63**(6): p. 061508.
85. Al-Jarro, A., et al., *Direct calculation of Maxwell stress tensor for accurate trajectory prediction during DEP for 2D and 3D structures*. Journal of Physics D: Applied Physics, 2007. **40**(1): p. 71.
86. Schwalbe, J.T., P.M. Vlahovska, and M.J. Miksis, *Vesicle electrohydrodynamics*. Physical Review E, 2011. **83**(4): p. 046309.
87. MacQueen, L.A., M.D. Buschmann, and M.R. Wertheimer, *Mechanical properties of mammalian cells in suspension measured by electro-deformation*. Journal of Micromechanics and Microengineering, 2010. **20**(6): p. 065007.
88. Jones, T.B., *Electromechanics of particles*. 2005, Cambridge; New York: Cambridge University Press.
89. Rosales, C. and K.M. Lim, *Numerical comparison between Maxwell stress method and equivalent multipole approach for calculation of the dielectrophoretic force in single-cell traps*. ELECTROPHORESIS, 2005. **26**(11): p. 2057-2065.
90. Pethig, R., *Review article-dielectrophoresis: status of the theory, technology, and applications*. Biomicrofluidics, 2010. **4**(2): p. 022811 (35 pp.).
91. COMSOL, *MEMS Module User's Guide: The Electromechanics Interface*. 1998–2011
92. Chen, J., et al., *Electrodeformation for single cell mechanical characterization*. Journal of Micromechanics and Microengineering, 2011. **21**(5): p. 054012.
93. Muñoz, J., R. Valencia, and C. Nieto, *COMSOL and MATLAB® Integration to Optimize Heat Exchangers Using Genetic Algorithms Technique*, in *Proceedings of the COMSOL Conference 2008*.
94. E. Pelster, a.D.W., W.E. GmbH, and D. Ulm, *Design Optimization of an Electronic Component with an Evolutionary Algorithm Using a MATLAB-COMSOL Based Model*, in *COMSOL conference 2011*: Stuttgart.
95. COMSOL, *Introduction to LiveLink™ for MATLAB®*. 2009–2011.
96. Center, M.D., *Genetic Algorithm Terminology*, 1994-2013 The MathWorks, Inc.
97. Gascoyne, P.R.C., Xiao-Bo, Wang, Ying, Huang, Becker, F. F., , *Dielectrophoretic separation of cancer cells from blood*. Industry Applications, IEEE Transactions on, 1997. **33**(3): p. 670-678.



98. Labeed, F.H., Coley, Helen M., Thomas, Hilary, Hughes, Michael P., *Assessment of Multidrug Resistance Reversal Using Dielectrophoresis and Flow Cytometry*. Biophysical journal, 2003. **85**(3): p. 2028-2034.
99. Lee, M.-H., Wu, Pei-Hsun., Staunton, Jack Rory., Ros, Robert., Longmore, Gregory D., Wirtz, Denis., *Mismatch in Mechanical and Adhesive Properties Induces Pulsating Cancer Cell Migration in Epithelial Monolayer*. Biophysical journal, 2012. **102**(12): p. 2731-2741.
100. Leporatti, S., Vergara, D., Zacheo, A., Vergaro, V., Maruccio, G., Cingolani, R., Rinaldi, R., *Cytomechanical and topological investigation of MCF-7 cells by scanning force microscopy*. Nanotechnology, 2009. **20**(5): p. 055103 (6 pp.).
101. Guck, J., Schinkinger, Stefan., Lincoln, Bryan., Wottawah, Falk., Ebert, Susanne., Romeyke, Maren., Lenz, Dominik., Erickson, Harold M., Ananthakrishnan, Revathi., Mitchell, Daniel., Käs, Josef., Ulvick, Sydney., Bilby, Curt., , *Optical Deformability as an Inherent Cell Marker for Testing Malignant Transformation and Metastatic Competence*. Biophysical journal, 2005. **88**(5): p. 3689-3698.
102. Hou, H., Li, Q., Lee, G., Kumar, A., Ong, C., Lim, C., *Deformability study of breast cancer cells using microfluidics*. Biomedical Microdevices, 2009. **11**(3): p. 557-564.
103. Lincoln, B., Erickson, Harold M., Schinkinger, Stefan, Wottawah, Falk, Mitchell, Daniel, Ulvick, Sydney, Bilby, Curt, Guck, Jochen, , *Deformability-based flow cytometry*. Cytometry Part A, 2004. **59A**(2): p. 203-209.
104. Suresh, S., Spatz, J., Mills, JP., Micoulet, A., Dao, M., Lim, CT., Beil, M., and Seufferlein, T., *Connections between single-cell biomechanics and human disease states: gastrointestinal cancer and malaria*. Acta Biomaterialia, 2005. **1**(1): p. 15-30.
105. Nikkhah, M., Strobl, Jeannine S., Schmelz, Eva M., Agah, Masoud, *Evaluation of the influence of growth medium composition on cell elasticity*. Journal of biomechanics, 2011. **44**(4): p. 762-766.

## Appendix

### A.1: *model.m* , MATLAB function for transferring the result and modified parameters to COMSOL Desktop

```
function out = model
import com.comsol.model.*
import com.comsol.model.util.*

model = ModelUtil.create('Model');

model.modelPath('C:\...');%Insert the source COMSOL simulation file%

model.modelNode.create('mod1');

model.geom.create('geom1', 3);

model.mesh.create('mesh1', 'geom1');

model.physics.create('solid', 'SolidMechanics', 'geom1');
model.physics.create('es', 'Electrostatics', 'geom1');

model.study.create('std1');
model.study('std1').feature.create('stat', 'Stationary');

model.geom('geom1').lengthUnit([native2unicode(hex2dec('00b5'),
'Cp1252') 'm']);

model.param.set('x1', ['30[' native2unicode(hex2dec('00b5'), 'Cp1252')
'm]']);
model.param.descr('x1', 'Length of electrodes');
model.param.set('x2', ['30[' native2unicode(hex2dec('00b5'), 'Cp1252')
'm]']);
model.param.descr('x2', 'Distance between electrodes');
model.param.set('x3', '90[deg]');
model.param.descr('x3', 'Tip angle');
model.param.set('x4', '40[1]');
model.param.descr('x4', 'Medium permittivity');
model.param.set('x5', ['20[' native2unicode(hex2dec('00b5'), 'Cp1252')
'm]']);
model.param.descr('x5', 'Vertical distance between electrodes');
model.param.set('x6', ['0[' native2unicode(hex2dec('00b5'), 'Cp1252')
'm]']);
model.param.descr('x6', 'Cell position');
model.param.set('r1', ['10[' native2unicode(hex2dec('00b5'), 'Cp1252')
'm]']);
model.param.descr('r1', 'Cell radius');
model.param.set('tt', ['0.5[' native2unicode(hex2dec('00b5'), 'Cp1252')
'm]']);
model.param.descr('tt', 'Cell Thickness');

model.geom('geom1').feature.create('wp1', 'WorkPlane');
```

```

model.geom('geom1').feature('wp1').geom.feature.create('b1',
'BezierPolygon');
model.geom('geom1').feature('wp1').geom.feature('b1').set('degree',
[1]);
model.geom('geom1').feature('wp1').geom.feature('b1').set('p', {'0'
'0'; '0' '0'});
model.geom('geom1').feature('wp1').geom.feature('b1').set('w', {'1'
'1'});
model.geom('geom1').feature('wp1').geom.feature('b1').set('degree', [1
1]);
model.geom('geom1').feature('wp1').geom.feature('b1').set('p', {'0' '0'
'0'; '0' '0' '0' '0'});
model.geom('geom1').feature('wp1').geom.feature('b1').set('w', {'1' '1'
'1' '1'});
model.geom('geom1').feature('wp1').geom.feature('b1').set('degree', [1
1 1]);
model.geom('geom1').feature('wp1').geom.feature('b1').set('p', {'0' '0'
'0' '0' '0'; '0' '0' '0' '0' '0'});
model.geom('geom1').feature('wp1').geom.feature('b1').set('w', {'1' '1'
'1' '1' '1' '1' '1' '1'});
model.geom('geom1').feature('wp1').geom.feature('b1').set('degree', [1
1 1 1]);
model.geom('geom1').feature('wp1').geom.feature('b1').set('p', {'0' '0'
'0' '0' '0' '0'; '0' '0' '0' '0' '0' '0' '0' '0'});
model.geom('geom1').feature('wp1').geom.feature('b1').set('w', {'1' '1'
'1' '1' '1' '1' '1' '1' '1' '1' '1' '1'});
model.geom('geom1').feature('wp1').geom.feature('b1').set('degree', [1
1 1 1 1]);
model.geom('geom1').feature('wp1').geom.feature('b1').set('p', {'0' '0'
'0' '0' '0' '0' '0'; '0' '0' '0' '0' '0' '0' '0' '0' '0'});
model.geom('geom1').feature('wp1').geom.feature('b1').set('w', {'1' '1'
'1' '1' '1' '1' '1' '1' '1' '1' '1' '1' '1' '1'});
model.geom('geom1').feature('wp1').geom.feature('b1').setIndex('p', '-
x2/2', 0, 0);
model.geom('geom1').feature('wp1').geom.feature('b1').setIndex('p', '-
x2/2-x1*cos(x3/2)', 0, 1);
model.geom('geom1').feature('wp1').geom.feature('b1').setIndex('p',
'x1*sin(x3/2)', 1, 1);
model.geom('geom1').feature('wp1').geom.feature('b1').setIndex('p', '-
x2/2-x1*cos(x3/2)', 0, 2);
model.geom('geom1').feature('wp1').geom.feature('b1').setIndex('p',
'x1*sin(x3/2)+x5', 1, 2);
model.geom('geom1').feature('wp1').geom.feature('b1').setIndex('p', '-
x2/2-x1*cos(x3/2)-x5', 0, 3);

```

```

model.geom('geom1').feature('wp1').geom.feature('b1').setIndex('p',
'x1*sin(x3/2)+x5', 1, 3);
model.geom('geom1').feature('wp1').geom.feature('b1').setIndex('p', '-
x2/2-x1*cos(x3/2)-x5', 0, 4);
model.geom('geom1').feature('wp1').geom.feature('b1').setIndex('p', '-
1*(x1*sin(x3/2)+x5)', 1, 4);
model.geom('geom1').feature('wp1').geom.feature('b1').setIndex('p', '-
x2/2-x1*cos(x3/2)', 0, 5);
model.geom('geom1').feature('wp1').geom.feature('b1').setIndex('p', '-
1*(x1*sin(x3/2)+x5)', 1, 5);
model.geom('geom1').feature('wp1').geom.feature('b1').setIndex('p', '-
x2/2-x1*cos(x3/2)', 0, 6);
model.geom('geom1').feature('wp1').geom.feature('b1').setIndex('p', '-
x1*sin(x3/2)', 1, 6);
model.geom('geom1').feature('wp1').geom.feature('b1').setIndex('p', '-
x2/2', 0, 7);
model.geom('geom1').feature('wp1').geom.runAll;
model.geom('geom1').runAll;
model.geom('geom1').feature('wp1').geom.run('b1');
model.geom('geom1').feature('wp1').geom.feature.create('fill',
'Fillet');
model.geom('geom1').feature('wp1').geom.feature('fill').selection('poin
t').set('b1', [7]);
model.geom('geom1').feature('wp1').geom.feature('fill').set('radius',
'1');
model.geom('geom1').feature('wp1').geom.runAll;
model.geom('geom1').feature('wp1').geom.run('fill');
model.geom('geom1').feature('wp1').geom.feature.create('mir1',
'Mirror');
model.geom('geom1').feature('wp1').geom.feature('mir1').selection('inpu
t').set({'fill'});
model.geom('geom1').feature('wp1').geom.feature('mir1').set('keep',
'on');
model.geom('geom1').feature('wp1').geom.runAll;
model.geom('geom1').run('wp1');
model.geom('geom1').feature.create('ext1', 'Extrude');
model.geom('geom1').feature('ext1').setIndex('distance', '0.5', 0);
model.geom('geom1').runAll;

model.view('view1').set('transparency', 'on');
model.view('view1').set('renderwireframe', true);

model.geom('geom1').run('ext1');
model.geom('geom1').feature.create('blk1', 'Block');
model.geom('geom1').feature('blk1').setIndex('size',
'2*(x2/2+x1*cos(x3/2)+x5)', 0);
model.geom('geom1').feature('blk1').setIndex('size',
'2*(x1*sin(x3/2)+x5)', 1);
model.geom('geom1').feature('blk1').setIndex('size', '60', 2);
model.geom('geom1').feature('blk1').setIndex('pos', '-x2/2-
x1*cos(x3/2)-x5', 0);
model.geom('geom1').feature('blk1').setIndex('pos', '-
1*(x1*sin(x3/2)+x5)', 1);
model.geom('geom1').runAll;
model.geom('geom1').run('blk1');
model.geom('geom1').feature.create('sph1', 'Sphere');

```

```

model.geom('geom1').feature('sph1').setIndex('pos', ['r1+1['
native2unicode(hex2dec('00b5'), 'Cp1252') 'm']'], 2);
model.geom('geom1').feature('sph1').set('r', 'r1');
model.geom('geom1').feature('sph1').setIndex('pos', 'x6', 0);
model.geom('geom1').runAll;
model.geom('geom1').run('sph1');
model.geom('geom1').feature.create('sph2', 'Sphere');
model.geom('geom1').feature('sph2').set('r', 'r1-tt');
model.geom('geom1').feature('sph2').setIndex('pos', ['r1+1['
native2unicode(hex2dec('00b5'), 'Cp1252') 'm']'], 2);
model.geom('geom1').feature('sph2').setIndex('pos', 'x6', 0);
model.geom('geom1').runAll;
model.geom('geom1').run('sph2');
model.geom('geom1').feature.create('dif1', 'Difference');
model.geom('geom1').feature('dif1').selection('input').set({'sph1'});
model.geom('geom1').feature('dif1').selection('input2').set({'sph2'});
model.geom('geom1').runAll;
model.geom('geom1').run('dif1');
model.geom('geom1').feature.create('sph3', 'Sphere');
model.geom('geom1').feature('sph3').set('r', 'r1-tt');
model.geom('geom1').feature('sph3').setIndex('pos', 'x6', 0);
model.geom('geom1').feature('sph3').setIndex('pos', ['r1+1['
native2unicode(hex2dec('00b5'), 'Cp1252') 'm']'], 2);
model.geom('geom1').runAll;
model.geom('geom1').runAll;
model.geom('geom1').run('fin');

model.material.create('mat1');
model.material('mat1').name('Chrome');
model.material('mat1').propertyGroup('def').set('relpermittivity',
{'12' '0' '0' '0' '12' '0' '0' '0' '12'});
model.material('mat1').propertyGroup('def').set('electricconductivity',
{'7.9e6' '0' '0' '0' '7.9e6' '0' '0' '0' '7.9e6'});
model.material('mat1').set('family', 'plastic');
model.material.create('mat2');
model.material('mat2').propertyGroup.create('Enu', 'Young's modulus
and Poisson's ratio');
model.material('mat2').name('Cell');
model.material('mat2').propertyGroup('def').set('heatcapacity',
'1700[J/(kg*K)]');
model.material('mat2').propertyGroup('def').set('relpermittivity',
{'80' '0' '0' '0' '80' '0' '0' '0' '80'});
model.material('mat2').propertyGroup('def').set('thermalexpansioncoeffi
cient', {'280e-6[1/K]' '0' '0' '0' '280e-6[1/K]' '0' '0' '0' '280e-
6[1/K]'});
model.material('mat2').propertyGroup('def').set('density',
'1150[kg/m^3]');
model.material('mat2').propertyGroup('def').set('thermalconductivity',
{'0.26[W/(m*K)]' '0' '0' '0' '0.26[W/(m*K)]' '0' '0' '0'
'0.26[W/(m*K)]'});
model.material('mat2').propertyGroup('def').set('electricconductivity',
{'0.1' '0' '0' '0' '0.1' '0' '0' '0' '0.1'});
model.material('mat2').propertyGroup('Enu').set('youngsmodulus',
'600[Pa]');
model.material('mat2').propertyGroup('Enu').set('poissonsratio',
'0.37');
model.material('mat2').set('family', 'plastic');

```

```

model.material.create('mat3');
model.material('mat3').propertyGroup('def').func.create('eta',
'Piecewise');
model.material('mat3').propertyGroup('def').func.create('Cp',
'Piecewise');
model.material('mat3').propertyGroup('def').func.create('rho',
'Piecewise');
model.material('mat3').propertyGroup('def').func.create('k',
'Piecewise');
model.material('mat3').propertyGroup('def').func.create('cs',
'Interpolation');
model.material('mat3').name('Medium');
model.material('mat3').propertyGroup('def').func('eta').set('arg',
'T');
model.material('mat3').propertyGroup('def').func('eta').set('pieces',
{'273.15' '413.15' '1.3799566804-0.021224019151*T^1+1.3604562827E-
4*T^2-4.6454090319E-7*T^3+8.9042735735E-10*T^4-9.0790692686E-
13*T^5+3.8457331488E-16*T^6'; '413.15' '553.75' '0.00401235783-
2.10746715E-5*T^1+3.85772275E-8*T^2-2.39730284E-11*T^3'});
model.material('mat3').propertyGroup('def').func('Cp').set('arg', 'T');
model.material('mat3').propertyGroup('def').func('Cp').set('pieces',
{'273.15' '553.75' '12010.1471-80.4072879*T^1+0.309866854*T^2-
5.38186884E-4*T^3+3.62536437E-7*T^4'});
model.material('mat3').propertyGroup('def').func('rho').set('arg',
'T');
model.material('mat3').propertyGroup('def').func('rho').set('pieces',
{'273.15' '553.75' '838.466135+1.40050603*T^1-
0.0030112376*T^2+3.71822313E-7*T^3'});
model.material('mat3').propertyGroup('def').func('k').set('arg', 'T');
model.material('mat3').propertyGroup('def').func('k').set('pieces',
{'273.15' '553.75' '-0.869083936+0.00894880345*T^1-1.58366345E-
5*T^2+7.97543259E-9*T^3'});
model.material('mat3').propertyGroup('def').func('cs').set('table',
{'273' '1403'; '278' '1427'; '283' '1447'; '293' '1481'; '303' '1507';
'313' '1526'; '323' '1541'; '333' '1552'; '343' '1555'; '353' '1555';
'363' '1550'; '373' '1543'});
model.material('mat3').propertyGroup('def').func('cs').set('interp',
'piecewisecubic');
model.material('mat3').propertyGroup('def').set('electricconductivity',
{'15e-3[S/m]' '0' '0' '0' '15e-3[S/m]' '0' '0' '0' '15e-3[S/m]'});
model.material('mat3').propertyGroup('def').set('relpermittivity',
{'60' '0' '0' '0' '60' '0' '0' '0' '60'});
model.material('mat3').propertyGroup('def').addInput('temperature');
model.material('mat3').set('family', 'plastic');
model.material.create('mat4');
model.material('mat4').name('Cytoplasm');
model.material('mat4').propertyGroup('def').set('relpermittivity',
{'40' '0' '0' '0' '40' '0' '0' '0' '40'});
model.material('mat4').propertyGroup('def').set('electricconductivity',
{'0.1' '0' '0' '0' '0.1' '0' '0' '0' '0.1'});
model.material('mat4').set('family', 'plastic');
model.material('mat4').selection.set([4]);
model.material('mat1').selection.set([1 5]);
model.material('mat2').selection.set([3]);
model.material('mat3').selection.set([2]);

model.physics('solid').selection.set([3]);

```

```

model.material('mat3').propertyGroup('def').set('relpermittivity',
{'x4'});
model.material('mat4').propertyGroup('def').set('relpermittivity',
{'60'});

model.physics('solid').feature.create('bndl1', 'BoundaryLoad', 2);
model.physics('solid').feature('bndl1').selection.set([16 17 18 19 20
21 22 23 24 25 26 27 28 29 30 31]);
model.physics('solid').feature('bndl1').set('FperArea', {'es.nTx_FDEF'
'es.nTy_FDEF' '0'});
model.physics('es').feature.create('fcall', 'ForceCalculation', 3);
model.physics('es').feature('fcall').selection.set([3]);
model.physics('es').feature('fcall').set('ForceName', 1, 'FDEF');
model.physics('solid').feature.create('displ', 'Displacement1', 1);
model.physics('solid').feature('displ').selection.set([32 35 36 39 42
45 54 55]);
model.physics('solid').feature('displ').set('Direction', 3, '1');
model.physics('solid').feature.create('disp2', 'Displacement1', 1);
model.physics('solid').feature.create('disp3', 'Displacement1', 1);
model.physics('solid').feature('disp2').selection.set([33 34 37 38 47
49 51 53]);
model.physics('solid').feature('disp2').set('Direction', 2, '1');
model.physics('solid').feature('disp3').selection.set([40 41 43 44 46
48 50 52]);
model.physics('solid').feature('disp3').set('Direction', 1, '1');
model.physics('es').feature.create('pot1', 'ElectricPotential', 2);
model.physics('es').feature('pot1').selection.set([6 10 12 13 14 15]);
model.physics('es').feature('pot1').set('V0', 1, '5');
model.physics('es').feature.create('pot2', 'ElectricPotential', 2);
model.physics('es').feature('pot2').selection.set([32 33 35 36 37 39]);
model.physics('es').feature('pot2').set('V0', 1, '-5');

model.mesh('mesh1').run;

model.sol.create('sol1');
model.sol('sol1').study('std1');
model.sol('sol1').feature.create('st1', 'StudyStep');
model.sol('sol1').feature('st1').set('study', 'std1');
model.sol('sol1').feature('st1').set('studystep', 'stat');
model.sol('sol1').feature.create('v1', 'Variables');
model.sol('sol1').feature.create('s1', 'Stationary');
model.sol('sol1').feature('s1').feature.create('sel', 'Segregated');
model.sol('sol1').feature('s1').feature('sel').feature.remove('ssDef');
model.sol('sol1').feature('s1').feature('sel').feature.create('ss1',
'SegregatedStep');
model.sol('sol1').feature('s1').feature('sel').feature('ss1').set('segev
ar', {'mod1_V'});
model.sol('sol1').feature('s1').feature.create('il', 'Iterative');
model.sol('sol1').feature('s1').feature('il').set('linsolver', 'cg');
model.sol('sol1').feature('s1').feature('sel').feature('ss1').set('lins
olver', 'il');
model.sol('sol1').feature('s1').feature('il').feature.create('mg1',
'Multigrid');
model.sol('sol1').feature('s1').feature('il').feature('mg1').set('prefu
n', 'amg');

```

```

model.sol('sol1').feature('s1').feature('sel').feature.create('ss2',
'SegregatedStep');
model.sol('sol1').feature('s1').feature('sel').feature('ss2').set('segv
ar', {'mod1_u'});
model.sol('sol1').feature('s1').feature.remove('fcDef');
model.sol('sol1').attach('std1');

model.result.create('pg1', 3);
model.result('pg1').set('data', 'dset1');
model.result('pg1').feature.create('surfl', 'Surface');
model.result('pg1').feature('surfl').set('expr', {'solid.mises'});
model.result('pg1').name('Stress (solid)');
model.result('pg1').feature('surfl').feature.create('def', 'Deform');
model.result('pg1').feature('surfl').feature('def').set('expr', {'u'
'v' 'w'});
model.result('pg1').feature('surfl').feature('def').set('descr',
'Displacement field (Material)');
model.result.create('pg2', 3);
model.result('pg2').set('data', 'dset1');
model.result('pg2').feature.create('mslc1', 'Multislice');
model.result('pg2').feature('mslc1').set('expr', {'V'});
model.result('pg2').name('Electric Potential (es)');

model.sol('sol1').runAll;

model.result('pg1').run;
model.result.create('pg3', 'PlotGroup3D');
model.result('pg3').run;
model.result('pg3').feature.create('surfl', 'Surface');
model.result('pg3').feature('surfl').set('expr', 'u');
model.result('pg3').run;
model.result('pg3').feature('surfl').feature.create('def1', 'Deform');
model.result('pg3').run;
model.result('pg3').run;
model.result.numerical.create('int1', 'IntVolume');
model.result.numerical('int1').selection.set([3]);
model.result.numerical('int1').set('expr', '1');
model.result.table.create('tbl1', 'Table');
model.result.table('tbl1').comments('Volume Integration 1 (1)');
model.result.numerical('int1').set('table', 'tbl1');
model.result.numerical('int1').setResult;
model.result.numerical.remove('int1');
model.result('pg3').run;
model.result('pg3').run;

out = model;

```



## A.2: Trapping-stretching procedure of MDA-MB-231 cells

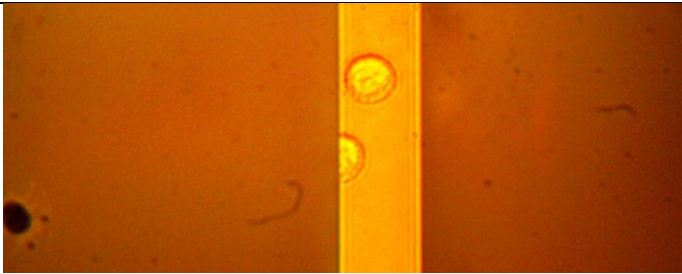
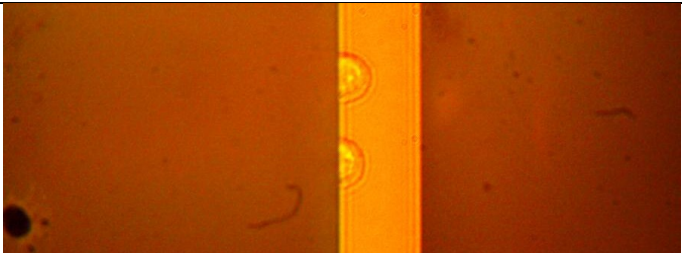
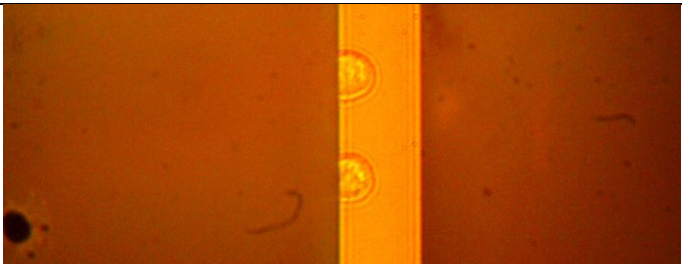
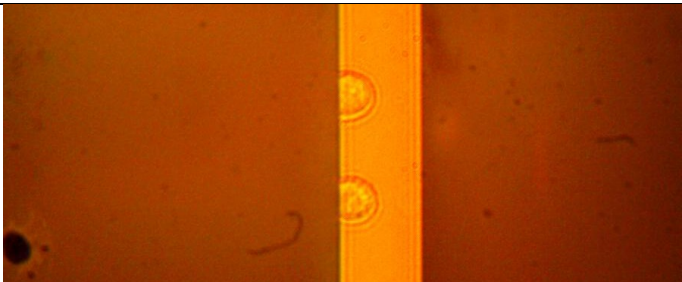
Upon applying 2 volts		
Upon applying 20 volts		
After 5 minutes of exposure of 20 volts		
After 10 minutes of exposure of 20 volts		

Figure A.2 Trapping-stretching procedure of MDA-MB-231 sample cells

### A.3: Elastic parameters of MCF10A and MDA-MB-231 cells in different growth media [105]

**Table 2**

Elastic parameters for non-malignant, non-metastatic MCF10A and highly metastatic MDA-MB-231 breast cells in different growth media.

	<b>n</b>	<b>E (kPa)</b>
<b>MDA-MB-231</b>		
M1: RPMI+10%FBS	47	0.50 ± 0.35
M2: RPMI+5%FBS	55	0.41 ± 0.22
M3: DMEM+5%FBS	79	0.40 ± 0.22
M4: RPMI+5%FBS+EGF	64	0.36 ± 0.20
M5: DMEM+5%HS+EGF+CT+INS+HC	78	0.37 ± 0.25
<b>MCF10A</b>		
M1: RPMI+10%FBS	59	1.11 ± 0.85**
M2: RPMI+5%FBS	61	1.0 ± 0.68
M3: DMEM+5%FBS	38	0.98 ± 0.49
M4: RPMI+5%FBS+EGF	100	0.88 ± 0.57
M5: DMEM+5%HS+EGF+CT+INS+HC	108	0.72 ± 0.54

E: elastic modulus, n: number of the cells analyzed. Data are presented in mean ± standard deviation (\*\* $p < 0.002$ , comparing M1 to M5).